Final Report

IMAGE ENHANCEMENT AND ADVANCED INFORMATION EXTRACTION TECHNIQUES FOR ERTS-1 DATA

William A. Malila
Richard F. Nalepka
Jane E. Sarno

INFRARED AND OPTICS DIVISION

JUNE 1975

Prepared for
NATIONAL AERONAUTICS AND SPACE ADMINISTRATION

Goddard Space Flight Center,
Greenbelt, Maryland 20771
Contract NAS5-21783, Task VII
E. F. Szajna, Code 430, Technical Monitor

1136A

ENVIRONMENTAL
RESEARCH INSTITUTE OF MICHIGAN
FORMERLY WILLOW RUN LABORATORIES, THE UNIVERSITY OF MICHIGAN
BOX 618 • ANN ARBOR • MICHIGAN 48107

TECHNICAL REPORT STANDARD TITLE PAGE

1. Report No. NASA CR-ERIM 193300-66-F	2. Government Accession No.	3. Recipient's Catalog No.
4. Title and Subtitle IMAGE ENHANCEMENT AND ADVANCED INFORMATION EXTRACTION TECHNIQUES FOR ERTS-1 DATA		5. Report Date June 1975 6. Performing Organization Code
7. Author(s) William A. Malila, Richard F. Nalepka, Jane E. Sarno		8. Performing Organization Report No. 193300-66-F
9. Performing Organization Name and Address Environmental Research Institute of Michigan Infrared and Optics Division Post Office Box 618 Ann Arbor, Michigan 48107		10. Work Unit No. Task VII 11. Contract or Grant No. NAS5-21783
12. Sponsoring Agency Name and Address Goddard Space Flight Center Greenbelt, Maryland 20771		13. Type of Report and Period Covered Final Report, June 12, 1972-October 31, 1974 14. Sponsoring Agency Code

15. Supplementary Notes

Mr. E. F. Szajna, Code 430, was Technical Monitor; Mr. G. Grebowsky was Scientific Monitor.

16. Abstract

This is the final report of an investigation carried out under the Earth Resources Technology Satellite (ERTS-1) program. The effort focussed on digital processing of multispectral scanner (MSS) data. Previously developed advanced digital processing techniques were applied and tested to determine their effectiveness in improving the quality of extracted information by understanding and alleviating degrading effects in the data, especially data covering large areas on the ground. The three areas of investigation were: (1) atmospheric effects in received signals, (2) signature extension techniques for enabling recognition in areas removed in space and time from training areas, and (3) pixel proportion estimation techniques for improving the accuracy of area estimates above those obtained with conventional recognition processing.

As a result of this investigation it was demonstrated and concluded that (1) the atmosphere has significant effects on ERTS MSS data which can seriously degrade recognition performance; (2) the application of selected signature extension techniques developed at ERIM serve to reduce the deleterious effects of both the atmosphere and changing ground conditions on recognition performance; and (3) a proportion estimation algorithm developed at ERIM, to overcome problems in acreage estimation accuracy resulting from the coarse spatial resolution of the ERTS MSS, was able to significantly improve acreage estimation accuracy over that achievable by conventional techniques, especially for high contrast targets such as lakes and ponds.

17. Key Words		18. Distribution Statement
ERTS data use	Classification	Initial distribution is indicated at the end of this document.
Remote sensing	Processing	
Multispectral	Atmospheres	
Scanners	Radiative transfer	
Interpretative techniques	Scientific satellites	
	Optics	

19. Security Classif. (of this report)	20. Security Classif. (of this page)	21. No. of Pages	22. Price
Unclassified	Unclassified	141	

PREFACE

This final report presents results of an investigation carried out at the Environmental Research Institute of Michigan (ERIM) for NASA's Goddard Space Flight Center. The work reported herein was accomplished under Task VII of Contract NAS5-21783 the objective of which was to adapt techniques existing at ERIM for application to ERTS-1 data, to assess the practicability of these techniques by applying them to selected ERTS-1 data, and to identify any additional problems that might be associated with such processing of satellite multispectral scanner data. Three areas were studied: (1) atmospheric effects; (2) signature extension; and (3) proportion estimation. Mr. E.F. Szajna was Technical Monitor for this contract, while Mr. G. Grebowsky served as Scientific Monitor.

The reported work was performed within ERIM's Infrared and Optics Division, directed by Mr. Richard R. Legault, under the supervision of Dr. Jon D. Erickson, Head of the Information Systems and Analysis Department. A number of individuals other than the authors participated in and contributed to various aspects of this investigation. Dr. Robert Turner provided consultation on the topic of atmospheric effects in ERTS data. Mr. James P. Morgenstern performed some of the recognition processing and analysis. Mr. Arthur McCleer participated in the development of the procedure for computer-assisted correlation of ERTS data and Earth coordinate systems. Mr. Ross H. Hieber contributed to both these efforts, and provided computer programming support and consultation throughout the investigation. Mr. James Reyer assisted with adaptive processing. Dr. Harold Horwitz, Mr. John T. Lewis, and Mr. J.P. Livisay assisted in the proportion estimation processing and analysis. Secretarial assistance was provided throughout this contract period by Ms. D. Dickerson, Ms. L. Parker, and Ms. G. Sotomayor.

Dr. Gene R. Safir and other Michigan State University personnel provided ground-truth information.

PAGE 2 INTENTIONALLY BLANK

TABLE OF CONTENTS

4
PAGE INTENTIONALLY BLANK

FIGURES

TABLES

SYMBOLS

E_s = Extraterrestial solar irradiance
L = Radiance
L_I = Intrinsic radiance
L_p = Path radiance
L_0 = Radiance at target
m = Estimated signature mean
p = True proportion
$\hat{p}$ = Estimated proportion
T = Atmospheric transmittance
t = Time
Δ = Mean level adjusted difference
θ = Angle of scan from nadir
θ_0 = Solar zenith angle
λ = Wavelength
μ_0 = Cosine of the solar zenith angle
ρ = Target reflectance
ρ = Probability of rejection parameter (Sec. 5)
ρ_B = Background albedo
τ = Optical thickness of atmosphere
τ = Water proportion threshold parameter (Sec. 5)
ϕ = Relative azimuth angle

ACRONYMS

ASCS	Agriculture Stabilization and Conservation Service
ERIM	Environmental Research Institute of Michigan
ERTS	Earth Resources Technology Satellite
GSFC	Goddard Space Flight Center, Greenbelt, Maryland
MASC	Multiplicative and Additive Signature Correction algorithm
MLA	Mean Level Adjustment
MSS	Multispectral Scanner
MSU	Michigan State University, East Lansing, Michigan
NWS	National Weather Service
Pixel	Picture element
SR&T	Supporting Research and Technology Program, Earth Observations Division, Johnson Space Center, Houston, Texas

IMAGE ENHANCEMENT AND ADVANCED INFORMATION EXTRACTION TECHNIQUES

1

SUMMARY, CONCLUSIONS AND RECOMMENDATIONS

This report describes an investigation in which a variety of computer techniques* for processing and analysis of remote sensor data were applied to data from the Earth Resources Technology Satellite (ERTS-1). Only data from the multispectral scanner (MSS) were analyzed, principally in digital form on computer-compatible tapes.

Advanced processing techniques developed on other NASA contracts were applied and tested, because conventional data processing and information extraction techniques fall short of providing the information required by the user in some applications. The three areas of the investigation were directed at factors which can seriously degrade the user's ability to extract necessary information: (1) atmospheric effects in received signals; (2) changes in signals as one moves in space and time from known areas used for training recognition processors; and (3) the relatively coarse spatial resolution of the sensor in comparison to the size of scene features being recognized.

Atmospheric effects in ERTS data were analyzed through both a radiative transfer model and empirical data. It was concluded that: (1) the atmosphere has significant effects on ERTS signals and makes major contributions to their magnitudes; (2) the major factors determining atmospheric contributions are optical thickness (haze content) and background albedo; (3) scan-angle-related effects are substantial in ERTS MSS data, even though the scan coverage is $\pm 6^{o}$; (4) signal variations attributable to the atmosphere can degrade recognition performance if not corrected; (5) measurement of optical thickness is preferred over visual range measurements as a method for characterizing atmospheric state. It is recommended that atmospheric effects on recognition be further quantified, that effects of aerosol absorption be studied, and that additional efforts be expended to verify and improve existing radiative transfer models for future use.

Methods for improving computer recognition of scene classes over large areas were studied by the application of existing recognition processing procedures and several signature

*These techniques were developed by ERIM for the Earth Observations Division of the Johnson Space Center of NASA under Contracts NAS9-9784 and NAS9-14123, as a part of the Supporting Research and Technology (SR&T) Program.

extension techniques which compensate for changes in signals caused by atmospheric effects and/or changing ground conditions. It was demonstrated and/or concluded that: (1) recognition processing performance degrades when signatures are applied directly to areas removed in space or time from the training data; (2) the signature extension techniques developed earlier at ERIM can alleviate the deleterious effects in the data and improve recognition performance in non-local areas (several techniques were tested: mean level adjustment, adaptive processing with a decision-directed Kalman filter, multiplicative and additive signature correction (MASC), and adjustment based on radiative transfer model calculations); (3) performance on field-center pixels (picture elements) was better than on full sections; (4) recognition performance depends on the procedures used for training and the type and quality of ground truth information. It is recommended that the various signature extension techniques be tested and evaluated in a more operational context on a more extensive data base and that their sensitivity to training procedures be explored.

Finally, problems related to the size of the ERTS spatial resolution element were addressed through the application of ERIM's proportion-estimation algorithm which operates on either individual pixels or averaged pixels. Mis-recognition of pixels that contain mixtures of two or more materials can cause errors in area estimation. Two area-determination applications were studied: mapping of surface water and agricultural acreage inventory. It was demonstrated and/or concluded that: (1) for surface water, the ERIM proportion-estimation algorithm detected water bodies and identified their acreages more accurately than did other available techniques; (2) the largest improvement was achieved on the smaller lakes and ponds which usually were not detected by more conventional techniques; (3) the algorithm exhibited little or no performance improvement for the agricultural scene over that achievable by conventional techniques; (4) the result of (3) is due in part to the availability of only three of the ERTS bands and the relatively wide spectral bandwidth of ERTS, but some restrictions imposed by the original algorithm were more clearly identified. It is recommended that recent modifications of the ERIM proportion-estimation algorithm be fully tested and evaluated to establish their performance characteristics.

2
INTRODUCTION

The state-of-the-art of remote sensing of earth resources took a giant step forward with the launch of the first Earth Resources Technology Satellite (ERTS). This event placed in orbit advanced sensing devices which would monitor the Earth from the vantage point of space and which would repeatedly pass over ground points at 18-day intervals. For the first time the

remote-sensing community had at its disposal a system which was a forerunner of operational remote sensing systems of the future. It was then up to that community (the users, the technique developers and the sensor developers) to quantify the characteristics of this new system, to demonstrate its utility and to identify and develop means to overcome its limitations.

Clearly, with a new sensing system operating from a new vantage point, there was a great deal to be learned and many problems to be solved. Not all of the problems were unanticipated. As a result of previous experience with the aircraft remote-sensing program of which ERIM was a charter member, certain of the problems were identified and/or anticipated, and in fact were being dealt with prior to the launch of ERTS.

These problems included quantifying the effects of the atmosphere on the radiation received at the sensor; developing data-processing techniques which would overcome the inherent variability of the data (thus enabling one to take full advantage of the large-scale view of the sensor); and devising a means for reducing the limitations on area measurement accuracy caused by the relatively coarse spatial resolution of the sensors. Each of these problems had been previously and was still being investigated by ERIM with NASA support. Candidate techniques for the solution of the latter two problems had been developed, while a radiative transfer model had been constructed to address the first.

As a part of this investigation, therefore, we undertook to utilize the available technology, to adapt it for use on the ERTS-1 MSS data, to quantify the effects of the atmosphere on those data, and to determine the effectiveness of the available advanced data processing and information extraction techniques. Sections 3, 4, and 5 of this report discuss the investigation and its results on the subjects of atmospheric effects, signature extension, and proportion estimation, respectively.

3
ATMOSPHERIC EFFECTS IN ERTS-1 DATA

The atmosphere strongly influences ERTS-1 data. For example, the lesser contrasts in ERTS Band 4 images, as compared with those in ERTS Band 5, are in part due to the greater influence of the atmosphere in the shorter-wavelength channel. Differences in atmospheric conditions within a given frame or between frames can change the spectra of received radiances, thereby hampering image-interpretation efforts and degrading recognition processing and other information extraction with computers.

In this section, the major factors which determine atmospheric effects in ERTS data are discussed and illustrated with sample calculations. Methods of correcting data for atmospheric effects are discussed primarily in Section 4.

3.1 GENERAL DESCRIPTION OF ATMOSPHERIC EFFECTS

The basic equation for the total radiance received at a sensor is:

$$L_{Total} = \underbrace{L_0 T}_{= \text{Beam}} + \underbrace{L_p}_{= \text{Path}} \tag{1}$$

where L_0 is the radiance at the surface of the target material

T is the transmittance of the atmosphere between the target and the sensor

L_p is the path radiance

The product $L_0 T$ is sometimes called the "beam radiance" because it represents the direct beam of radiation from the target which reaches the sensor after attenuation by the atmosphere. Path radiance is extraneous radiance that does not come from the target; it is scattered by atmospheric constituents into the receiving beam of the sensor, either directly from the sun or after reflection from background materials.

All quantities in Eq. (1) depend on characteristics of the atmosphere and on viewing conditions. For satellite-sensed radiation, for instance, transmittance (T) depends on τ_0 (the optical thickness of the atmosphere), θ (the angle of scan from nadir), and λ (the wavelength of interest). Path radiance depends on these parameters as well as on θ_0 (the solar zenith angle), ϕ (the relative azimuth angle between the solar plane and the view plane), ρ_B (the background albedo), t (the time of year), and the atmospheric state. The surface radiance of the target may be expressed in simplified form as:

$$L_0 = E_0\left(\frac{1}{\pi}\right)\rho \tag{2}$$

where E_0, the irradiance at the surface, depends on τ_0, λ, θ_0, ρ_B, t, and the atmospheric state, and ρ is the diffuse reflectance of the target. In more complex situations, the target reflectance depends on the solar and viewing geometries.

Atmospheric effects are difficult to measure, especially for satellite sensors. Radiative transfer models provide a mechanism for predicting the effects of the atmosphere on ERTS signals and exploring the sensitivity of these effects to changes in the various parameters that determine them.

A radiative transfer model has been developed by Dr. Robert Turner at ERIM [1-6] under the sponsorship of NASA.* This model and calculations made with it were used under this contract to study atmospheric effects in ERTS data. The model is a practical one in the sense that

*NASA Contracts NAS9-9784 and NAS9-14123 under the Supporting Research and Technology (SR&T) Program of the Earth Observations Division, Johnson Space Center, Houston, Texas.

it uses very little computer time as compared to other models based upon more involved mathematical procedures. All types of atmospheric conditions can be represented, from heavy hazes with a visual range of 2 km to the pure Rayleigh atmosphere with a horizontal visual range of ~340 km. Auxiliary programs can be run to generate additional, non-standard conditions if necessary. The radiative-transfer program will compute spectral radiances, irradiances and transmittances in terms of view angles, sun angles, optical thickness, wavelength and time of year. Comparisons have been made between calculations based upon this model and those of Coulson et al. [7] for a pure Rayleigh atmosphere and also for experimental data on sky radiance. In all cases the agreement is very good with significant deviations occurring only for large sun angles ($\theta_0 \gtrsim 80^0$). The main assumptions in the model as developed so far are: (1) Lambertian surface; (2) uniform density of the medium in the horizontal plane; (3) a spatially uniform background surface; and (4) no gaseous absorption. Additional details are presented in Appendix A.

3.2 EFFECTS OF OPTICAL THICKNESS OF THE ATMOSPHERE

At the wavelengths under consideration, the optical thickness of the atmosphere is the most important factor in predicting or estimating atmospheric effects in ERTS data. Optical thickness (and the altitude profile of optical depth) is the basic parameter in the Turner radiative-transfer model. It is desirable to have measurements of optical thickness for analysis of specific data sets. But, in the absence of specific measurements and for system-related parametric calculations, one can resort to values for standard atmospheric profiles. The Turner model incorporates characteristics for a series of standard atmospheres, described by Elterman [8], each of which is associated with a specific horizontal visual range.

There are two competing atmospheric effects on remotely sensed radiation. Atmospheric attenuation of radiation emanating from the surface tends to reduce the magnitude of sensed radiation, whereas scattering (and/or emission) from atmospheric constituents produces the additive path radiance term.

Figure 1 illustrates the dependence of both total spectral radiance and path radiance at a satellite on the amount of atmospheric haze present, as denoted by the visual range of standard atmospheres. This figure is for a long wavelength of 0.95 μm (ERTS Band 7) where atmospheric effects are less than for shorter wavelengths, but a fairly substantial path-radiance contribution is evident. Note that, depending on the surface albedo, the radiance received from a 32% reflector may either increase or decrease as the visual range decreases (amount of haze increases).

The spectral dependence of path radiance is illustrated in Figure 2. The amount of path radiance is several times greater at 0.55 μm than at 0.95 μm. The relative magnitudes of total and path radiance at 0.55 μm can be seen in Figure 3. (The dependence of these quantities on surface reflectance is discussed later.)

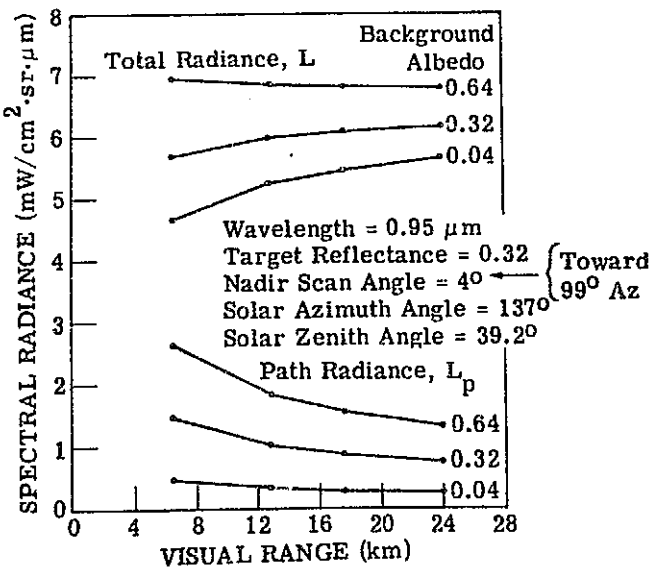

FIGURE 1. DEPENDENCE OF RADIANCE AT SATELLITE ON VISUAL RANGE, 0.95 μm [9]

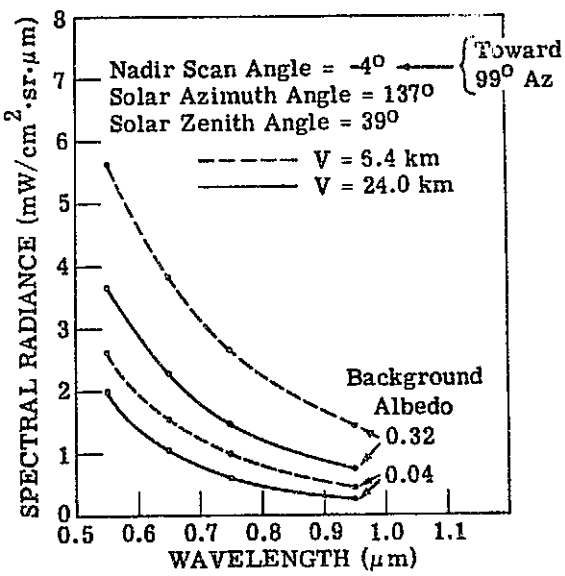

FIGURE 2. SPECTRAL DEPENDENCE OF PATH RADIANCE [9]

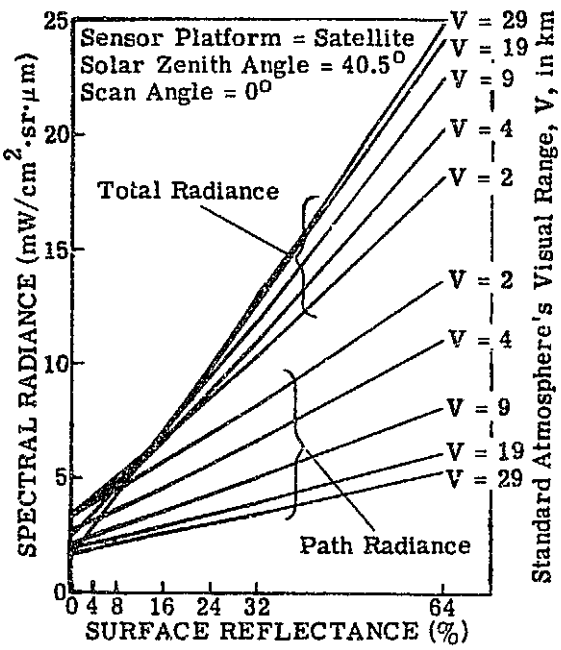

FIGURE 3. DEPENDENCE OF 0.55 μm RADIANCES ON SURFACE REFLECTANCE

An alternative display of the information in Figure 3 is presented in Figure 4, where total radiance is plotted versus path radiance. As before, the path radiance is greatest for the haziest atmosphere.

The pattern of Figure 4 is found at longer wavelengths as well. Figure 5 shows that path radiance is still a significant contributor to total radiance at 0.75 μm.

3.3 EFFECTS OF BACKGROUND ALBEDO

A striking feature in Figure 3 is the cross-over of total radiance lines for the different amounts of haze, when the surface reflectance is varied (the observed target and surrounding background reflectances were made equal and the view angle taken normal to the surface for this graph). The implication is that there is a surface reflectance value at which the sensed radiance is essentially independent of the amount of haze present in the atmosphere. For reflectances smaller than this cross-over value, the radiance for a hazy atmosphere is greater than that for a clear one, while the opposite is true for surface reflectances greater than the cross-over value. The cross-over effect is observed in Figure 4 as a change in sign of the slope of those primarily horizontal lines which denote different background reflectance values.

The cross-over effect was observed in calculations for longer wavelengths as well (see, for example, the results in Figure 5 for 0.75 μm). Interestingly, the cross-over region was for surface reflectances between 10 and 12% at wavelengths of 0.55, 0.65, 0.75, and 0.95 μm under the conditions considered. It is not known what patterns would result from calculations for different sun positions.

The strong dependence of path radiance on the albedo of background surfaces, as evidenced in the figures discussed above, is also noteworthy. Background albedo can be as large a factor as haze content (visual range) in determining the path radiance contributions.

3.4 EFFECTS ON SUN ANGLE (AND LATITUDE) ON ERTS DATA

ERTS passes over the continental United States in a few minutes' time on each orbit. The sun's position relative to any one point on the Earth's surface does not change appreciably during that time, but there are substantial changes in the local solar zenith angle at points along the satellite ground track. These in turn cause noticeable changes in total and path radiance quantities. We here include some calculations and discussion, generated by Dr. Turner under the aforementioned SR&T program [6], to provide a more complete description in this report of atmospheric effects in ERTS data.

Calculations of beam radiance (L_0T in Eq. 1) and path radiance were made for simulated passes of ERTS from north to south across the western part of the United States during mid-morning hours on a clear day. Results are presented in Figure 6 for summer (21 June 1973)

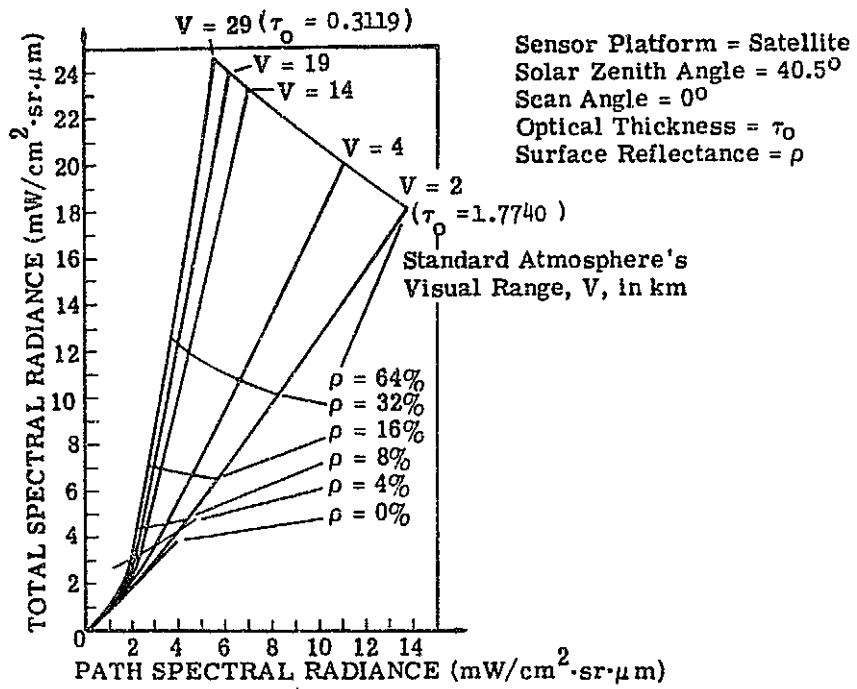

FIGURE 4. INTERDEPENDENCE OF 0.55 μm RADIANCES FOR DIFFERING ATMOSPHERIC HAZE AND SURFACE REFLECTANCE

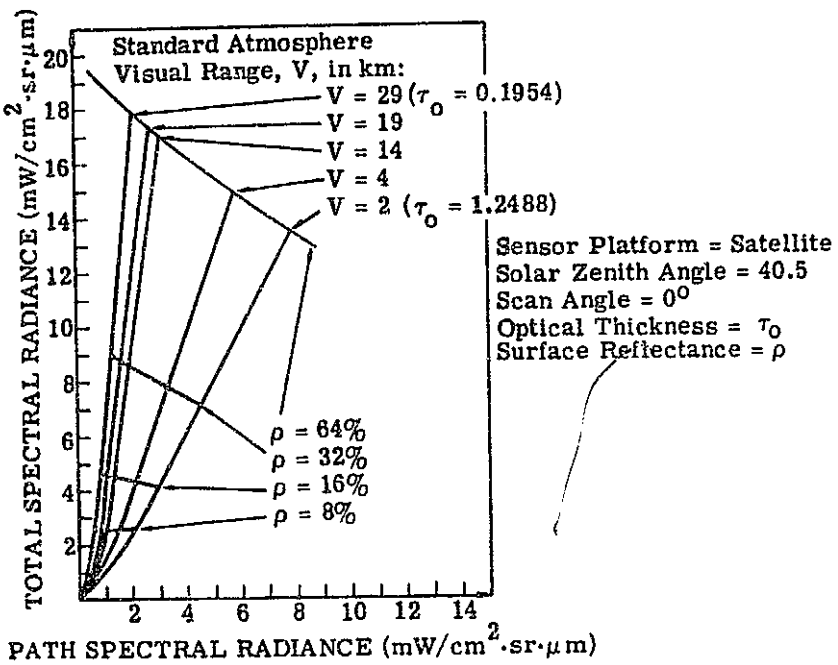

FIGURE 5. INTERDEPENDENCE OF 0.75 μm RADIANCES FOR DIFFERING ATMOSPHERIC HAZE AND SURFACE REFLECTANCE

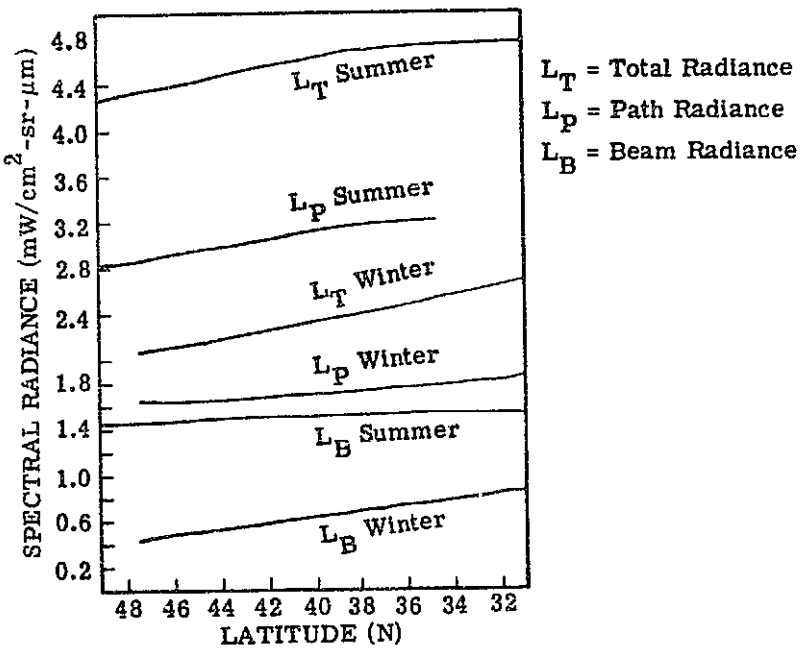

FIGURE 6. SPECTRAL RADIANCES FOR SIMULATED ERTS PASSES. Wavelength = 0.55 μm; visual range = 23 km; reflectance = 0.05.

and winter (18 December 1973) passes. A minor but not negligible effect in the calculations is a 6 to 7% increase in exo-atmospheric solar irradiance from winter to summer, a change caused by variations in the Earth-Sun distance.

The major effect on radiances is the change in solar zenith angle as a function of latitude. As the latitude decreases the angle between the nadir view angle and the solar zenith angle decreases, resulting in a higher backward scattering of radiation and therefore an increase in path radiance. The effect is more pronounced in summer than in winter because the angle is smaller.

A question arises: should one correct the satellite data by a simple multiplicative operation using the sun angle? The answer is that it would be advisable to use another correction procedure because the additive path radiance term, a major component of the total radiance, is a rather complicated function of sun angle. For a Lambertian surface we can define an intrinsic radiance L_I which is the radiance the surface would exhibit in the absence of the atmosphere:

$$L_I = \frac{\rho}{\pi} \mu_o E_s \tag{3}$$

where ρ is the target reflectance, μ_o is the cosine of the solar zenith angle, and E_s is the extra-terrestrial solar irradiance at the top of Earth's atmosphere.

Figure 7 illustrates the variation in the ratio of the radiances to the intrinsic radiance as a function of latitude for a 5% surface reflectance. It can be seen that the ratio L_B/L_I is almost constant. It is the path radiance term that has a strong solar-angle variation, introducing a corresponding variation in total radiance which would not be sufficiently corrected by a simple multiplicative operation. The problem is much more severe for winter than for summer, and the trends of the L_T/L_I curves on Figure 7 have opposite slopes for the two seasons. The curves would be flatter at longer wavelengths where the path radiance comprises a smaller fraction of the total radiance.

3.5 EFFECTS OF SCAN ANGLE

Scan angle is another observation parameter. Large "scan-angle effects" often have been observed in airborne MSS data where scan angles much larger than the $\pm 6^o$ of ERTS are employed. While one would not necessarily expect to find them to be of significance in ERTS data, indications are that they can be.

The lengths of observation paths through the atmosphere are longer for off-nadir scan angles than for nadir. The corresponding lower transmission of radiation tends to reduce signals received from off-nadir angles. An opposite effect is caused by scattering (and emission) in the atmosphere which adds extraneous path radiance to received signals. The relative balance

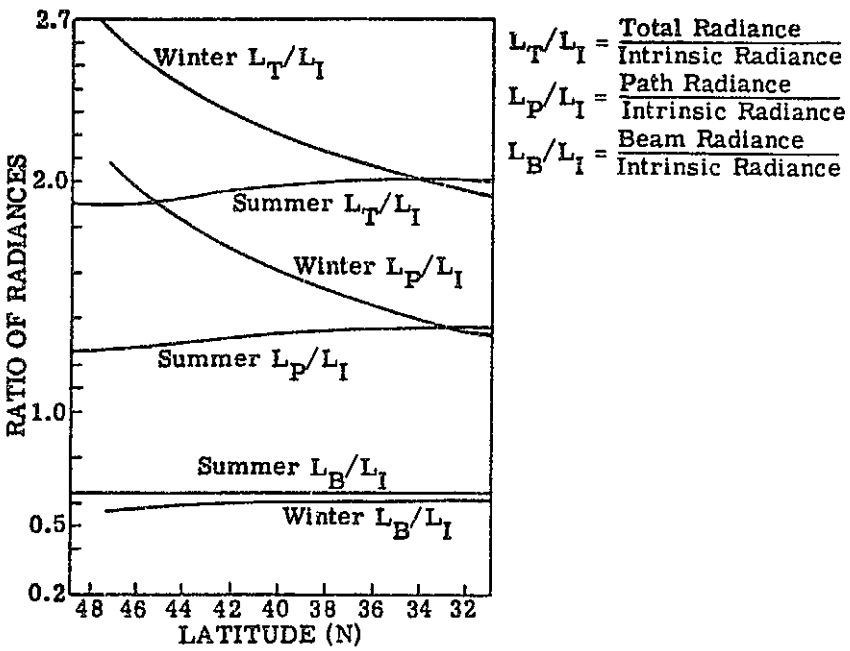

FIGURE 7. RADIANCE RATIOS FOR SIMULATED ERTS PASSES.
Wavelength = 0.55 μm; visual range = 23 km; reflectance = 0.05.

between these two opposite effects depends on the direction of scan relative to the sun's position. Path radiance usually dominates when the scanner looks away from the sun, while the transmittance effect usually is greater when the scanner looks toward the sun's azimuth. In addition to these atmospheric scan angle effects, there can be bidirectional reflectance effects in the surface materials observed.

Figure 8 illustrates the scan-angle dependence of 0.55 μm total and path radiances on a clear day. The variations, due to atmosphere alone, are as much as 8% of the minimum value of total radiance for an 8% diffuse reflector. Percentage variations in path radiance are even greater. The curves in Figure 8 are for different background albedos. Figure 9 presents a graph for which visual range was the parameter varied to obtain different curves of radiance for a fixed (8%) background albedo. Note that the visual range has little effect on total radiance for scan angles toward the sun but does affect it for angles away from the sun.

Calculations for slightly different clear-day conditions were made and are presented in Table 1. Percentage changes are calculated for wavelengths of 0.55 μm and 0.75 μm and $\pm 6^{\circ}$ off-nadir scan angles. Again, path radiance changes are large, and percentage changes in total radiance are significant even though they are 1/2 to 1/3 of the path radiance changes. For instance, there would be a 10% change in 0.55 μm total radiance across an ERTS frame and over 6% in 0.75 μm total radiance.

3.6 ESTIMATES OF VISUAL RANGE

It was noted earlier that optical thickness, the key parameter in radiative transfer calculations, could be approximated by standard atmospheres tagged by visual ranges for some applications. Airports regularly determine and report visibility conditions, so we explored the possible use of these readings from stations scattered throughout an ERTS frame (1033-15580, 25 August 1972) over southwestern Michigan. ERTS signals from water bodies located near these stations were extracted, analyzed, and compared with predictions of signals made using the Turner model and the airport visual range readings.

The reflectance of water is essentially zero in ERTS Band 7, very low in Band 6, and a few percent in Bands 4 and 5 where it depends somewhat on the depth and turbidity of the water and the bottom color. Therefore, we believe that clear open-water signal levels in Bands 6 and 7 well represent path radiance and, in Bands 4 and 5, are still largely due to path radiance.

Calculations were made with the radiative transfer model for the sun angle, scan angle, and visual range that existed for each of the five stations. A zero reflectance surface was assumed for water in Bands 6 and 7 and a 5% reflectance surface was assumed for Bands 4 and 5. The computed spectral radiances for three different background albedos are listed in Table 2. The right-hand column gives the maximum variation between stations, as a percentage of the

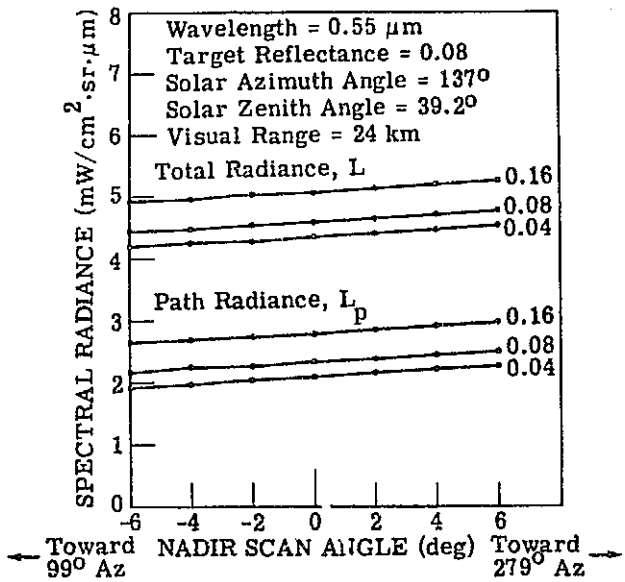

FIGURE 8. DEPENDENCE OF RADIANCE AT SATELLITE ON SCAN ANGLE, 0.55 μm

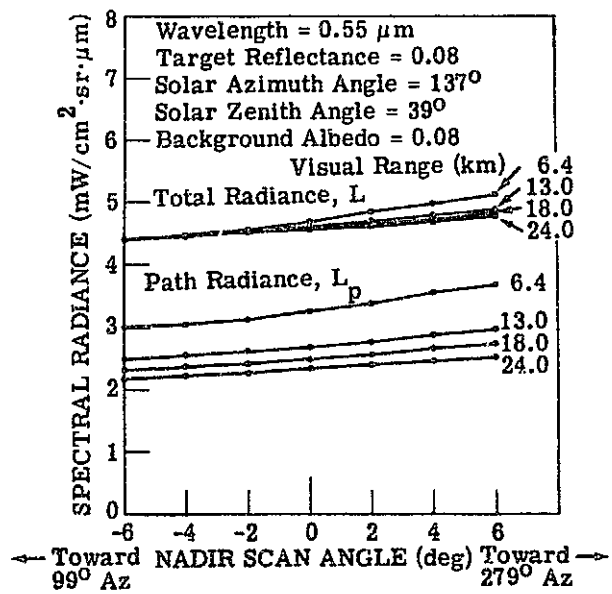

FIGURE 9. COMBINED SCAN-ANGLE AND VISUAL-RANGE EFFECTS ON RADIANCE AT SATELLITE, 0.55 μm

TABLE 1. SCAN ANGLE EFFECTS ATTRIBUTABLE TO THE ATMOSPHERE

Azimuth Relative to Sun (ϕ)	Scan Angle Relative to Nadir (θ)	Spectral Radiances* ($mW/cm^2 \cdot sr \cdot \mu m$) $\lambda = 0.55\ \mu m$ Path	$\lambda = 0.55\ \mu m$ Total	$\lambda = 0.75\ \mu m$ Path	$\lambda = 0.75\ \mu m$ Total	Percent Change from Nadir ($\theta = 0^o$) Value $\lambda = 0.55\ \mu m$ Path	$\lambda = 0.55\ \mu m$ Total	$\lambda = 0.75\ \mu m$ Path	$\lambda = 0.75\ \mu m$ Total
38^o	(-) 6^o	2.51	4.70	0.98	2.78	-7.3	-4.2	-7.2	-2.8
	0^o	2.71	4.90	1.06	2.86	0	0	0	0
218^o	6^o	2.98	5.17	1.17	2.96	10.2	5.5	10.1	3.7

Percent Change from One Side of Nadir to Other

Scan Angle Change	$\lambda = 0.55\ \mu m$ Path	$\lambda = 0.55\ \mu m$ Total	$\lambda = 0.75\ \mu m$ Path	$\lambda = 0.75\ \mu m$ Total
-6^o to $+6^o$	18.9	10.1	18.7	6.6

*Target Reflectance = Background Albedo = 8%
Solar Zenith Angle = 39^o
Optical Thickness of Atmosphere = 0.3812 for 0.55 μm and 0.2854 for 0.75 μm.

TABLE 2. MODEL CALCULATIONS OF TOTAL SPECTRAL RADIANCE AT SATELLITE FROM LOCATIONS THROUGHOUT FRAME 1033-15580

WAVELENGTH	TARGET REFLECTANCE	BACKGROUND ALBEDO	COMPUTED SPECTRAL RADIANCE AT VARIOUS REPORTING STATIONS ($mW/cm^2 \cdot Sr \cdot \mu m$)					MAXIMUM VARIATION ACROSS FRAME
λ	ρ_T	ρ_B	MUSKEGON	GRAND RAPIDS	KALAMAZOO	BATTLE CREEK	LANSING	Max-Min / Min
(μm)								(%)
.55	.05	.05	3.786	3.545	3.674	3.531	3.462	9.3
		.10	4.172	3.837	4.151	3.945	3.857	8.7
		.20	4.960	4.430	5.123	4.789	4.661	15.6
.65	.05	.05	2.640	2.514	2.600	2.517	2.485	6.2
		.10	2.926	2.726	2.962	2.825	2.777	8.6
		.20	3.506	3.153	3.694	3.449	3.368	17.1
.75	0	.10	1.074	0.815	1.222	1.045	0.981	49.9
		.30	1.907	1.417	2.290	1.943	1.831	61.6
		.50	2.759	2.030	3.386	2.863	2.700	66.8
.95	0	.10	0.509	0.370	0.607	0.506	0.474	64.0
		.30	0.988	0.716	1.223	1.022	0.963	70.8
		.50	1.474	1.065	1.851	1.546	1.459	73.8
REPORTING VISIBILITY (ST. MILES) @ 11 a.m. 8/25/72			8+	15	5*(Haze)	7	8	

*12 NOON REPORT SINCE NONE AVAILABLE @ 11 a.m.

minimum value for the given albedo. The variation ranges from 6 to 17% in Bands 4 and 5 and from 50 to 74% in Bands 6 and 7. Thus, it is seen that appreciable differences can exist due to atmospheric effects.

Empirical values in Bands 5 and 7 from lakes near four of the reporting stations are plotted versus location along a transect from Muskegon to Kalamazoo to Lansing (see Figure 10, parts (a) and (b) respectively). Also on the figures are corresponding computed values extracted from Table 2. The agreement between the shapes of the theoretical and empirical plots is striking. The one departure is the Band 7 value extracted from Reed Lake near Grand Rapids. This is a small lake; we are uncertain of its condition, and it was used only because no larger lakes exist nearby. The differences in magnitude between the two types of data are not fully understood, but are influenced by the particular target reflectance and/or background albedo selected for calculation and plotting and the radiance calibration of the ERTS data.

From the foregoing, it would appear that a radiative transfer model and surface visual range estimates can be used to predict the general shape of variation that is present in ERTS data throughout a scene. However, further analysis and examples should be used for confirmation and to resolve the differences found between magnitudes of calculated and empirical radiances.

A word of caution is in order regarding the use of National Weather Service visibility estimates. Aside from the fact that they indicate only ground-level conditions, depend upon the experience of the observer, and may not adequately characterize the entire atmospheric path, one must also understand the reporting procedures and be familiar with the visibility markers available at the stations of interest. Private conversations with NWS personnel have produced the following information: Seven miles is considered to be unlimited visibility as far as NWS and flight controllers are concerned; longer ranges depend on the reporting station having suitable markers at longer distances. The NWS observation manual states that "When the prevailing visibility is more than seven miles and is also estimated to be more than twice the distance to the most distant marker visible, encode the visibility as twice the distance to that marker, rounded to the nearest reportable value, or seven miles which ever is the greater, and if the visibility is estimated to be greater than the coded value, add a plus." Therefore, even on an exceptionally clear day a station with restricted view (e.g., because of trees and terrain) and an absence of suitable markers might never report a visibility greater than seven miles, while another might have suitable markers at 30 miles or more distance and report corresponding values. In sum, ground visibility readings can provide useful information for analysis of ERTS data, but one can be misled if restrictions on the reporting stations are not known and considered.

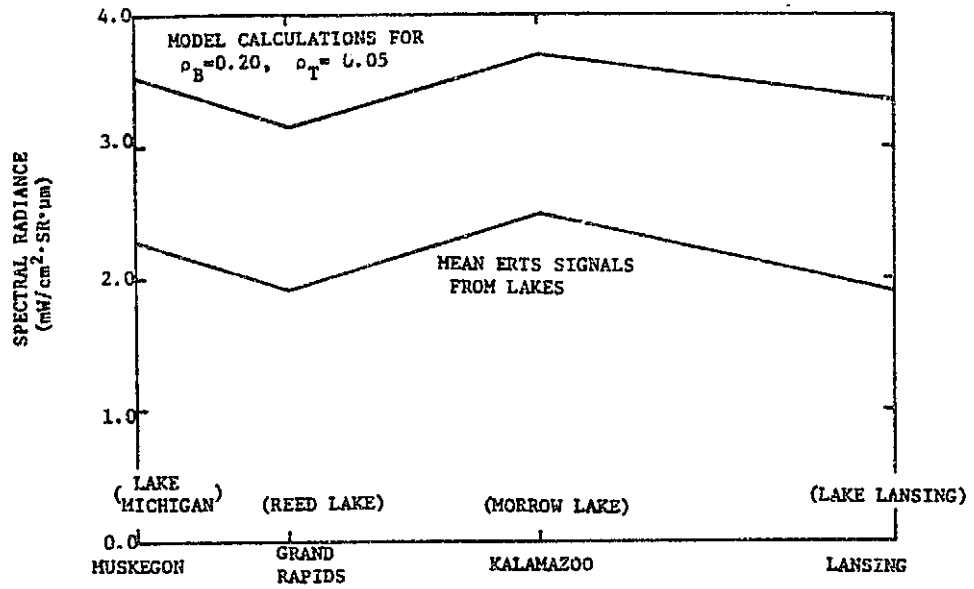

(a) Muskegon to Lansing Transect (λ_c = 0.65 μm)

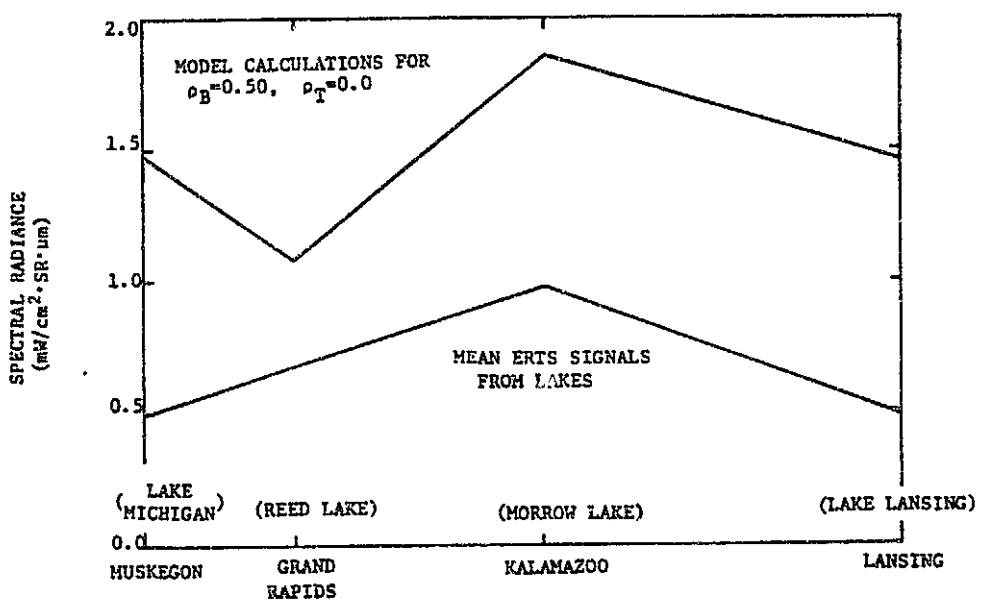

(b) Muskegon to Lansing Transect (λ_c = 0.95 μm)

FIGURE 10. COMPARISON OF MODEL CALCULATIONS WITH RADIANCES EXTRACTED FROM ERTS DATA FOR WATER BODIES

3.7 UNCERTAINTIES IN ASSOCIATING OPTICAL THICKNESSES WITH VISUAL RANGE READINGS

The preferred method for obtaining detailed information on atmospheric effects for a given location is to measure the optical thickness directly. The reason is that one may have the same horizontal visual range at ground level and still experience considerable variation in optical thickness due to varying altitude profiles of atmospheric constituents. R. Turner has made calculations of the sensitivity of total radiance to such profile differences. One set of calculations is presented here for completeness of the discussion [6].

At each of several visual ranges, the optical thickness from the standard atmosphere was adjusted by ±15% and ±50% of the optical thickness associated with aerosol scattering to obtain new profiles. Total radiances calculated for these different profiles are presented in Figure 11 for 0.55 μm; corresponding path radiances are presented in Figure 12. These profiles correspond to one- and two-standard-deviation variations of the profiles averaged by Elterman to obtain the standard atmospheres used in the model. These results quantitatively indicate a limitation that should be kept in mind when horizontal visual range estimates are used to characterize atmospheres.

The model results discussed to this point have been for scattering, non-absorbing atmospheres only. Investigators are also examining the effects of absorption by aerosols (Turner, [5 and 6]) and by water vapor (Pitts, et al., [10]). Water vapor absorption primarily affects ERTS Band 7, while aerosol absorption affects all bands, especially the shorter wavelengths.

3.8 EMPIRICAL METHODS FOR ESTIMATING ATMOSPHERIC EFFECTS

There are empirical methods that have been used to estimate atmospheric effects in ERTS data. One of these involves "darkest object" location. The water signal analysis discussed in Section 3.6 is an example of this procedure.

One scans through the data to locate the darkest objects separately in each spectral band. These objects may be surface water which has nearly zero reflectance in ERTS Band 7; in other bands dark soil, shadowed areas, or some other dark material may be used. These signals primarily represent path radiance, because the direct beam radiance from the surface is very low. Corrections based on such darkest-object signals can be made to reduce atmospheric effects in the ERTS data.

Application of another empirical procedure, which uses analysis of data clusters in two or more different areas, is discussed in the context of preprocessing for signature extension in Section 4. Both multiplicative and additive correction factors are determined and applied to transform one data set to the equivalent atmospheric state of another, which is then used for training the recognition processor.

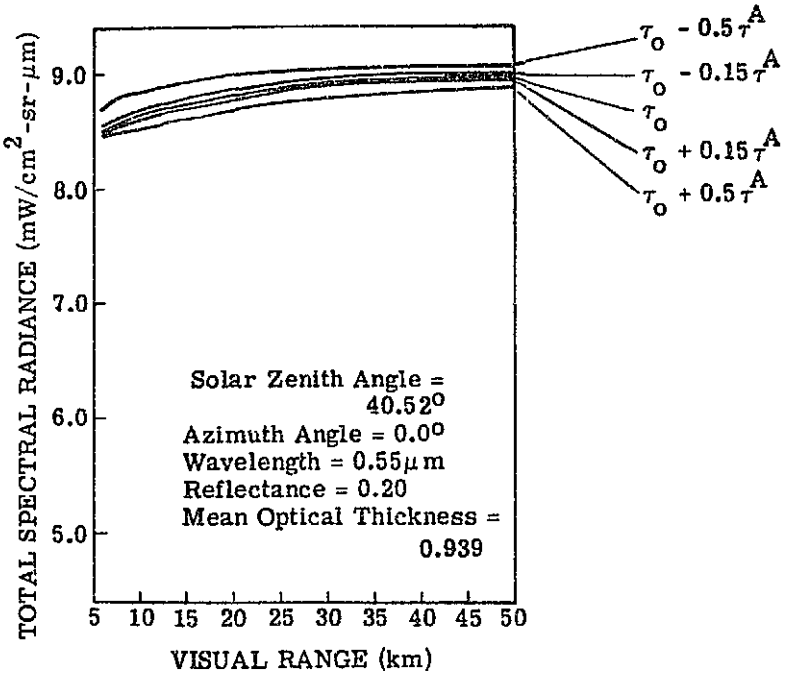

FIGURE 11. DEPENDENCE OF TOTAL SPECTRAL RADIANCE ON VISUAL RANGE FOR VARIOUS ATMOSPHERIC PROFILES

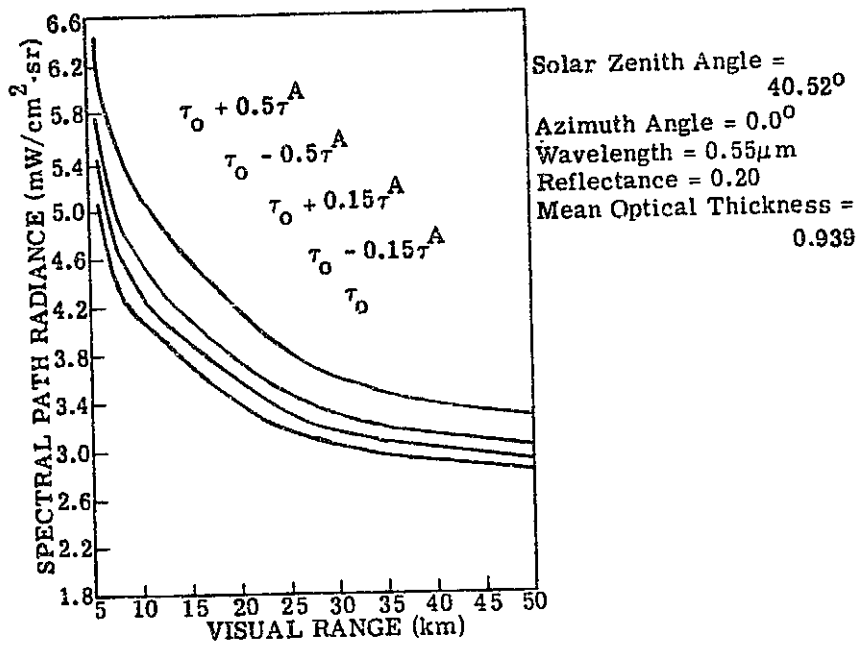

FIGURE 12. DEPENDENCE OF PATH RADIANCE ON VISUAL RANGE FOR VARIOUS ATMOSPHERIC PROFILES

In a study aimed at obtaining quantitative information on atmospheric effects, the ERIM multispectral scanner was flown on a series of multialtitude passes in synchronism with the ERTS-1 pass on 25 August 1972. Reflectance panels were placed on the flight line. Airborne signals from large fields, resolvable in ERTS data, were compared to signals from the reflectance panels and equivalent reflectance values, called secondary standards, were assigned to these fields. Average values were then extracted from ERTS data for each of the secondary standards and converted to radiances. (The maximum radiance values listed in Table G.2-2, page G-14, of the ERTS Data Users Handbook were assigned to computer-compatible-tape levels 127, 127, 127 and 63 for ERTS Bands 4, 5, 6 and 7, respectively.)

Figure 13 presents plots of ERTS radiance versus target reflectance for the four ERTS bands. bands. The dashed lines are least-squares fits to the values obtained for the secondary standards. Also on the figures are trios of lines that represent approximate calculations made with the radiative transfer model for different background albedos. The visual range used for these calculations was 24 km (15 stat. mi).

The slopes of the theoretical lines and the empirical fits agree well, but the magnitudes differ in Bands 4 and 5 (especially in Band 4) for reasonable background albedos. The reason(s) for these differences is not known with certainty, but there are several possibilities. (1) The theoretical radiance values were obtained by merely multiplying band-center spectral radiances by factors of 0.1, 0.1, and 0.3 to approximate the ERTS spectral bandwidths; more detailed spectral calculations are desirable. (2) The reflectances assigned to the secondary standards for the empirical plots appear to be too low; higher values would improve agreement. (3) The model might be in error, although checks elsewhere of sky radiance predictions have shown good agreement with measurements and with exact calculations for a pure Rayleigh atmosphere. (4) The atmospheric profile used in the calculations was less hazy than the condition in the test area (24 km visual range as opposed to 13 km). (5) It is possible that the ERTS calibrations are biased or we have misinterpreted the calibration procedures. Despite the differences seen, the strong influence of the atmosphere on ERTS data has been shown in both theoretical and empirical studies.

3.9 COMPARISON OF ATMOSPHERIC EFFECTS AND OTHER SOURCES OF VARIATION IN ERTS SIGNALS

The preceding sections have shown the variation in total radiance (and, therefore, in ERTS signals) that can occur because of atmospheric effects. It is of interest to compare these with other sources of variation in ERTS signals.

One source of variation is in the differences which occur in the calibrated outputs of the six detector channels which make up each of the four ERTS spectral bands. In some instances,

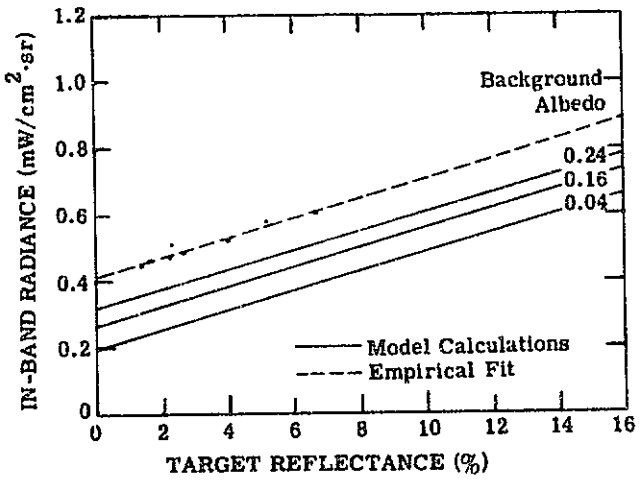

(a) ERTS Band 4 (0.5 - 0.6 μm)

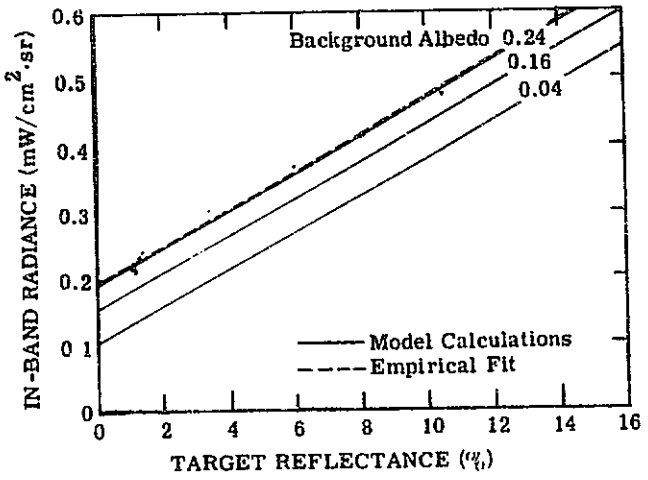

(b) ERTS Band 5 (0.6 - 0.7 μm)

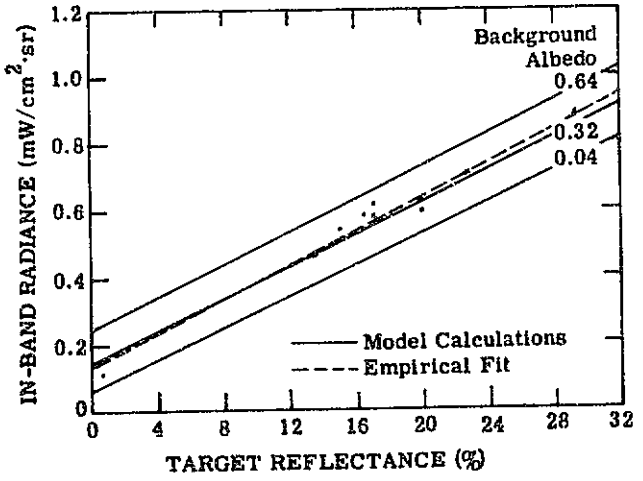

(c) ERTS Band 6 (0.7 - 0.8 μm)

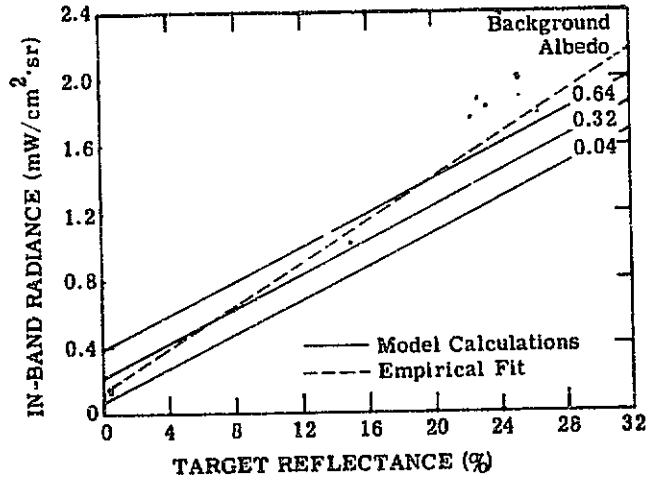

(d) ERTS Band 7 (0.8 - 1.1 μm)

FIGURE 13. COMPARISON OF EMPIRICAL AND THEORETICAL RADIANCES

these differences have been seen as striping and/or banding effects on ERTS images, sometimes referred to as "every-sixth-line effects." Even when not particularly noticeable in the ERTS images, there are detectable differences in the digital outputs on computer-compatible tapes. We possessed two digital versions of the same frame, the second having been requested because of major sixth-line problems in ERTS Band 6. Means and standard deviations of signals were computed for several thousand points from an agricultural scene, and points from every sixth line were grouped to give results for each detector channel, as presented in Table 3. The standard deviation of means varied between 0.1 and 0.6 digital counts for all but ERTS Band 6, for which it was greater. The ratio, standard deviation ÷ mean (called the coefficient of variation), was computed for each case and varied between 0.6% and 2.2% for the three best channels. These values agree with results of similar analyses of other data sets. Added to these more or less systematic variations should be the random variations associated with noise in the individual channels.

Another source of variation in the signals is the variation in reflectance of the surfaces being mapped. Signal statistics gathered for individual fields and combined to form recognition signatures include all the noise sources discussed so far. An examination of signatures generated as part of the processing discussed in Section 4 shows coefficients of variation of 3 to 1 8% or more, depending on the characteristics of the scene class under consideration.

Presumably, there would be little random variation due to the atmosphere in a localized area of an ERTS image in the absence of clouds. The question remains as to how great atmosphere-induced variations might be over a larger area, (e.g., an entire ERTS frame). Duggin [11] and others have considered the variability that could exist throughout an ERTS frame by making measurements throughout individual days and at scattered locations. In Ref. [11], coefficients of variation of 3.6 to 7.3% in irradiance were determined as indicators of atmospheric transmittance differences throughout a frame for a given set of conditions. The graphs presented earlier in this section indicate changes of this magnitude, and substantially greater can occur if the atmospheric haze levels vary appreciably from one part of the frame to another. Even without that variability, the radiative transfer model calculations have shown 6 to 10% variations in total radiance from one side of an ERTS frame to another, due solely to scan-angle effects on a relatively clear day.

Changes of the magnitude discussed herein are sufficient to cause problems in computer recognition over extended areas of ERTS frames unless corrections are applied.

3.10 CONCLUSIONS AND RECOMMENDATIONS

The effect of Earth's atmosphere on remotely sensed multispectral data is by no means simple. In this section it has been shown that a multiplicative factor involving the sun angle

TABLE 3. COMPARISON OF SIGNAL CHARACTERISTICS ON ORIGINAL CCT AND NEW CCT FOR FRAME 1033-15580

Each entry computed for 4800 points from an agricultural scene

DETECTOR	ERTS BAND 4		ERTS BAND 5		ERTS BAND 6		ERTS BAND 7	
GROUP	MEAN	STD. DEV.	MEAN	STD. DEV.	MEAN	STD. DEV.	MEAN	STD. DEV.
1 new	25.56	2.21	18.14	3.54	44.23	6.50	24.90	4.45
old	24.52	2.17	17.28	3.44	45.07	6.56	24.90	4.45
2 new	24.82	2.00	17.35	3.63	43.91	6.28	25.20	4.46
old	25.78	1.98	17.62	3.59	44.29	6.33	25.20	4.43
3 new	24.95	2.07	17.38	3.59	43.28	6.17	25.37	4.55
old	25.20	2.08	17.44	3.65	43.24	5.98	25.37	4.52
4 new	25.38	1.98	17.35	3.74	40.24	9.86	25.49	4.78
old	25.38	1.91	17.48	3.76	43.73	6.06	25.49	4.76
5 new	25.77	2.23	17.52	3.72	44.09	6.63	25.24	4.73
old	25.77	2.23	17.52	3.72	17.76	18.78	25.24	4.73
6 new	25.62	2.07	17.78	3.86	45.22	6.47	25.70	4.66
old	25.58	1.91	17.51	3.58	45.25	6.78	25.71	4.63
	New	Old	New	Old	New	Old	New	Old
Mean of Means (m)	25.35	25.37	17.59	17.48	43.50	39.89	25.32	25.32
Std. Dev. of Means (s)	0.41	0.57	0.25	0.11	1.71	10.9	0.27	0.27
Ratio, s/m	1.6%	2.2%	1.4%	0.6%	3.9%	27.2%	1.1%	1.1%

*Anomalous value due to bad detector channel, Group 5.

alone is not likely to be sufficient for the correction of space data for recognition processing over large areas. This is especially true for conditions of light haze in which multiple scattering is of lesser importance and the scattering proportions of the atmosphere depend strongly upon the anistropic character of single scattering by an aerosol particle. The resulting angular variations in the data depend upon the angle between the viewing direction and the solar beam as well as other quantities such as spatial variations in atmospheric turbidity throughout a region covered by an ERTS frame.

It also has been shown that significant changes can occur in total radiance at the satellite due to atmosphere-related scan angle effects across an ERTS frame, amounting to 5 to 10% of the total radiance on a clear day.

It has been shown that the relationship between total spectral radiance, surface reflectance and visual range is rather involved. The background surface albedo was shown to be a major determinant of path radiance, being comparable to haze content for many situations. There does appear to be a narrow range of reflectance values for which the total radiance is nearly independent of haze content.

It has been demonstrated that a measurement of horizontal visual range near the surface can be a rather poor indicator of atmospheric state and that optical thickness is a much better measure, although it is more difficult to obtain.

Variations attributable to atmospheric effects in ERTS data can be as large or larger than those due to sensor noise and surface reflectance variations within well defined classes of ground cover.

Unresolved differences were found between radiances obtained by applying the published calibration constants to ERTS-1 MSS data and those calculated with the radiative transfer model.

Finally we conclude, in conjunction with results presented in Section 4, that a signature extension algorithm can be used to correct multispectral data for variable atmospheric effects. One must be careful, however, in the specification of the relevant parameters on which signature extension transformations are based.

It is recommended that additional studies be made to further quantify the effects of atmosphere-related variability in ERTS signals on multispectral recognition. In particular, it would be desirable to relate signal changes directly to changes in recognition performance. Also, more effort should be devoted to effects of absorption by aerosols, especially for remote sensing in the vicinity of urban areas. Finally, additional effort should be expanded to verify and/or improve current radiative transfer models to make them more valuable in future studies and applications of satellite remote sensing.

4
RECOGNITION PROCESSING AND SIGNATURE EXTENSION

Computer recognition of multispectral scanner signals provides an automated method for interpretation of remote sensor data and a potential capability for conducting operational surveys of large areas. Multispectral scanner (MSS) data can be processed by computers which have been trained to recognize the spectral characteristics of various classes of ground cover found in a scene. The spectral characteristics of each ground-cover class are usually described by statistical parameters (a mean vector and a variance-covariance matrix) of the MSS signals, a description called the "recognition signature" of the class. The training of the recognition computer normally entails an extraction of signal statistics and a correlation of these with known types of ground cover in a "training" area.

Recognition carried out on data collected in the same locale as the data used for training is termed "local recognition." "Non-local recognition" occurs when areas distant in time and/or space from the training area are recognized.

When large areas are surveyed from space, there exists a high probability that environmental and observational conditions will change from day to day, frame to frame, or even within a frame. Resulting changes in signal levels received from each class of ground cover can result in degraded machine recognition performance and reduced quality of other extracted information. One way to combat such changes is to have available substantial amounts of ground-truth information from throughout the survey area; however, this can be expensive. Another way is to adjust the signatures and/or data in non-local areas to counteract the effects of the changes [12]. We use the term "signature-extension techniques" to describe methods and procedures that are used to obtain improved non-local recognition processing and, thereby, more efficient, accurate and effective area survey information.

4.1 APPROACH

There are many situations in which signature extension is required and many techniques for extending signatures. Two situations are considered in this report: (1) extension of signatures between areas on a given day and (2) extension of signatures from one day to another for the same area. Four different methods of signature extension were applied. Three of them include adjustment of signature means, based on: (1) average signal values in the two areas; (2) the time-and-space dependent characteristics of signals recognized as each of the classes (adaptive processing); and (3) theoretical calculations based on a radiative transfer (atmospheric effects) model and ground-based optical depth measurements. The fourth method performs multiplicative and additive transformations of the signature means and scales the dispersion matrices.

Three different data sets are considered in this section. The first (25 August) is over a test area in Michigan, the test site to which processing efforts on this contract were primarily devoted; the second (21 August) and third (10 and 11 June) are in neighboring states. Some results obtained at ERIM under the previously noted NASA SR&T contract are presented in addition to those obtained under this contract, to provide a more complete characterization of the potential of advanced techniques for processing ERTS data. Consequently, all techniques were not applied to each data set.

In the first part of each analysis, training procedures were used to establish signatures. Then, generally after local recognition was performed, non-local recognition without signature adjustment was performed and followed by use of one or more signature-extension techniques. Results were always obtained for field-centers, but in some instances they were obtained for full sections that contained several fields and boundaries.

4.2 DISCUSSION OF RECOGNITION AND SIGNATURE EXTENSION METHODS

Local recognition was carried out for each of the sites using the ERIM linear decision rule. With this rule [13], the distribution of signals from each signature is assumed to be multivariate normal. The signal space is partitioned by a series of linear discriminants, which implement a pairwise decision rule to decide to which class the pixel belongs. Then, a quadratic calculation is made to determine whether the observation is sufficiently likely to have come from that class to be assigned to it; if not, it is rejected and assigned to a null class. A threshold value corresponding to a 0.001 probability of false rejection was used for the results presented here. This rule has performed with accuracies comparable to conventional quadratic decision rules, with a susubstantial saving in computer time.

Non-local recognition was carried out between pairs of sites by applying the local signatures from one site to the other without any adjustment of either signatures or data. Substantial decreases in recognition accuracy from local levels were noted. After various signature extension techniques were applied, improved results were obtained.

4.2.1 SIGNATURE EXTENSION BY MEAN LEVEL ADJUSTMENT

The mean level adjustment (MLA) procedure used is one which adds constants to the means of recognition signatures from one area for use in another area. The constant is determined for each channel from the difference in average signal values of the two areas.

The MLA procedure is based on two assumptions. The first is that some overall, constant, additive change has occurred in the spectral characteristics of all classes in going from one area to the next, such as a change in atmospheric conditions affecting path radiance. The second assumption,

implicit in the procedure for computing the adjustment, is that the two areas have identical percentages of each type of ground cover present. If there is a constant difference between the two areas, this method should be able to make a good adjustment and give recognition accuracies approaching the local recognition results.

Mathematically, the procedure can be expressed as follows:

$$\hat{m}_A^i = m_B^i + \Delta_{A|B}^i \tag{4}$$

where $\hat{m}_A^i$ is the estimated signature mean for area A in channel i

m_B^i is the corresponding signature mean for area B

$\Delta_{A|B}^i$ is the mean level adjustment difference $\left(\mu_A^i - \mu_B^i\right)$, where μ_A^i and μ_B^i are averages of data values over specified portion(s) of each area.

4.2.2 SIGNATURE EXTENSION BY ADAPTIVE PROCESSING

The second signature extension method employed was adaptive processing with a decision-directed Kalman filter developed at ERIM by Dr. Robert Crane [14], following earlier work by Dr. Frank Kriegler, et al. [15]. In this method, the means of recognition signatures are adjusted in response to the signal values of pixels that are recognized as each particular class. The adjustments are small dynamic adaptations to changes in the signals from each ground cover, as opposed to the single discrete shift of MLA. This method, like the mean-level-adjustment procedure used, keeps the covariances constant as the means shift. The use of constant covariance simplifies the algorithm substantially and is not unreasonable for data sets which span a moderate amount of change in scene conditions.

The Kalman filter method of adaptive processing is a more subtle method than mean level adjustment and is more likely to improve recognition accuracies in areas where recognition does fairly well. There are several ways in which adaptive processing might be applied to a data set, depending on the nature of changes between the training area and non-local areas of interest. First, one might process data continually from the training area to the non-local area, adapting along the way. Second, one might jump directly to the non-local area and let the signatures adapt to the new conditions, provided differences are not too great. This method is used when the intervening areas differ from the training area and non-local area of interest. Third, one might proceed as with the second method, after first making an adjustment to get the signatures into a closer correspondence with the non-local area (e.g., after first performing a MLA operation). The first two methods were examined in this study.

The first way represents the optimum situation, providing the non-local areas covered are composed of the same ground covers as are found in the training area. An important condition

for successful adaptive processing is that unique signatures represent all ground covers present. A common problem to all adaptive methods is that a signature could adapt to the false alarms of a ground cover for which no signature exists and be "captured" by the other cover. A captured signature would not only give many false alarms but might adapt to such an extent that it could no longer recognize the ground cover it was meant to recognize.

There are parameters of the Kalman filter that can be adjusted between repeated processing trials. Two were varied in this investigation. θ_1 determines the updating rate, which controls the speed with which signatures are allowed to adapt. Values of θ_1 are related to the number of data points (or number of lines of fixed length) that would be processed before a signature mean approach a new value following a step change in the crop signals. θ_2 controls the interaction between the means of the various signatures.

4.2.3 SIGNATURE EXTENSION BY MULTIPLICATIVE AND ADDITIVE SIGNATURE CORRECTION (MASC)

The MASC (Multiplicative and Additive Signature Correction) algorithm for signature extension was recently developed at ERIM by Dr. Robert Henderson [16] under the previously identified SR&T contract. With this algorithm, a signature correction transformation is determined for extending signatures from one site to another. The transformation applies both a multiplicative and an additive correction term to each signature to more accurately reflect changes that occur between data sets than is possible with a simple additive correction. For example, the MASC correction for transforming signature means of one crop from one site, W, for use in another site, F, is:

$$\hat{m}^i_F = a^i_{F|W} m^i_W + b^i_{F|W} \tag{5}$$

where m^i_W is the mean value for the crop in channel i for area W

$a^i_{F|W}$ and $b^i_{F|W}$ are the multiplicative and additive correction coefficients, respectively, for transforming W signatures to F conditions

$\hat{m}^i_F$ is the adjusted signature mean value in channel i for use in area F

The factors $\left\{a^i_{F|W}\right\}$ are also used to scale the signature variance-covariance matrices.

While the transformation coefficients $\{a^i, b^i\}$ could be determined from radiometric and atmospheric measurements made in the two sites at the time of data collection, such measurements are not usually taken. Alternatively, these coefficients can be based on the results of unsupervised pixel-by-pixel data clustering procedures in the two sites of interest. The clusters are paired between sites and used in conjunction with a linear regression program which computes the coefficients. It is not necessary to identify the ground cover classes associated with

the various clusters, because they are paired according to their relative signal values. Furthermore, it is not necessary that the proportions of the cover classes be the same, although ideally the same cover classes should be present in both sites.

4.2.4 SIGNATURE EXTENSION BY ATMOSPHERIC CORRECTION

Given information on the differing atmospheric states and viewing geometries of two data sets, one can use a radiative transfer model to compute differences in path radiances and transmittance for use in signature corrections. For the data set considered in this report, photometer readings were available with which to compute optical thicknesses for the atmosphere on two days over the same site.

4.3 RECOGNITION OF DIFFERENT AREAS ON SAME DAY

Recognition capabilities were analyzed for two data sets with three of the four signature extension techniques. The analyses of these two data sets are presented and discussed separately, beginning with the 25 August set and ending with the 21 August set.

4.3.1 DATA SET FROM 25 AUGUST 1972

Recognition results obtained with the various procedures are presented, following descriptions of the ERTS data set, ground truth, training procedures, and a special procedure developed for pixel selection.

4.3.1.1 Data and Ground Truth Descriptions

The major data set for this contract was collected by ERTS-1 on 25 August 1972 over Eaton, Ionia, and Clinton Counties in Michigan (Frame 1033-15580). These counties are in the vicinity of Lansing, Michigan, and the test sites are primarily agricultural in nature. The primary test site was a 3 × 11 km (2 × 7 mile) area in Eaton County, Michigan, in which extensive field observations had been made. Ground-truth information also was available for the surrounding area and in Clinton and Ionia Counties, through Agricultural Stabilization and Conservation Service (ASCS) Records, photointerpretation of low-altitude aerial photography (collected on the same day as the ERTS pass by the ERIM C-47 aircraft) and high-altitude aerial photography (collected on 15 September 1972 by the NASA RB-57 aircraft). Areas 3 × 3 km (2 ×2 mile) in size were analyzed in Clinton and Ionia Counties.

The above sites and data were used in common with another ERTS-1 investigation (MMC-321, NAS5-21834, Michigan State University (MSU), East Lansing, Michigan) in which ERIM participated as a subcontractor, carrying out recognition processing and analysis. Most of the ground truth information was provided by MSU. Both local recognition and non-local recognition without signature extension techniques were carried out cooperatively between the two contracts and have been reported earlier [17, 18], but are summarized in this report for comparison with

signature extension results. Also, a procedure for correlating ERTS MSS pixels (picture elements) with analysis areas specified on aerial photographs and/or topographic maps for use both in training and in evaluating recognition results was developed under joint support of the two contracts (see Section 4.3.1.3). The problem is partly due to the size of ERTS resolution elements. The fields in the sites are relatively small in terms of the number of ERTS pixels that can be found that represent resolution elements entirely within field boundaries. Yet they are typical of those in much of the country, so this procedure should be useful for many other investigations.

The ERTS-1 MSS data for 25 August were found to have anomalous values in every sixth line of Band 6, so Band 6 was omitted from our recognition processing of those data.

4.3.1.2 Training Procedures

Training for local recognition of the 2 × 7 mile area in Eaton County was performed by extracting signal statistics from 58 of the largest fields in the ground-truth area (some outside the _ × 7 mile area) and analyzing them with a signature clustering procedure. Based on this analysis and knowledge of the crops present, statistics for 23 of the fields were combined into 12 recognition signatures for the five major classes of ground cover: corn, soybeans, trees, bare soil, and senescent (or senescing) cover. The last category included field beans, alfalfa, and grasses. Later, for both adaptive processing and the proportion estimation processing discussed in Section 5, groups of these 12 signatures were combined to form fewer signatures to represent the major classes.

Training for local recognition in Ionia and Clinton Counties were somewhat different from that in Eaton County, because of differences in ground truth and crop types present. Whereas the species of most fields in Eaton County were identified, many fields in the Ionia-Clinton site were called "senescent vegetation" by the photointerpreters. Field beans, for example, were not noted as being present in Ionia-Clinton, although they were one of the prominent crops in the Eaton site. A seven-signature set was defined for the five major classes in the Ionia-Clinton site, using a representative sample of the available fields in each class. In contrast to the Eaton site, small fields were used as well as large ones; half of all fields in a class, up to a maximum of ten, were used to form the recognition signature.

4.3.1.3 Pixel Selection

Recognition results were evaluated both for field-center pixels only and for larger areas that contained many fields, the boundaries between them, and roads and farmsteads. In the early stages of selecting field-center pixels, it was found that purely manual techniques were inadequate and inconsistent. Therefore, the previously mentioned computer-assisted procedure for selecting and assigning pixels to specific fields was developed. Details of the procedure are presented

in Refs. [19-21]. In brief, the procedure utilizes an empirical map transformation derived by least squares calculations from a local network of control points in and around the area of interest. This transformation is used to warp Earth coordinates to match ERTS coordinates, effectively computing the location of each pixel, so pixel assignments are made without any movement or interpolation of ERTS data values. Another feature of the procedure is a capability to define inset distances away from polygonal boundaries of fields so as to exclude boundary pixels which represent more than one type of surface cover.

4.3.1.4 Results for Local Recognition and Non-Local Recognition Without Signature Extension

Results for local recognition and non-local recognition without signature extension are presented for comparison with the signature extension results discussed in succeeding sections. The local results were generated cooperatively with the previously mentioned Michigan State University ERTS-1 contract.

4.3.1.5 Recognition Results for Signature Extension by Mean Level Adjustment

In Section 4.2.1, two assumptions of the MLA procedure are listed. The validity of these assumptions was checked on the 25 August data set. Then recognition results were obtained both for field centers and for full sections.

Check of Assumptions. Of the two assumptions, the second, that percentages of ground covers are identical in the areas used to determine the adjustments, was easily checked with the aid of complete ground truth for both areas. Table 4 gives the ground truth percentages for four of the major ground covers in the areas used to compute two different mean level adjustments. These four ground covers have roughly the same proportions in the two sites but account for only half of the total area, the rest consisting mainly of senescing vegetaion, brush, home sites and urban areas. Considering these other ground cover types, the two areas differ in that the Ionia-Clinton 2×4 mile area includes part of the village of Westphalia while the Eaton 2×7 mile area is bisected by the Thornapple River with its brushy, tree-lined banks. Because the two areas do not meet the ideal of identical proportions of the various ground covers, cover percentages were calculated twice. The first set of percentages (MLA-I) is based on all the sections in the two areas; and there is fairly close agreement for the ground covers shown, with the exception of trees. The second set of ground truth percentages displayed in Table 4 (MLA-II) was calculated by omitting those sections which contributed to the differences between the two areas. In Clinton County, the section containing the village of Westphalia was omitted from the calculations. In Eaton County, two sections through which the Thornapple River passes, and an exceptionally brushy section were excluded. These deletions gave closer agreement

TABLE 4. PERCENTAGES OF VARIOUS GROUND COVERS IN AREAS USED TO COMPUTE MEAN LEVEL ADJUSTMENTS

	Percentages In Areas Used For Mean Level Adjustment I		Percentages In Areas Used For Mean Level Adjustment II	
Ground Cover	Eaton County*	Ionia-Clinton Counties**	Eaton County†	Ionia-Clinton Counties‡
Corn	28	30	31	30
Soybeans	5	5	5	4
Trees	10	6	6	7
Bare Soil	8	10	10	10
Total	54	51	52	51

*2 × 7 mi area

**2 × 4 mi area

† Excludes brushy sections

‡ Excludes urban area

between the percentages for all ground covers except soybeans. The overall percentages were also improved.

Regarding the assumption of some overall, constant difference, it can be noted that on 25 August 1972 there was a frontal weather system passing through Michigan; parts of the area covered by the ERTS frame were cloud covered. Airport visibility readings varied throughout the frame which suggests that, although neither the Eaton or Ionia-Clinton area were cloud covered, there could well have been a difference in atmospheric conditions over the two areas.

The average signal values for the Ionia-Clinton and Eaton County areas are shown in Table 5. The values were higher in the Ionia-Clinton area for all three channels. The differences, Δ_i, between the signal values of the two areas (Ionia-Clinton minus Eaton) were added to each of the Eaton recognition signatures means and subtracted from the Ionia-Clinton recognition signature means. The two adjusted signatures sets created in this way were then used for non-local recognition.

To study how sensitive the mean level adjustment method is to differences in the ground cover composition of two areas, average signal values were recalculated, omitting those areas which were known to contribute to the differing percentages in the two areas. The new average signal values for the Ionia-Clinton area (Table 6) are almost identical to those in the previous table. The absence of the village did not alter the average values for any channel, because there were a substantial number of dark trees within and near the village, which offset the brighter signals from homes and roads of the village in the first two bands.

The averages did change, however, in Eaton County when the brushy areas were omitted from the calculations, so the adjustments between the two areas depend on which sections are used to compute the average signal values. The differences, Δ_i, in Table 6 are slightly lower than those calculated using all sections for Bands 4 and 5 but are higher for Band 7. These changes are consistent with a lower proportion of healthy green vegetation in the remaining Eaton sections. Adjusted signatures based on either or both of these tables should give better results for non-local recognition that unadjusted signatures, but it would be expected that local signatures would give the best recognition results.

Field Center Recognition Results with Mean Level Adjustments. Non-local recognition results obtained for field centers in the two areas using two different sets of mean-level-adjusted signatures are summarized* in Table 7. Percentages of correct recognition of field-center

*More results are presented later in this section, and Appendix B contains complete recognition performance matrices.

TABLE 5. AVERAGE SIGNAL VALUES USED TO COMPUTE MEAN LEVEL ADJUSTMENT I

Band	Average Signal: Ionia-Clinton*	Average Signal: Eaton**	Difference (Δ_i)
4	26.89	25.38	1.52
5	19.09	17.53	1.56
6	Not Used		
7	26.62	25.39	1.23

*2 × 4 mi area

**2 × 7 mi area

TABLE 6. AVERAGE SIGNAL VALUES USED TO COMPUTE MEAN LEVEL ADJUSTMENT II

Band	Average Signal: Ionia-Clinton*	Average Signal: Eaton**	Difference (Δ_i)
4	26.90	25.45	1.45
5	19.10	17.68	1.42
6	Not Used		
7	26.62	25.25	1.36

*Excludes urban area (Westphalia 5)

**Excludes brushy sections (Benton 6, Chester 12, and Roxand 24)

TABLE 7. NON-LOCAL AND LOCAL RECOGNITION RESULTS SHOWING EFFECTS OF USING MEAN-LEVEL-ADJUSTED SIGNATURES

	Percent Correct Recognition for Various Signature Sets							
	Eaton County Area				Ionia-Clinton Area			
Signatures: / True Class	Ionia-Clinton	I-C MLA-I	I-C MLA-II	Local	Eaton	Eaton MLA-I	Eaton MLA-II	Local
Corn	57.0	64.2	64.9	77.0	57.3	61.3	67.0	77.4
Soybeans	66.7	74.5	74.5	88.2	92.6	88.9	88.9	85.2
Trees	93.3	73.3	76.0	88.0	55.3	91.5	89.4	87.2
Bare soil	80.6	77.8	75.0	97.2	100.0	86.3	88.7	94.3
Senescent	61.6	86.8	86.0	78.3	64.0	55.0	59.2	76.5
Ave. over points	63.1	72.9	73.1	79.9	64.4	64.0	68.1	79.4
Ave. over plots	63.3	78.1	78.4	78.5	64.1	60.1	63.9	75.6

pixels are given for five classes, as well as overall percentages averaged both over pixels and over plots (defined field centers). Overall local recognition accuracies were approximately 80% in both areas, but non-local recognition accuracies with non-adjusted signatures fell to 63 to 64%.

Both mean level signature adjustments improved overall non-local recognition results by about 10% for Ionia-Clinton signatures in the Eaton area. Improvements were not as great in the Ionia-Clinton area, being only +4% for MLA-II and slightly negative for MLA-I. As just discussed, MLA-I was based on signal averages over all sections while, for MLA-II, sections containing scene cover types that were not common to both were excluded.

Upon examining the results for the individual ground covers, it is apparent that they do not mirror the overall results. The trend for each of the ground covers is the same in most cases for both adjusted signature sets, and the following remarks apply for either set, except when otherwise noted.

In both areas, mean level adjustment improved corn recognition, although the recognition results are still reduced as compared to local recognition results.

Soybeans and bare soil were well recognized in the Ionia-Clinton area regardless of the signature set used. In fact, bare soil recognition is best for the unadjusted Eaton County signature set. Soybeans and bare soil were not as well recognized using non-local signatures in the Eaton County area as they were in the Ionia-Clinton area. Both sets of adjusted Ionia-Clinton signatures porduced an 8% increase in soybean recognition, compared to that with unadjusted signatures, but bare soil recognition decreased slightly, with the second set of adjusted signatures giving the lowest recognition accuracy. Local signatures gave the best results for both ground covers.

In the Ionia-Clinton area, approximately 90% of the trees were recognized with adjusted Eaton signatures. This accuracy is slightly greater than the local recognition result of 87% and much greater than the 55% obtained for non-local recognition with unadjusted signatures. Local recognition accuracy for trees in Eaton County was as high as that in the Ionia-Clinton area but the unadjusted non-local signatures gave higher results than did local signatures. Use of the adjusted signatures resulted in reduced recognition accuracies.

For the senescent cover class, the Eaton County area had a higher recognition accuracy with adjusted signatures than with either unadjusted non-local or local signatures. On the other hand, the Ionia-Clinton area had lower recognition accuracy with the adjusted signatures than with unadjusted non-local signatures. In each area, non-local signatures gave a reduced recognition accuracy compared to local signatures.

Tables 8 and 9 give information about two ways of evaluating incorrectly recognized pixels. (See Appendix B for complete tables of recognition results.) Missed detections refer to those pixels of a ground cover which are not recognized by its signature. False alarms are those pixels which are recognized by a particular signature class but do not belong to that class.

Table 8 indicates which classes account for 10% or more of the missed detections of each other class. In the Ionia-Clinton area, ≥10% of corn pixels were misclassified as senescent cover by all signature sets; corn pixels also were misclassified as trees by the two adjusted signature sets. In Eaton County, the senescent cover signatures were responsible for missed corn detections by all of the signature sets except the unadjusted non-local. In this area, corn was also misclassified as trees by the unadjusted non-local and the local signature sets. Soybean missed detections never reached the 10% level for any signature class in the Ionia-Clinton area, but in Eaton County ≥10% of soybeans were misclassified as a senescent cover by all signature sets except the local set. Trees tended to be recognized as corn by the Eaton County signature sets in all cases, but trees never had a significant number of missed detections when an Ionia-Clinton signature set was used. Bare soil was misclassified as senescent cover when mean-level-adjusted signature sets were used in either area and by the unadjusted non-local signature set in Eaton County. In the Ionia-Clinton area, the senescent cover class was misclassified as soybeans and bare soil for all signature sets and also was misclassified as corn when the first mean-level-adjusted signature set was used. In Eaton County, only the unadjusted non-local signature set had a significant amount of the senescent cover class misclassified as corn.

The false alarms, displayed in Table 9, are expressed as percentages of the total number of field-center pixels evaluated for each area. Corn signatures have relatively low percentages of false alarms, all well below 5% except the unadjusted non-local signature set in Eaton County (7.4%). Both soybeans and bare soil signatures always gave very low percentages of false alarms in Eaton County, but they display differing patterns in the Ionia-Clinton area. Here, bare soil continues to have a relatively low false alarm rate ranging from 1.3% for the local signatures to 5.3% for the unadjusted non-local set. The soybean signature retains a low (4.4%) false alarm rate with the local signatures, but the non-local signature sets have higher percentages ranging from 7.0 to 8.6%.

The tree signatures produced highly variable false alarms. For the Ionia-Clinton area, the local and the unadjusted non-local signatures have low percentages of false alarms in Table 9. The same is true for both mean level adjusted signature sets in Eaton County; but the adjusted sets in the Ionia-Clinton area have high false alarms rates, 11.8% for I and 8.9% for II. The local Eaton County signature set has 5.6% false alarms, but the non-local set incorrectly recognized over 20% of the total number of pixels as trees.

TABLE 8. SIGNATURE CLASSES ACCOUNTING FOR 10% OR MORE OF THE MISSED DETECTIONS OF ANOTHER GROUND COVER CLASS

	Eaton County Area				Ionia-Clinton Area			
Signatures: / True Class	Ionia-Clinton	I-C MLA-I	I-C MLA-II	Eaton	Eaton	Eaton MLA-I	Eaton MLA-II	Ionia-Clinton
Corn	T	V	V	T,V	V	T,V	T,V	V
Soybeans	V	V	V	-	-	-	-	-
Trees	-	C	C	C	C	-	-	-
Bare soil	V	V	V	-	-	V	V	-
Senescent	C	-	-	-	S,B	C,S,B	S,B	S

Key: C = Corn, S = Soybeans, T = Trees, B = Bare soil, V = Senescent vegetation

TABLE 9. FALSE ALARMS FOR EACH RECOGNITION CLASS, EXPRESSED AS PERCENTAGE OF ALL FIELD-CENTER PIXELS IN AREA

	Eaton County Area				Ionia-Clinton Area			
Signatures: / Recognition Class	Ionia-Clinton	I-C MLA-I	I-C MLA-II	Eaton	Eaton	Eaton MLA-1	Eaton MLA-II	Ionia-Clinton
Corn	7.4	2.0	2.1	3.6	2.9	4.4	3.4	2.3
Soybeans	0.8	0.9	0.9	1.4	8.2	8.6	7.0	4.4
Trees	20.4	2.9	1.6	5.6	0.1	11.8	8.9	3.7
Bare soil	0.9	1.5	1.5	2.1	5.3	3.8	3.8	1.3
Senescent	3.3	19.6	17.8	6.6	18.9	6.6	6.6	7.5

In comparison to the other ground cover classes, the senescent cover class consistently has fairly high numbers of false alarms. The percentages range from 6.6% for both mean-level-adjusted signatures to 18.9% for the unadjusted non-local signatures in the Ionia-Clinton area. The local set has 7.5% false alarms. In Eaton County, the non-local signature set has the lowest percentage of false alarms (3.6%) for the senescent cover class, while the local signature set has 6.6%. Both of the mean level adjusted signature sets have high percentages of false alarms for senescent covers, 19.6% for I and 17.8% for II.

Full-Section Recognition Results With Mean Level Adjustments. Recognition results for the MLA procedures were also tabulated for full sections, and the proportion of each class in each section was calculated. Table 10 gives both ground truth proportions and proportion estimates obtained by using the local, the unadjusted non-local, and the first MLA recognition signature sets. These results are based on all the pixels in each section, including boundary pixels, farmsteads and roads, not just on field-center pixels. The ground truth proportion of the senescent covers was not calculated in the Eaton County area and is, thus, omitted from Table 10. Composite proportions and the RMS error are also presented for each ground cover in both areas. The method used for calculating the RMS error is indicated in a footnote of Table 10.

As would be expected, the local recognition proportions generally come closest to the ground truth proportions for both areas and have the lowest RMS error. Mean-level-adjustment results appear to be slightly better than non-adjusted results. The direction of the errors in the estimates for both non-local signature sets tend to be the opposite for the two areas; for example, the bare soil estimates are higher than the ground truth proportions in the Ionia-Clinton area and lower Eaton County.

4.3.1.6 Recognition Results for Signature Extension by Adaptive Processing

Eaton County recognition signatures were used with adaptive processing to determine if non-local recognition accuracies in the Ionia-Clinton area could be improved. In an attempt to avoid possible problems with signature capture, a seven-signature set was formed from the 12 signatures by combining redundant ground cover signatures.

Approach. Our first adaptive processing with the combined Eaton signatures in the Ionia-Clinton area was started locally in the Eaton County area and continued to and through the Ionia-Clinton area.

In a second application, processsing with the Eaton County signatures began directly in the Ionia-Clinton area. The second method was used because the interval between the two areas included part of the Looking Glass River and large tracts of brushy and uncultivated land. Because there were no distinct signatures for these types of ground cover, it was believed that

Table 10. FULL-SECTION RECOGNITION RESULTS FOR THE EATON AND IONIA/CLINTON AREAS

	CORN				TREES				BARE SOIL				SOYBEANS				SENESC. VEG.			
SECTION	GT	LR	NLR	MLA	GT	LR	NLR	MLA	GT	LR	NLR	MLA	GT	LR	NLR	MLA	GT	LR	NLR	MLA
EATON CO.																				
019	24	19	29	9	6	4	13	2	5	8	2	2	16	14	11	11		54	44	75
030	32	31	38	20	8	8	6	6	11	8	8	10	3	2	2	2		51	28	58
031	20	20	29	15	14	9	18	8	18	19	12	14	1	3	2	2		49	36	59
R24	12	22	24	13	14	9	16	8	8	16	8	7	15	14	13	12		40	35	55
R25	33	29	36	22	0	2	10	1	8	6	4	4	11	15	11	11		48	36	60
R36	26	23	34	12	8	4	11	3	10	15	8	7	6	7	4	5		52	42	72
C01	18	21	28	9	3	6	13	4	4	8	2	1	6	4	4	3		61	51	81
C12	19	34	37	22	21	12	23	7	4	4	1	0	0	4	2	2		48	37	67
C13	39	33	41	31	18	12	20	9	12	10	3	3	2	1	0	0		45	32	56
C24	41	32	38	15	1	3	11	1	12	12	7	8	6	4	4	4		49	36	70
B06	42	38	27	34	7	14	35	7	4	7	3	2	0	5	2	2		36	30	53
B07	20	38	44	34	31	15	27	9	3	4	2	3	0	0	1	0		43	22	52
B18	23	27	26	21	10	8	18	3	3	10	4	3	0	1	1	0		54	48	70
B19	41	38	35	20	4	4	18	2	3	4	2	2	2	2	4	3		52	41	72
COMPOSITE EATON	28	29	33	20	10	8	18	5	8	9	5	5	5	5	4	4		49	37	64
RMS ERROR**		7.9	10.8	12.7		6.1	10.2	8.2		3.4	3.8	3.6		2.4	2.1	2.1				
IONIA CO.																				
P1	25	20	17	21	3	5	2	11	12	8	19	13	6	8	10	11	47	57	43	51
P2	24	21	13	20	3	2	0	6	20	15	35	26	0	3	5	6	50	54	41	46
P11	42	29	23	32	5	5	1	13	7	4	14	9	0	1	5	5	43	59	38	55
P12	28	23	17	21	6	7	3	15	5	5	15	12	5	8	12	12	51	52	53	40
CLINTON CO.																				
W5	26	21	10	24	5	2	1	16	6	5	26	12	9	5	7	7	42	61	41	56
W6	32	28	25	18	8	7	2	5	14	10	21	18	7	7	7	7	31	45	45	50
W7	30	23	20	22	15	10	0	16	6	5	19	11	7	3	3	5	36	55	52	45
COMPOSITE IONIA-CLINTON	30	24	18	23	6	6	2	12	10	7	21	14	5	5	7	8	43	55	52	42
RMS ERROR		6.7	12.4	8.0		2.4	6.7	7.1		3.1	12.2	4.9		2.8	4.4	4.5		13.6	10.9	10.0

*GT = GROUND TRUTH MLA = MEAN LEVEL ADJUSTMENT OF NON-LOCAL SIGNATURES
LR = LOCAL RECOGNITION NLR = NON-LOCAL RECOGNITION WITHOUT ADJUSTMENT

** $\text{Error}_{\text{RMS/CROP}} = \sqrt{\frac{1}{N}\sum_{i=1}^{N}(p_i - \hat{p}_i)^2}$ p_i=Ground Truth Proportion $\hat{p}_i$=Recognized Proportion

N=No. of Sections

signature capture might be a problem while processing through this interval between the two areas. The potential for this problem was increased because, although one area was due north of the other, the non-north-south track of the ERTS satellite required a widening of the range of data points processed on each scan line. Thus substantial areas for which ground truth was not available, and which did not necessarily have the same composition as the areas of interest, were included. As a control for use in the analysis of results, the Ionia-Clinton signatures were used as starting signatures for local adaptive processing in the Ionia-Clinton area.

While processing with the Kalman filter, different values were used on repeated trials for two of its parameters, θ_1 and θ_2. Three different values of the update parameter θ_1 were used, corresponding to approximately 60, 190, and 600 lines. (The total area processed was ~550 lines.) Signature capture becomes more likely the more rapidly updating occurs. The slower the updating rate, the less the signatures change, until eventually the point is reached where no changes occur.

The signature interaction parameter, θ_2, is usually set at zero so that the signatures may adapt with complete independence with respect to one another. Since attempts at altering θ_2 gave greatly decreased recognition accuracies, only results with θ_2 set at zero are reported. For a complete discussion of the Kalman filter method of adaptive processing see Ref. [13].

Field-Center Recognition Results with Adaptive Processing. Recognition results for adaptive processing with a Kalman filter are presented in Table 11 for three values of the update parameter θ_1. Results are for the Ionia-Clinton area with (a) adaptation of the Ionia-Clinton signatures, (b) adaptation of Eaton County signatures within the Ionia-Clinton area only, and (c) adaptation of the Eaton County signatures, starting in Eaton County, continuing through the interval separating the two areas and through the Ionia-Clinton area itself. Table 12 gives the number of false alarms for each ground cover class and each variation of adaptive processing used. The number of unclassified pixels is listed beneath the false alarms so that the total is the total number of pixels which were not correctly identified. A table giving signatures primarily responsible for missed detections is not included for adaptive processing because the missed detections are essentially the same as for non-local recognition with unadjusted signatures (Table 8): the various adaptation parameters did affect the percentages of pixels assigned to the various categories.

The best recognition results were obtained with an updating rate which requires ~190 lines to come close to the new value of the signature mean after an abrupt change. Adaptation at this rate gave a slight improvement when the Ionia-Clinton signatures were used. When Eaton County signatures were adapted within only the Ionia-Clinton area, recognition results were greatly improved as compared to the unadapted. However, much of this improvement is due to the correct classification of pixels which were unclassified by the unadapted signatures.

TABLE 11. ADAPTIVE RECOGNITION RESULTS. Correct recognition in Ionia-Clinton field centers (%).

	Ionia-Clinton Signatures				Eaton Signatures					
					Adapted Only Within the Ionia-Clinton Area				Adapted from Eaton County	
	Adaptive Update Interval (Lines)				Adaptive Update Interval (Lines)				Adaptive Update Interval (Lines)	
True Class	Unadapted*	~600	~190	~60	Unadapted*	~600	~190	~60	~190	~60
Corn	77.4	77.8	78.1	75.4	64.0	64.0	64.0	51.2	45.5	7.1
Soybeans	85.2	85.2	85.2	85.2	85.2	85.2	85.2	85.2	85.2	66.7
Trees	87.2	87.2	87.2	89.4	51.1	51.1	51.1	44.7	44.7	19.1
Bare soil	94.3	94.3	94.3	92.5	100.0	100.0	100.0	100.0	100.0	100.0
Senescent	76.5	77.7	77.7	77.3	51.9	82.3	83.1	80.4	80.8	78.8
Av. Over Points	79.4	80.0	80.1	78.8	62.1	73.7	74.0	67.0	64.6	44.7
Av. Over Plots	75.6	77.1	77.3	76.0	60.2	71.4	71.7	67.2	65.4	47.7

*Conventional Recognition

TABLE 12. FALSE ALARMS WITH ADAPTIVE PROCESSING FALSE ALARMS
(No. of pixels)

Recognition Class	No. of True Pixels in Class	Ionia-Clinton Signatures				Eaton Signatures					
						Adapted Only Within the Ionia-Clinton Area				Adapted from Eaton County	
		Adaptive Update Interval (Lines)				Adaptive Update Interval (Lines)				Adaptive Update Interval (Lines)	
		Unadapted*	~600	~190	~60	Unadapted*	~600	~190	~60	~190	~60
Corn	297	16	17	17	16	22	22	20	23	23	19
Soybeans	27	30	30	30	32	13	13	13	13	12	7
Trees	47	25	24	24	35	1	1	1	0	0	0
Bare soil	53	9	15	15	14	32	32	32	39	39	49
Senescent	260	51	51	50	48	111	112	112	151	168	303
Unclassified		10				80					
Total		141	137	136	145	259	180	178	226	242	378

*Conventional Recognition

The adaptive processing method classified all pixels. When the Eaton County signatures were adapted beginning in Eaton County, greatly reduced recognition accuracies resulted from the fastest update rate (update interval of 60 lines). Apparently the signatures of the senescent cover class shifted so that they captured much of the corn and almost all of the tree pixels. The other update interval used (190 lines) gave a result slightly better than the unadapted result. A slower update rate was not used, although it should have been less sensitive to the atypical scene conditions between the training area (Eaton) and the test area (Ionia-Clinton); a very long update interval would give results comparable to the unadapted recognition performance with non-local signatures.

4.3.1.7 Discussion of Results

To summarize, local recognition of field centers averaged 80% correct in both Eaton and Ionia-Clinton areas, while non-local recognition fell to 63-64% correct without the use of signature extension techniques. Mean level adjustments of signature means improved the non-local recognition performance, making up 3/5 and 1/4 of the difference between non-local and local performance in Eaton County and Ionia-Clinton Counties, respectively. Adaptive processing produced only a very slight improvement in Ionia-Clinton local recognition, but it improved non-local recognition performance substantially over that achieved with mean-level adjustment (2/3 as opposed to 1/4 of the difference between local and non-adjusted non-local performance) when adaptation started in the Ionia-Clinton area. Results were poor when adaptation started in Eaton County, apparently because of signature wander in an intervening brushy, uncultivated area.

There are some interesting differences between performance of the various techniques on individual crops in the two areas. Corn recognition was about the same in both areas for each technique. Soybean recognition was the same locally in the two areas, but decreased with non-local signatures in Eaton County while increasing in Ionia-Clinton. Patterns of recognition performance for trees, bare soil and senescent cover were quite variable and not easily generalized. If anything, when a particular technique was better than another for one crop in one area, it generally was poorer for the same crop in the other area. With MLA, soybeans, trees and bare soil were better recognized in Ionia-Clinton than in Eaton (by 10 to 20%), while recognition of the senescent cover class was 30% higher in Eaton County. The notable results of non-local adaptive processing in Ionia-Clinton were excellent performances on senescent vegetation and bare soil, but a poor performance on trees. Corn and senescent cover were the classes with the greatest number of pixels (see Table 13). Since corn recognition was similar for all techniques, performance on the senescent vegetation class had a large impact on the comparative overall performance.

TABLE 13. PERCENTAGE OF FIELD-CENTER PIXELS IDENTIFIED AS EACH GROUND COVER, ACCORDING TO AVAILABLE GROUND TRUTH

	Eaton County	Ionia-Clinton
Corn	51.4	43.4
Soybeans	5.9	3.9
Trees	8.7	6.9
Bare Soil	4.2	7.7
Senescent Cover	29.9	38.0

The results obtained in the two areas highlight the importance of the training step in multispectral recognition. Different training procedures and different numbers of signatures were used in the two areas, and they were based on ground truth data collected in different ways, as discussed in Section 4.3.1.2. The major differences lie in the ground covers comprising the senescent cover class. Because of extensive field visits, a more detailed description of ground covers was available for Eaton County than for Ionia-Clinton, for which photointerpretation provided much of the data. Four recognition signatures were used for senescent cover in Eaton County and three in Ionia-Clinton; yet, after adjustment, the Ionia-Clinton signatures performed better in Eaton County than vice versa. As will be discussed later in this section, the sizes, shapes, and locations of the signature patterns varied between sites.

Mean-Level Adjustment. To examine the premise that a constant adjustment exists for each channel which can convert the signatures from one area for accurate recognition in another area, the signature means for six classes in Eaton County were plotted in Figure 14 against those in the Ionia-Clinton area. For simplicity in plotting, a signature set which combined duplicate signature types was used for the Eaton County means. (The signatures labeled "grass" were omitted since they are basically different in the two areas, the Eaton signature being based on a single field and the Ionia-Clinton including a variety of field types.) A 45° line was also plotted as a reference. For ERTS Bands 4 and 5, the 1.4 count adjustment in means, as indicated for MLA-II in Table 6, appears to be a reasonable estimate for all ground covers except bare soil. However, mean-level-adjusted bare soil recognition was always higher than overall recognition, due in part of the fact that in Bands 4 and 5 none of the other signature means are close to that of bare soil (see Fig. 14).

The plotted signature means for Band 7 are scattered, but for four of six ground covers Eaton County signature means have higher values than the corresponding Ionia-Clinton means, even though both calculated averages indicated the opposite. The signatures for senescent vegetation and soybeans are the only two that lie on the other side of the 45° line, with that for senescent vegetation being higher. It would appear that "senescent" vegetation in Ionia-Clinton was less senescent and more healthy than that in Eaton County. No consistent, additive difference seems to exist between the two areas for Band 7. This probably accounts for the fact that recognition accuracies obtained using mean level adjusted non-local signatures did not come closer the matching the local values.

The differences in the recognition signatures from the two areas are displayed in Figure 15. For each signature, the mean and an ellipse which represents the distribution in two channels for a χ^2 value of 1 are plotted; plots are presented for Bands 5 vs 7 and 4 vs 7. The Eaton County plots, Figures 15(a) and (c), show 12 signatures: two corn, two trees, two soybeans, two bare soil, two field beans, one grass and one alfalfa. Figures 15(b) and (d) display the seven

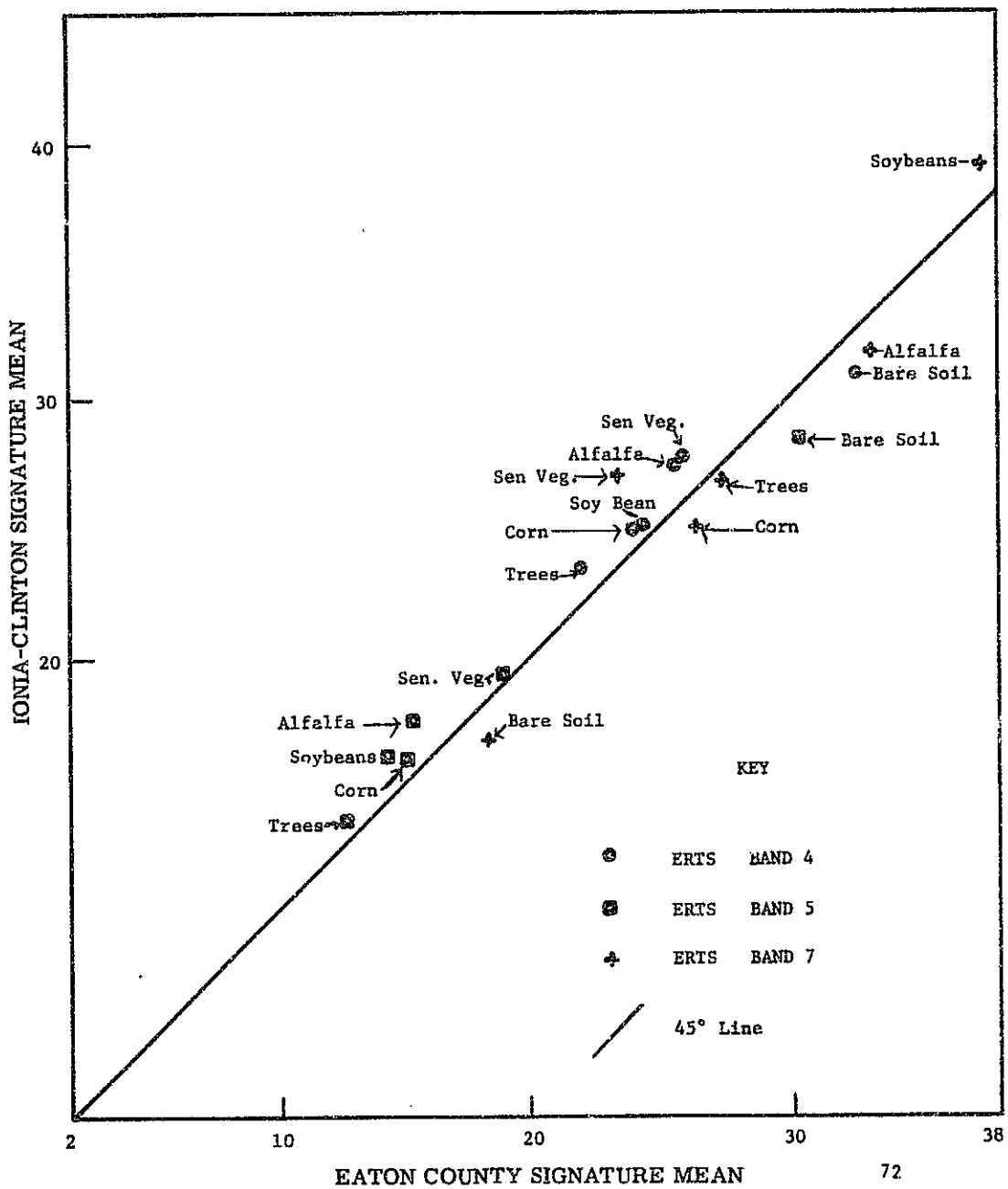

FIGURE 14. PLOT OF GROUND COVER SIGNATURE MEANS, EATON COUNTY VS IONIA-CLINTON COUNTY

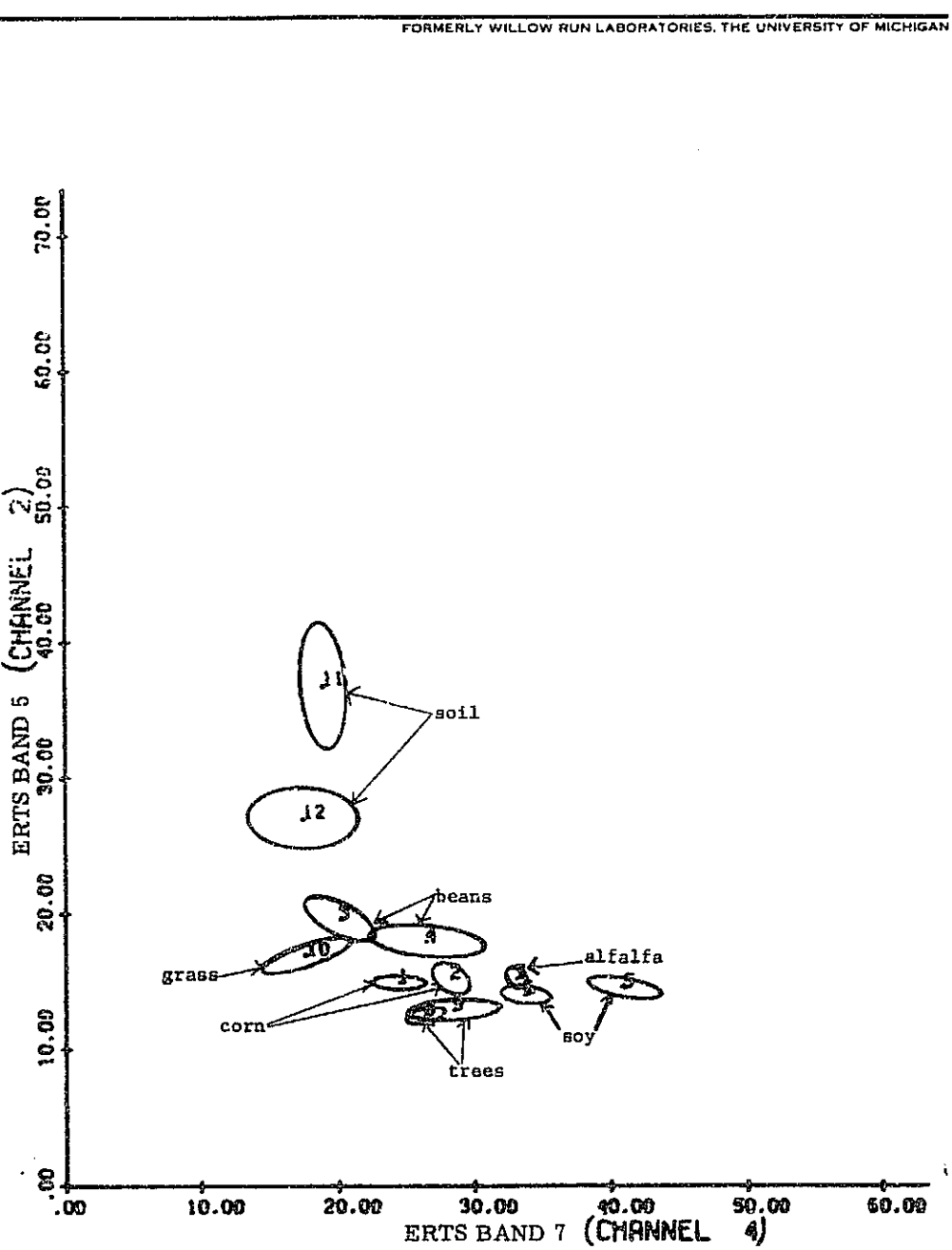

PLOT NUMBER 002 800557 9682 17 SEP 1974

(a) ERTS Band 5 vs Band 7, Eaton County Signatures

FIGURE 15. ELLIPSE PLOTS OF RECOGNITION SIGNATURES (Continued)

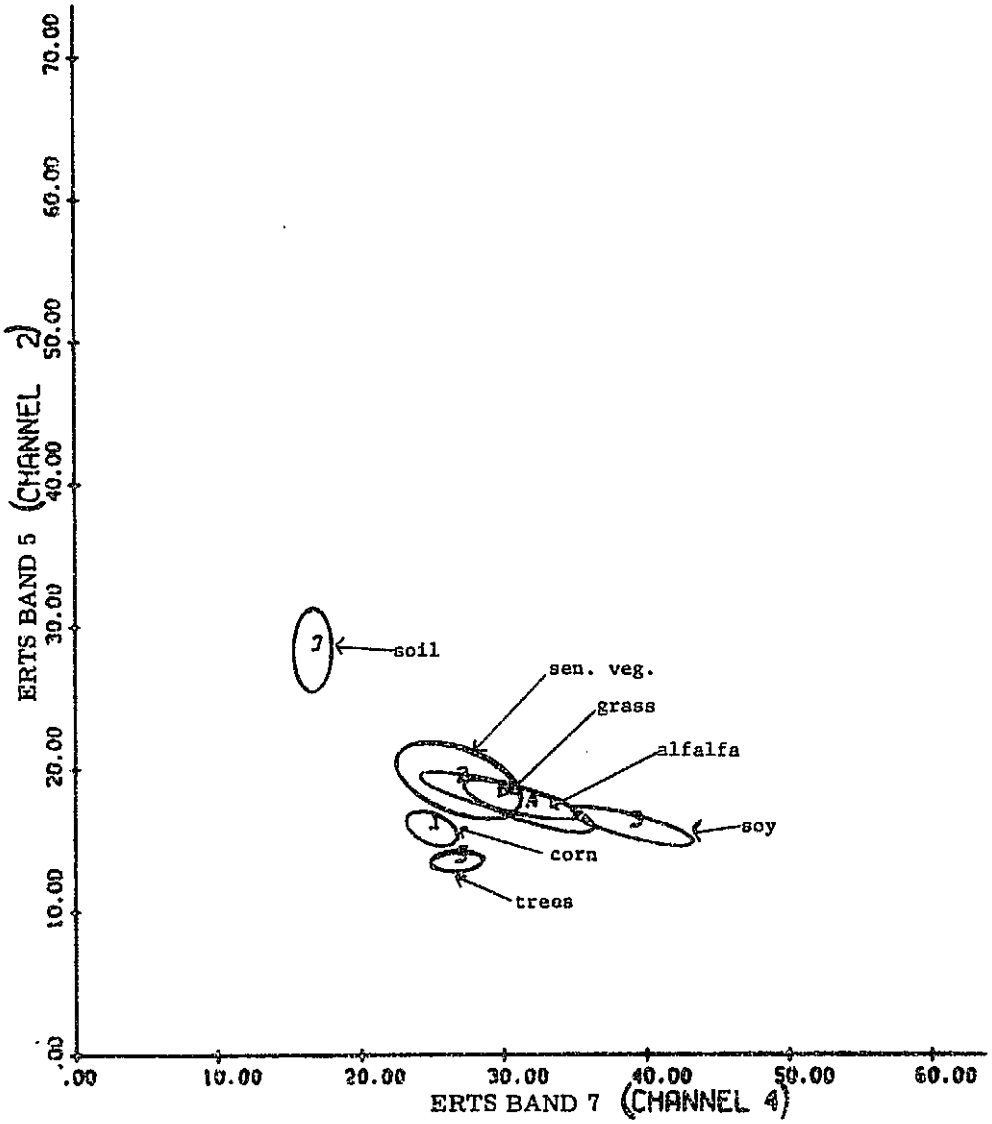

PLOT NUMBER 044 800567 S682 17 SEP 1974

(b) ERTS Band 5 vs Band 7, Ionia-Clinton Signatures

FIGURE 15. ELLIPSE PLOTS OF RECOGNITION SIGNATURES (Continued)

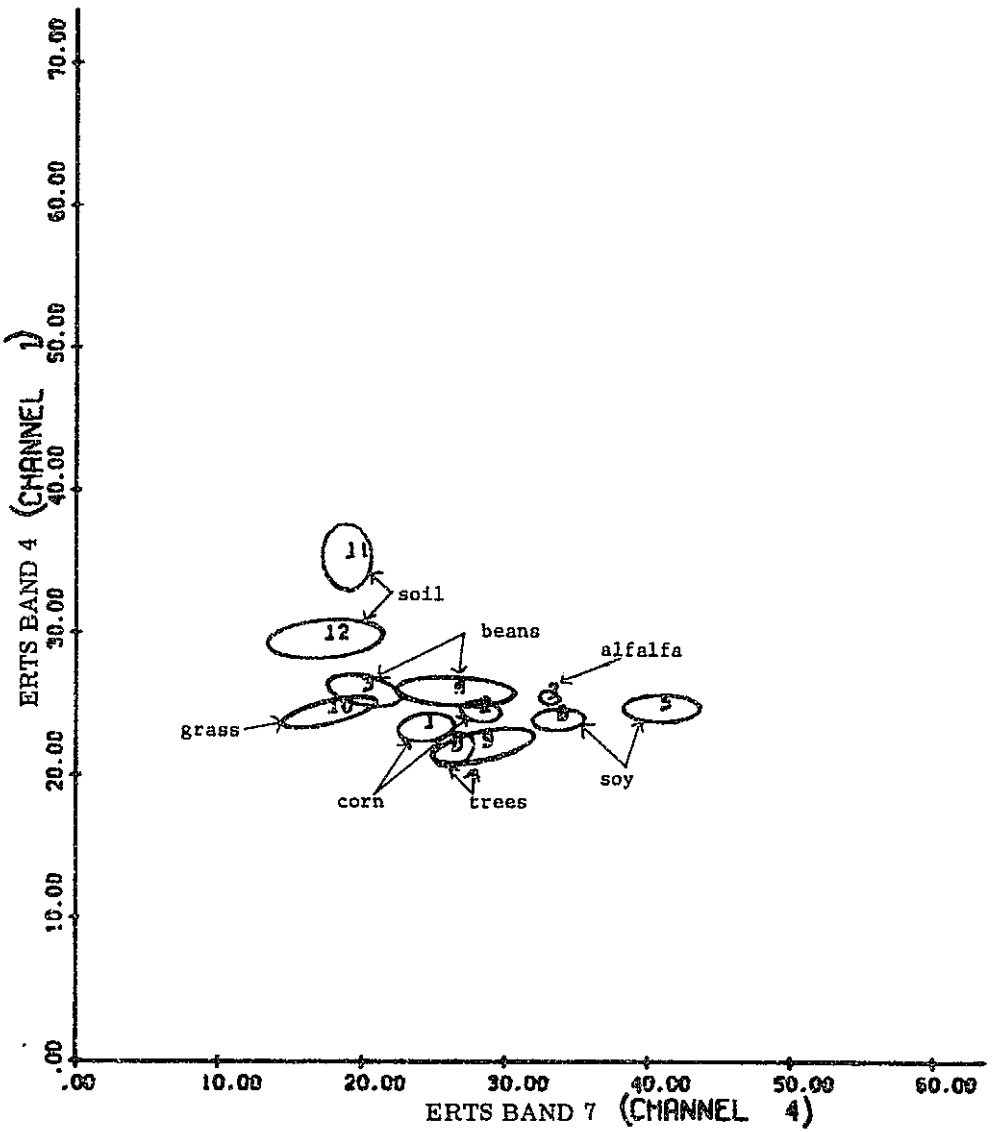

(c) ERTS Band 4 vs Band 7, Eaton County Signatures

FIGURE 15. ELLIPSE PLOTS OF RECOGNITION SIGNATURES (Continued)

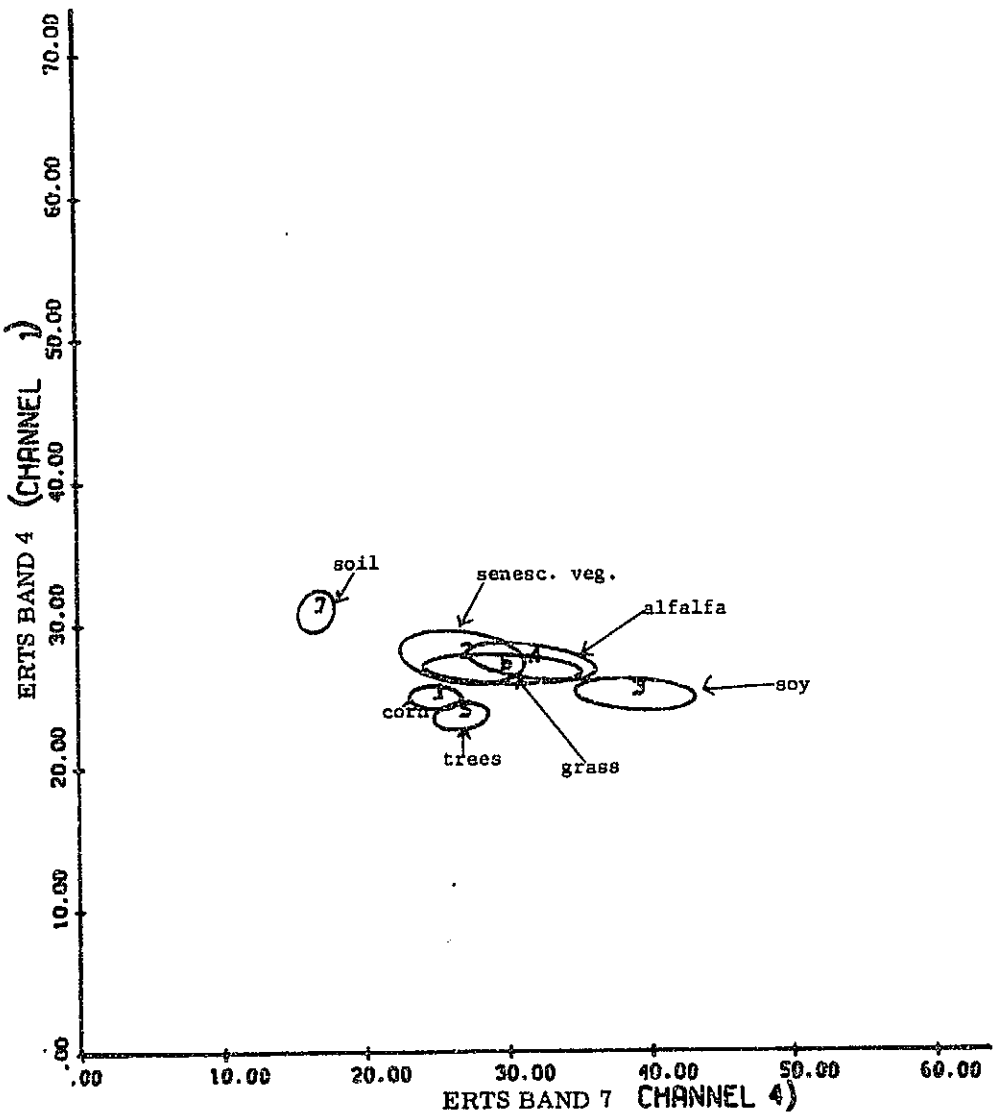

(d) ERTS Band 4 vs Band 7, Ionia-Clinton Signatures

FIGURE 15. ELLIPSE PLOTS OF RECOGNITION SIGNATURES (Concluded)

signatures from the Ionia-Clinton area: corn, trees, soybeans, bare soil, grass, alfalfa, and senescent vegetation. The greater the size of an ellipse, the greater is the variability of the class.

Because it is a composite class of various kinds of dying vegetation, and because different stages are likely to exist within the same field, the senescent cover class has a great deal of variability. In the Eaton County area, the two field bean signatures and the signatures for alfalfa and grass were used to define the senescent cover class. In the Ionia-Clinton area the senescent cover class is also a composite including the alfalfa and grass signatures as well as the senescent vegetation signature. Thus the senescent cover classes are not based on the same things in the two areas. The Ionia-Clinton signature for senescent vegetation exhibits more variability than the Eaton County signatures for field beans since it probably includes a variety of crop types.

Other observations can be made regarding the signature plots. Bare soil has two modes in Eaton County, one similar to the soil in Ionia-Clinton and the other substantially brighter in Bands 4 and 5. Also, the grass signatures are very different, for reasons already noted, both in location relative to the other signatures and in size. The Ionia-Clinton recognition signature for grass was formed by combining signatures from many fields including pastures, oats, wheat, hay, grass and weeds.

To determine whether or not the differences in the two grass recognition signatures were responsible for the different non-local recognition patterns with MLA, the percentages displayed in Tables 14 and 15 were calculated. Table 14 compares the percentages of pixels falsely recognized as soybeans and bare soil for all fields belonging to the senescent cover class with corresponding percentages for the subset of grass fields. Table 15 then compares the percentages of soybean and bare soil pixels recognized by all the senescent-cover-class signatures to the percentages falsely recognized by the grass signatures alone. The grass signatures did not falsely recognize any bare soil pixels (Table 15). However, a large portion of the senescent-cover pixels misclassified as bare soil were from grass fields. These misclassifications were largely due to recently harvested oat fields which at that time were mostly bare soil and were recognized as such.

Both area signature sets show an interaction between soybeans and the senescent cover class. The adjusted Eaton County soybean signatures recognize approximately 20% of the senescent cover pixels in Ionia-Clinton. Of the pixels so misclassified, 63% are grass pixels. The Ionia-Clinton adjusted signature set misclassified very few senescent pixels as soybeans, but 25% of the soybeans were falsely recognized by the senescent cover signatures. Of these, almost half were recognized

TABLE 14. MISCLASSIFICATIONS OF ENTIRE SENESCENT VEGETATION CLASS AND THE GRASSES WITH MEAN-LEVEL-ADJUSTED SOYBEANS AND BARE SOIL SIGNATURES

Area	Signatures	Recognized as Soybeans		Recognized as Bare Soil	
		% all Sen. Cover	% Grass	% All Sen. Cover	% Grass
Ionia Clinton	Eaton County I	22.3	14.2	10.0	7.3
	Eaton County II	18.1	11.5	10.0	7.3
Eaton County	Ionia Clinton I	2.7	0.4	5.0	4.3
	Ionia Clinton II	2.7	0.4	5.0	4.7

TABLE 15. FALSE ALARMS OF SOYBEANS AND BARE-SOIL PIXELS WITH MEAN-LEVEL-ADJUSTED SENESCENT-VEGETATION CLASS AND GRASS SIGNATURES

Area	Signatures	% of Soybeans Recognized by		% of Bare Soil Recognized by	
		Sen. Cover Class	Grass Signature	Sen. Cover Class	Grass Signature
Ionia Clinton	Eaton County I	3.7	0	13.2	0
	Eaton County II	3.7	0	11.3	0
Eaton County	Ionia Clinton I	25.5	11.8	16.7	0
	Ionia Clinton II	25.5	11.8	19.4	0

by the grass signature. The adjusted Eaton County grass signature recognized none of the soybean pixels, and very few soybeans were falsely recognized by the senescent cover signatures.

To summarize the foregoing analysis, the difference in the grass signatures of the two areas does not account for the differences in recognition of the senescent cover and soybeans classes with the two signature sets. Basically, the same trend is seen in grass as is seen in the entire class, but the grass signature only accounts for approximately half of the errors. Between senescent cover and bare soil, the grass signature is responsible for none of the missed detections of bare soil, and most bare-soil false alarms are due to recently harvested oat fields which probably should be called bare soil at the time. The difference in the amount of bare soil falsely recognized as senescent cover in the two areas is a result of the greater variability of the Ionia-Clinton senescent vegetation signature in comparison to the Eaton County field beans signatures.

Adaptive Processing. Adaptive processing improved recognition accuracies in the Ionia-Clinton area with both the Ionia-Clinton signature set and the Eaton County signature set. When processing with the Eaton set began in Eaton County and continued adapting through the Ionia-Clinton area, the recognition results were poor. Apparently, the brushy, uncultivated land around the Looking Glass River and possibly the brushy area within the 2×7 mile Eaton County area itself were responsible for the capture of one or more signatures.

Comparison of conventional processing results with results obtained with adaptive processing is complicated by differences between the two methods. Conventional methods usually classify with a threshold, in this case 0.001 probability of false rejection, to exclude pixels with wild values and ground covers for which there are no signatures. The adaptive processing method classifies every point although the point may be too far from the mean of the signature to affect the adapting significantly. This difference between the two methods had considerable effect in this case. Table 12 shows that 10 pixels were unclassified using the Ionia-Clinton signatures, and 80 pixels were not classified when the Eaton County signature set was used. The latter represents over one quarter of the pixels which were not correctly recognized by the conventional method. Because such a large portion of the incorrectly recognized pixels are really unclassified pixels, much of the improvement seen with adaptive processing may be due to the forced classification of all pixels. The conventional recognition accuracies, which are based on percentages of all pixels, would probably improve if processing were done without a threshold.

The results do show that adaptive processing with the updating rate representing the 190-line interval does improve recognition accuracies. It is not very likely that all 80 unclassified pixels would be correctly classified if there were no threshold; and thus, false alarms should

increase. Table 12 shows, however, that even with the threshold, the number of false alarms for conventional processing is 179 (= 259 - 80) compared to 178 for adaptive processing.

4.3.2 DATA SET FROM 21 AUGUST 1973

The 21 August data set is also agricultural in nature, consisting of two ground-truthed sites (F and W) separated by approximately 240 km (150 miles). The ERTS data collection date was 21 August 1973. Ground truth was obtained by ground observation for training data and by photointerpretation for test data.

Training was carried out only for site W. The signatures were obtained by combining statistics from several fields in each ground cover class. Only field-center pixels were considered. Five signatures were defined: corn, soybeans, quarry, pasture and trees. The resulting signatures were transformed for non-local recognition in the other site (F) by use of the MASC algorithm described in Section 4.2.3.

To obtain the signature-extension coefficients, clustering was performed on data from twenty 0.8 × 0.8 km areas in each site. The coefficients determined by the MASC procedure for transforming site W signatures for use in site F are presented in Table 16.

The final recognition categories were corn, soybeans and other. Recognitions with pasture, quarry, and tree signatures were assigned to the "other" class, along with unclassified pixels.

When untransformed signatures from site W were applied to data from site F, 240 km away, an overall recognition accuracy of only 28% was achieved for the 155 ground-truthed fields (1366 field-center pixels) in the site (see Table 17). Recognition of the major crops was especially poor, only 1.7% for corn and 10.0% for soybeans.

Greatly improved results, with an overall average of 80% correct, were obtained for site F through the MASC transformation of site W signatures. As shown in Table 18, corn and soybean recognition improved to 83% correct. These results are comparable to those obtained using local signatures on site F.

Two points are illustrated by this example. First, there are data differences that can cause substantial degradation in recognition performance for areas scattered throughout one or two ERTS frames on a given day. Second, signature extension procedures can adjust for these differences, at least under the condition of this example. The differences in signatures here are believed to be due primarily to atmospheric and illumination differences between the two sites.

TABLE 16. SIGNATURE TRANSFORMATION COEFFICIENTS FOR 21 AUGUST DATA, AS DETERMINED BY THE MASC PROCEDURE

Data Channel	Multiplicative Coefficient ($a_{F\|W}$)	Additive Coefficient ($b_{F\|W}$)
1	2.15	-22.449
2	2.23	-12.841
3	0.78	13.156
4	0.87	2.488

Notes: (1) Data channels 1-4 correspond to ERTS Bands 4-7, respectively.

(2) The MASC transformation is:

$$\hat{m}^i_F = a^i_{F|W} m^i_W + b^i_{F|W}$$

(3) Sites W and F are separated by approximately 240 km (150 mi).

TABLE 17. NON-LOCAL RECOGNITION RESULTS FOR 21 AUGUST DATA USTNG UNTRANSFORMED SIGNATURES

				NO. PIXELS RECOGNIZED AS:		
TRUE CLASS	NO. PLOTS	NO. PIXELS	% CORRECT	CORN	SOYBEANS	OTHER
CORN	43	356	1.7%	6	-	350
SOYBEANS	66	549	10.0%	-	55	494
OTHER	46	461	70.9%	126	8	327
TOTAL	155	1366		132	63	1171
AVERAGE OVER POINTS			28.4%			

TABLE 18 NON-LOCAL RECOGNITION RESULTS FOR 21 AUGUST DATA USING MASC-TRANSFORMED SIGNATURES

				NO. PIXELS RECOGNIZED AS:		
TRUE CLASS	NO. PLOTS	NO. PIXELS	% CORRECT	CORN	SOYBEANS	OTHER
CORN	43	356	83.4%	297	33	26
SOYBEANS	66	549	83.2%	28	457	64
OTHER	46	461	72.2%	110	18	333
TOTAL	155	1366		435	508	423
AVERAGE OVER POINTS			79.6%			

4.4 RECOGNITION OF SAME AREA ON DIFFERENT DAYS

When the same physical area is viewed on two successive days at the same time of day with no change in ground conditions (e.g., no rainfall), the major source of differences in signal levels is the intervening atmosphere. There are likely to be changes in the amount of atmospheric haze present on the two days. Also, it was shown earlier that a change in viewing geometry from one side of the ERTS frame to the other will introduce changes in signals even if the atmosphere is the same on both days.

It is difficult to find a data set which meets evaluation needs of substantial ground truth, atmospheric measurements, and differing amounts of haze on two successive days. One set meeting these criteria was available through a study being conducted under the previously referenced NASA SR&T program.

Signatures for trees and crops extracted from data collected on one day (Day 1) were applied to data from the preceding day (Day 2) over the same area. Recognition was substantially lower than with the Day 2 signatures applied to the same Day 2 data. Therefore, two signature extension techniques were applied to Day 1 signatures and recognition results determined with each. The first signature extension technique was a mean level adjustment procedure similar to that described earlier in Section 4.2.1. The second technique used adjustments based on photometer readings made on the two days at the time of the ERTS passes (see Section 4.2.4). These readings were used to calculate an optical depth at each wavelength for each day. The Turner radiative-transfer model was then used to compute total radiance and path radiance quantities for those optical depths and observation geometries. Signature adjustments based on these model calculations were applied to the Day 1 signatures and recognition processing was performed on Day 2 data.

To illustrate the results, the following example of tree recognition is given. First, an area that was classified as 100% trees on the first day was found and outlined on a recognition map. When the Day 1 signatures were applied to the Day 2 data, only 67% of the pixels were correctly classified as trees (symbol θ on Figure 16a). Then the signatures were adjusted by an amount determined by subtracting the mean level of signals over a larger nearby area on Day 1 from the mean levels computed for the same area on Day 2. A different adjustment was made for each channel. The adjusted signatures were used in the classifier and the classification percentage increased to 77% (Figure 16b).

With signature adjustments based on the model calculations, 88% of the pixels in the area were classified as trees, as shown in Figure 16c.

The above example is one of the more dramatic cases observed but, nevertheless, is indicative of the trend. The centers of a total of 27 wooded areas were delineated and tested.

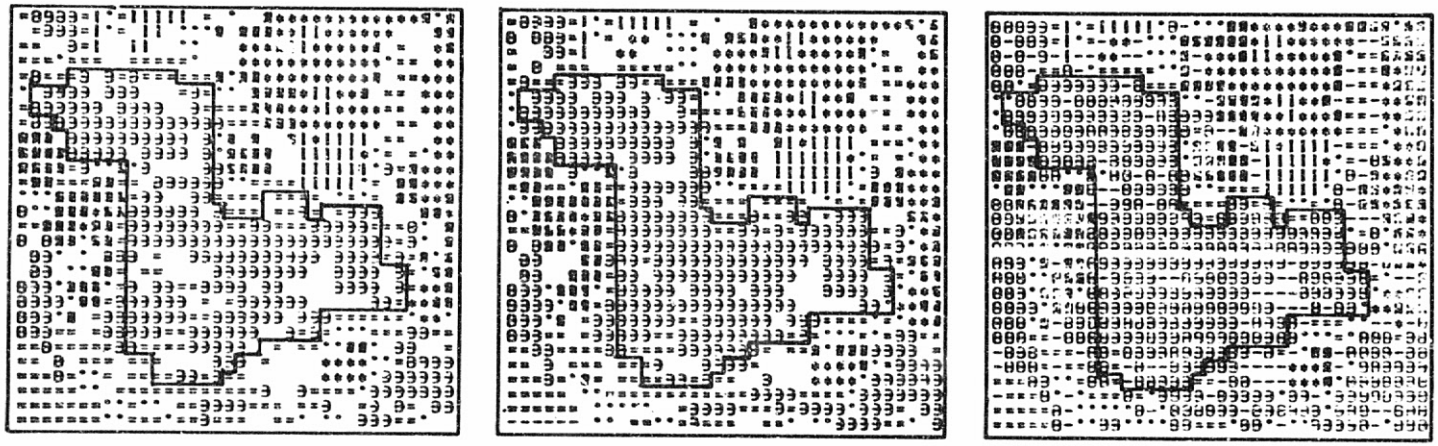

NO ADJUSTMENT OF SIGNATURES

(67% Called Trees)

EMPIRICAL MEAN LEVEL ADJUSTMENT

(77% Called Trees)

THEORETICAL MEAN LEVEL ADJUSTMENT

(88% Called Trees)

Outlined Area Completely Recognized as Trees for Same Day as Signatures.

FIGURE 16. EXAMPLE OF APPLYING SIGNATURES FROM ONE DAY TO ERTS DATA FROM PRECEDING DAY OVER SAME AREA

As shown in Table 19, the average classification accuracy fell from 96% to 88% with no adjustment of the signatures. The two signature extension techniques increased the correct classification accuracies to 92% and 91% respectively.

Results for field-center pixels of ten wheat fields also are presented in Table 19. Here, again the accuracy fell from 87% to 65% with no adjustment, and rose to 71% and 78% for the two types of signature extension procedures.

4.5 CONCLUSIONS AND RECOMMENDATIONS

ERTS-1 multispectral scanner data have been used to achieve reasonably high (80% correct) field-center recognition accuracies for agricultural crops on a local basis, i.e., with testing performed in the vicinity of training fields. It has been shown that recognition performance degrades when the signatures are applied directly to other areas displaced in space or time from the training area.

It has been demonstrated that signature extension techniques, previously developed at ERIM, can be applied to improve non-local recognition performance above that achievable without them. Several signature extension techniques were examined.

The first technique, mean level adjustment of signatures, produced some improvements although it was shown to be somewhat sensitive to the proportions of various ground covers in the areas used to determine adjustments. Also, it was found that one additive adjustment per channel did not produce an optimal match between local signatures and adjusted non-local signatures.

An example of the application of the multiplicative and additive signature correction (MASC) algorithm was presented which indicated a substantial improvement over the simple mean-level correction algorithm.

A different concept, that of adapting the means of the recognition signatures on the basis of decisions made along the flight track, was also tested. It performed best when adaptation was started in the non-local area, because atypical scene conditions existed in the region between training and test areas.

Finally, in the case studied, a radiative transfer model used in conjunction with ground-based measurements of optical thickness was shown to be capable of alleviating some of the deleterious effects of the atmosphere on multispectral recognition of non-local areas.

Recognition for full sections, as opposed to field centers, were examined only for unadjusted and mean-level-adjusted signatures. The results were not as encouraging as for field centers. Recognition was complicated by the presence of pixels which represented mixtures of two or more materials. Substantial number of such pixels were present in the data due to the relatively small size of fields in the area.

TABLE 19. SUMMARY OF CLASSIFICATION RESULTS FOR ONE AREA VIEWED ON TWO SUCCESSIVE DAYS

Signatures	Data Set	Wheat % Correct (10 Test Areas)	Trees % Correct (27 Test Areas)
Day 1	Day 1	87	96
Day 1	Day 2	65	88
Day 1 Adjusted*	Day 2	71	92
Day 1 Adjusted**	Day 2	78	91

*Empirical mean level adjustment

**Theoretical level adjustment (photometer plus model)

It was noted that training is a very important step in multispectral recognition and that recognition results for major crops depend on the adequacy and representativeness of signatures generated for other types of ground covers as well as for the major crops themselves. The class of senescing and senescent vegetation was quite variable in the time period analyzed and signatures with substantially different characteristics resulted from the use of both ground truth data of different quality, and different training procedures.

On the basis of the results reported and discussed herein it is recommended that the adaptive, MASC, and radiative-transfer-model signature extension techniques be tested and evaluated in a more operational context on a more extensive data base. Also, it is recommended that the sensitivity of these techniques to various methods of establishing recognition signatures be explored, e.g., to study whether it is better to have multiple modes for each ground cover class or to reduce the number by combining some of the modes. A related problem that should be investigated is the establishment of criteria for determining how much training data are required to obtain various levels of performance in a given application.

5
PROPORTION ESTIMATION

A third aspect of this ERTS investigation dealt with the test and evaluation* of advanced data processing and information extraction techniques whose purpose was to accurately determine the ground area encompassed by features in the scene as viewed by the ERTS-1 multispectral scanner.

5.1 DESCRIPTION OF THE PROPORTION ESTIMATION PROBLEM

Clearly, there is a serious problem in accurately determining the acreage of features smaller than the instantaneous field of view of the ERTS scanner. In addition, problems exist even for larger features since many of the ERTS MSS resolution elements, which view an instantaneous ground path 79 meters on a side, overlap the boundaries between these and adjoining features. As a result, the radiation represented in those pixels is a mixture of radiation reflected from two or more materials.

*The techniques to be tested here were initially conceived and developed at ERIM under NASA Contract NAS9-9784 and are being further developed and tested under NASA Contract NAS9-14123. Both contracts are administered by the Earth Observations Division, NASA Johnson Space Center, Houston, Texas.

The effect of simultaneously viewing two materials on the radiation reflected is illustrated in Figures 17 and 18. In Figure 17 the reflectance spectra are depicted for corn and bare soil as they would appear individually. If the sensor were to simultaneously view both corn and bare soil, the effective reflectance spectrum would be quite different. This is shown in Figure 18 for the combinations 20% corn - 80% bare soil and 50% corn - 50% bare soil. These spectra are simply weighted combinations of the pure spectra of Figure 17 and could represent the effect of viewing adjoining corn and bare soil fields in a single pixel.

Since the signals generated in such pixels are not characteristic of any one material, the use of conventional multispectral recognition processing techniques will result in the improper classification of those pixels. Therefore, the overall area assigned to each material class in a scene could be seriously in error. In ERTS data, at least 25% of the pixels covering a square field of 50 acres [20 hectares] will overlap its boundaries.) Such errors, if not eliminated or accounted for, could seriously degrade the utility of ERTS MSS data for applications such as the Large Area Crop Inventory Experiment (LACIE) which is being undertaken jointly by NASA. National Oceanic and Atmospheric Administration (NOAA), and the United States Department of Agriculture (USDA) to demonstrate present-day capabilities for using remotely sensed data to aid in estimating the productivity of wheat over large areas.

5.2 DESCRIPTION OF AN APPROACH TO PROPORTION ESTIMATION

Recognizing that problems of accurate acreage estimation were likely to exist in the future, ERIM, with NASA's support, began to develop special processing and information extraction techniques in the early 1970's [22-29]. In general, such techniques take advantage of the fact that the radiation emanating from each scene element is detected simultaneously in several spectral bands. This offers the possibility for classifying and accurately estimating the proportions of materials in a scene in which many samples are made up of mixtures of materials. The initial method developed at ERIM, which was tested and evaluated during this investigation, is briefly described in the following paragraphs. Additional details are presented in Appendix C.

Assume that a data set comprised of two spectral channels, λ_1 and λ_2, contains three pure and unique materials—A, B, and C. This situation can be depicted as in Figure 19, where the signature means for the three materials are shown in two-dimensional signal space. The signature simplex is the geometric figure formed by the lines connecting each pair of signature means. In the nondegenerate case, each pure signature is a distinct vertex of this simplex. If an unknown scene element consists of portions of all three materials, the signal generated by that scene element, X, lies within the simplex. An estimate of the proportion of each pure material constituting the unknown element is obtained by drawing a line from a vertex through the signal to be classified to the opposite leg of the simplex. The fraction of the line between the

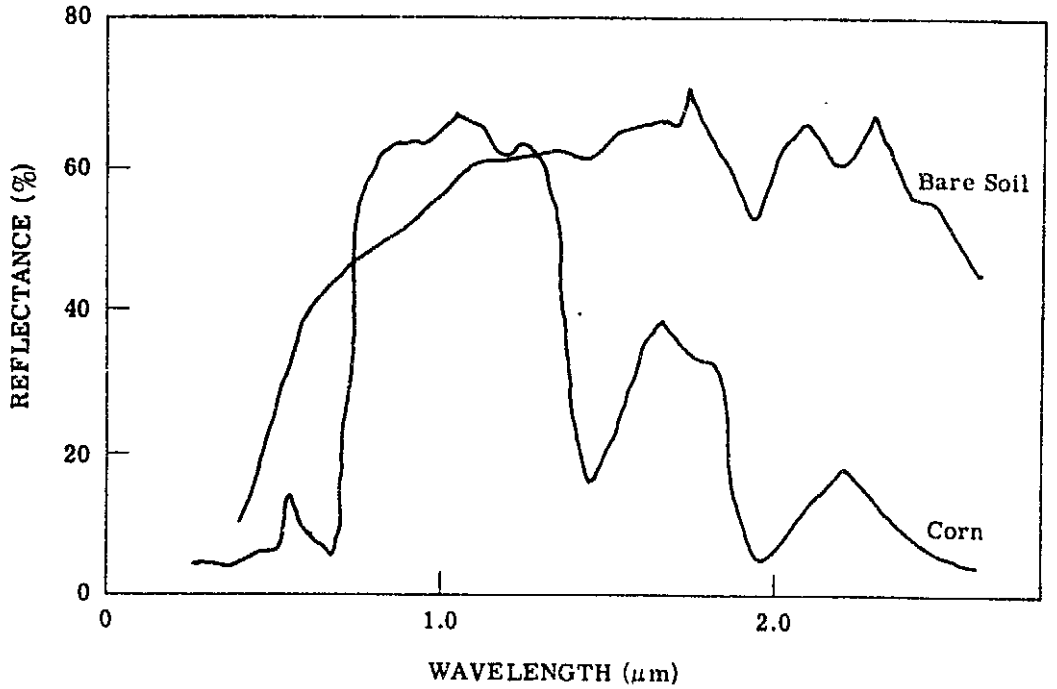

FIGURE 17. REFLECTANCE SPECTRA

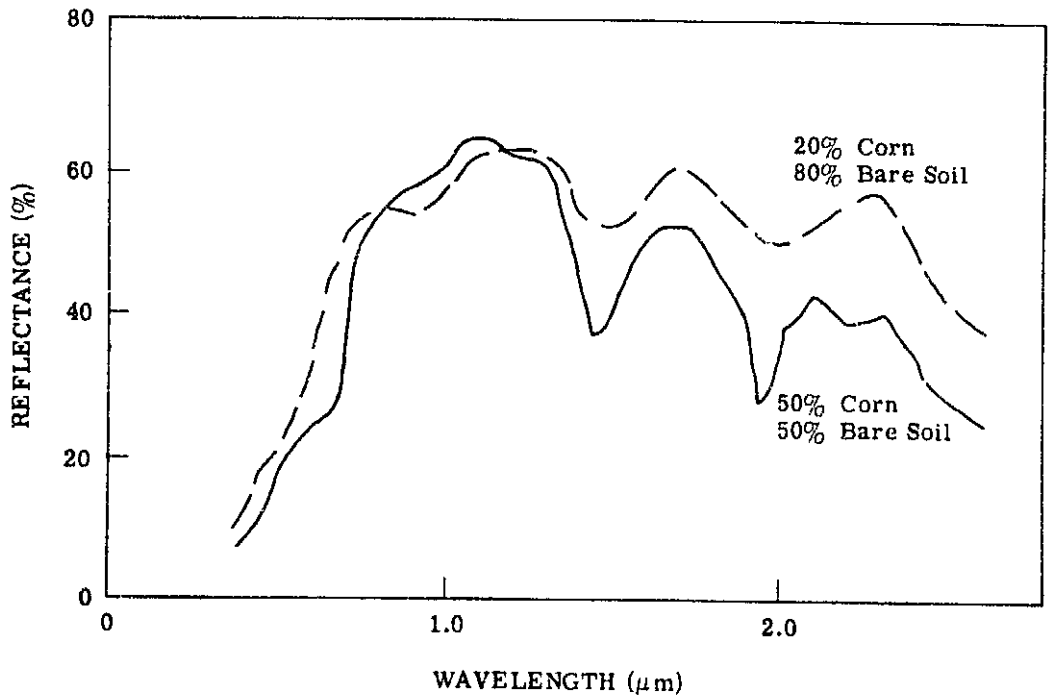

FIGURE 18. REFLECTANCE SPECTRA OF MIXTURES

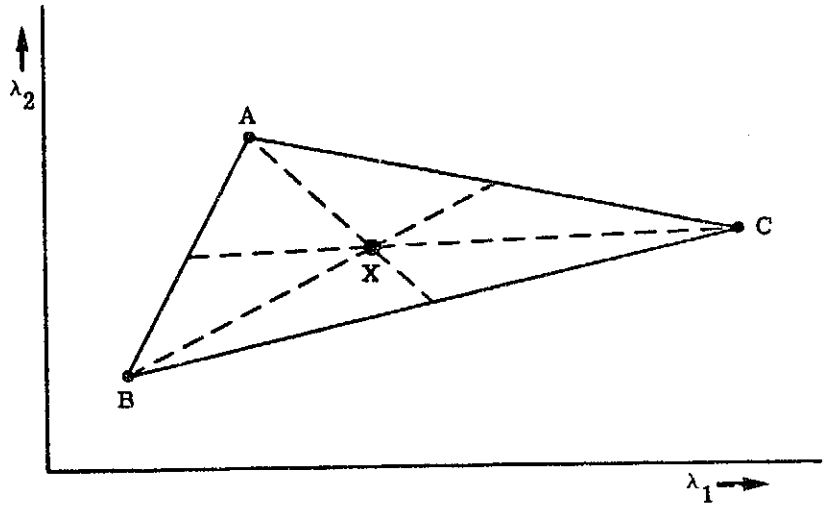

FIGURE 19. GEOMETRIC INTERPRETATION OF MEANS OF SIGNATURE MIXTURES. In the case illustrated, the unknown, X, is a combination of three pure materials (A, B and C) which form the vertices of the signature simplex.

crossover point and opposite side defines the proportion of the corresponding vertex material in the unknown. For the case illustrated in Figure 19, the unknown happens to lie at the centroid of the triangle, and its composition would be in the ratio of 1/3, 1/3, and 1/3 of materials A, B, and C, respectively. Cases requiring other geometric interpretations are shown in Figure 20. Figure 20a illustrates the occurrence of an unknown, Y, on the edge of the signature simplex. In this case the unknown would be comprised of only materials A and C. Figure 20b shows an unknown, Z, which lies completely outside the simplex. In this case, the unknown is said to be comprised of materials A and C in the proportion determined by finding the point in the simplex closest to the unknown. If the unknown, Z, were quite distant from the signature simplex (described in terms of a χ^2 distance), the algorithm will designate the unknown as an alien object or, in other words, an object composed of none of the simplex materials.

Although the above description has been limited to three pure and unique materials in two-dimensional signal space, the concept is easily expanded to situations where many object materials exist in spectral hyperspace. In applying the algorithm, however, it is necessary to observe two operational constraints. First, at least n - 1 spectral channels of information are required to satisfactorily estimate the proportions of n materials. Secondly, if the signatures for the materials in a mixture are similar or if one of them comes too close to a weighted average of the others, the estimates of the proportions may be poor. The latter condition is illustrated by Figure 21. Figure 21a shows a valid signal simplex for three signatures and two channels of data. Here covariance matrices interpretable in terms of loci of constant probability are shown. Figure 21b is a nearly degenerate signature simplex in which the vertex of one signature has come close to the weighted average of the other two signatures. A measure of what is "too close" is dependent upon the size and shape of the unit contour ellipsoid about the vertex, or more specifically upon the signature covariance matrix.

In many applications, proportions for each data point may not be required. For these cases, a reduction in computation time can be achieved by averaging all non-alien data points and then carrying out a single computation of the proportions of the objects appearing in the entire averaged region. This approach is not only much faster, but also provides the possibility for improved accuracy, since averaging would reduce the effect of the variability of sensor signals caused by the natural variation of the radiation received from any object class in the scene. In addition, the effects of random noise would be reduced.

As a part of the continuing investigations under Contracts NAS9-9784 and NAS9-14123, we have developed and begun testing modifications and improvements to the above approach for proportion estimation. (Other investigators [30-33] have also recently begun examining the proportion estimation problem.) One serious restriction imposed by our initial approach was that at least n - 1 spectral channels of information were required to satisfactorily estimate the

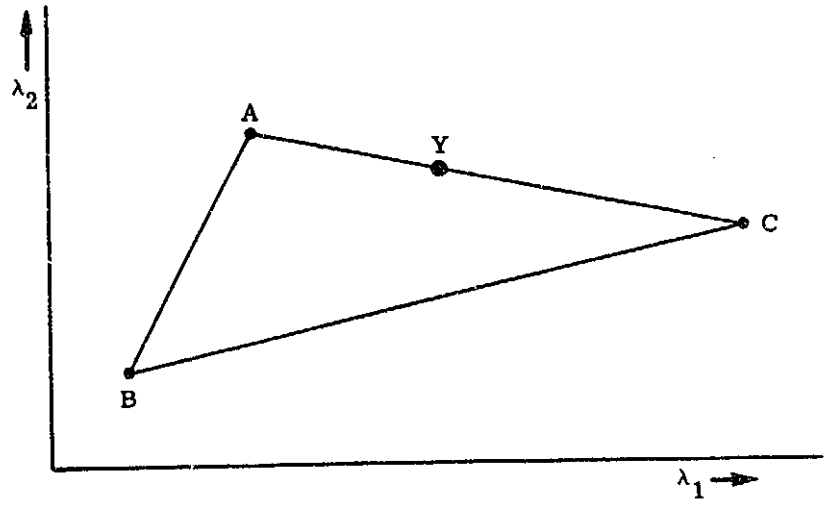

(a) The unknown, Y, lying on the margin of the signature simplex is a mixture of materials A and C.

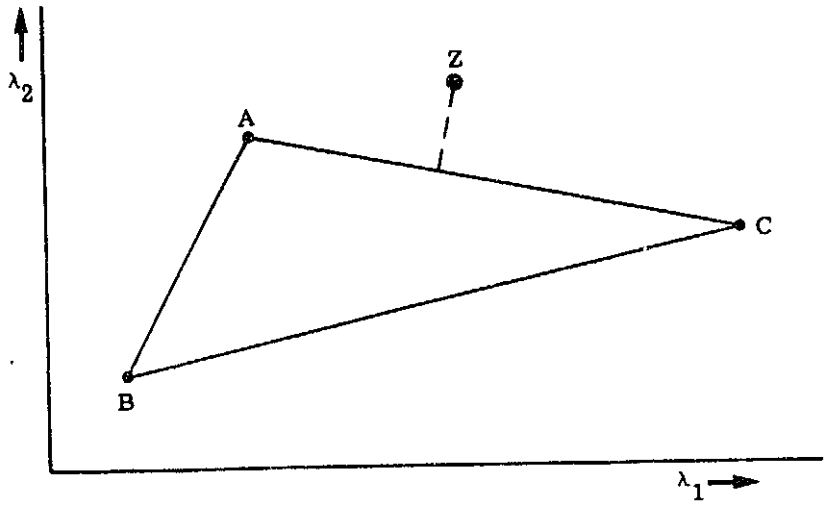

(b) The unknown, Z, lying outside the signature simplex is a mixture of materials A and C. If Z were too distant from the simplex, it would be declared an alien object.

FIGURE 20. GEOMETRIC INTERPRETATION OF ESTIMATE (SPECIAL CASES)

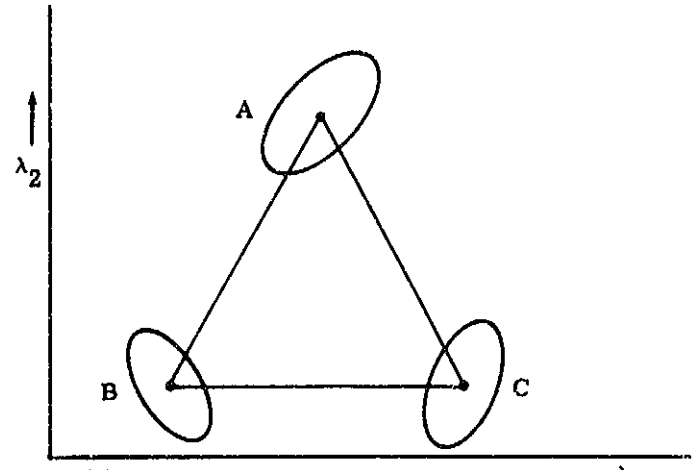

(a) Signature Simplex with Unit Contour Ellipsoids

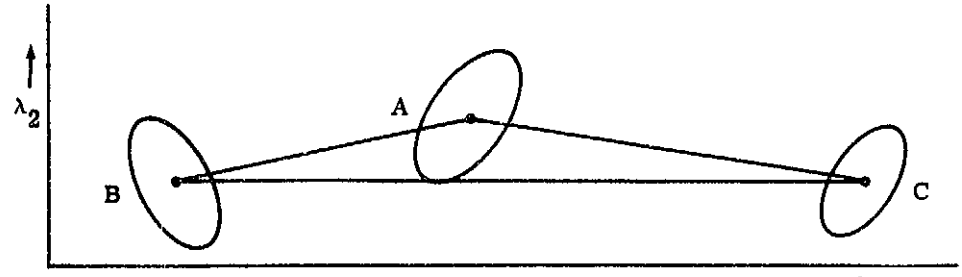

(b) Nearly Degenerate Signature Configuration

FIGURE 21. GEOMETRIC CONFIGURATIONS FOR THREE SIGNATURES AND TWO SPECTRAL CHANNELS

proportions of n materials. A recent modification [34] permits many more materials to be considered by assuming that, in a realistic scene, no more than four materials would appear within a single pixel. This is especially important for the ERTS MSS and its four spectral bands.

A more recent modification also takes advantage of the characteristics of surrounding pixels to help identify the most likely constituents of the central pixel.

5.3 TEST AND EVALUATION OF AN ERIM PROPORTION ESTIMATION TECHNIQUE

For the test and evaluation of ERIM proportion estimation techniques it was decided to examine two application disciplines: water and agriculture. These two disciplines represent tests of varying difficulty. The accurate estimation of ground area covered by water is less difficult since water exhibits high contrast with most backgrounds in the spectral regions covered by the ERTS MSS. In fact, it has been suggested [35] that a universal algorithm using two of the ERTS MSS spectral bands can be used to detect (but not necessarily accurately estimate the acreage of) all bodies of water 10 acres or larger in size.

The problem of accurately estimating the acreage of selected agricultural crops is much more difficult. This task is complicated by the variability of spectral characteristics of crops from field to field and during the growing season, the similarity in spectral characteristics of many crops, and the broadband spectral coverage of the ERTS MSS.

5.3.1 PROPORTION ESTIMATION FOR WATER

The goal of this test was to determine how accurately we could estimate the surface area of a number of lakes and ponds in a small portion of an ERTS frame. The region selected for processing is shown in Figure 22, a black-and-white aerial photograph of that region.

Using an enlargement of this photo, the surface area of the water bodies was determined. Two methods, dot grid and planimeter, were used to determine area; the results were calibrated by assuming a one mile separation between the section line roads apparent in the photo.

For purposes of comparison, the data were processed using two approaches in addition to the multi-channel proportion estimation algorithm. One of these was the conventional recognition algorithm in which each pixel was assigned to one and only one class. In the other approach, proportions were estimated using only one ERTS MSS band. In processing the data the first step was the establishment of training signatures for the major object classes in the scene. The primary scene components in this case were water, trees and soil. A number of pixels containing pure samples of each of these classes were located and the mean signal vector and associated covariance matrix were determined for each class. Since there were some data quality problems with ERTS Band 6, only Bands 4, 5 and 7 were used to establish signatures and for the ensuing processing.

FIGURE 22. TEST AREA FOR PROPORTION ESTIMATION FOR WATER

Having established the signatures, the three processing algorithms (multi-channel proportion estimation, single-channel proportion estimation, and conventional recognition) were applied to the data. In order to meaningfully compare the results generated using these algorithms, it was necessary to identify the thresholds which would be used in each. These threshold or parameter values would affect the trade-off between the detection rate and the false alarm rate. For this comparison, it was decided to utilize those parameter values which eliminated water false alarms in the scene (i.e., no non-water pixels would be classified as water) while at the same time maximizing the detection rate.

The multi-channel proportion estimation algorithm used for estimating water acreage depends upon the values used for two parameters. One of these parameters, ρ, is called the probability of rejection; the other, τ, is the water proportion threshold.

The purpose of the probability of rejection parameter ρ is to eliminate those signals representing pixels that contain insignificant coverage by a combination of water, bare soil and vegetation, or to eliminate signals representing pixels that contain significant coverage by combinations of other object classes. The probability of rejection parameter ρ operates as follows. If a signal x is not within a probability contour that contains $(1 - \rho)$ of the samples for a signature of some mixture of water, bare soil and vegetation, then the proportion of water estimated for the pixel represented by the signal x is taken to be zero.

The objective of the other parameter, the water proportion threshold τ, is to eliminate small proportion estimates of water for pixels which, in reality, contain no water. This parameter operates as follows. A tentative proportion estimate $\hat{p}$ of water is made for the pixel in question. If $\hat{p}$ is less than τ, then the estimated proportion of water is taken to be zero. If $\hat{p}$ is greater than or equal to τ, then $\hat{p}$ is taken as the estimated proportion of water.

Figure 23 gives the operating characteristics of the proportion estimation algorithm for this data set as functions of the probability of rejection and the water proportion threshold. The plots shown in this figure were determined as follows. All the pixels in the scene were classified by photo-interpretation into two classes: class W if they contained some water, or class G if they contained no water. The total amount of water surface area estimated for the pixels in class G, divided by the area of those pixels, was taken as the false alarm rate. The total amount of water surface area estimated for pixels in class W divided by the actual (as determined by photo-interpretation) surface area of water in class W was taken as the detection rate.

From the figure we see that for $\tau = 0.4$ or greater, the false alarm rate becomes zero, regardless of the probability of rejection ρ. For a specific value of ρ, we may increase the detection rate by decreasing τ, but the penalty is an increased false alarm rate. Examination of

the operating characteristics indicated that the combination of parameter settings with $\rho = 0$ and $\tau = 0.4$ yields near-optimum results: detection rate = 90.24% and false alarm rate = 0. This detection rate is based upon assigning to each pixel an area equal to 79 × 57 m.

The single-channel proportion estimation algorithm operates similarly to the multichannel proportion estimation algorithm, with probability of rejection parameter ρ and water proportion threshold parameter τ. In single-channel proportion estimation, the ρ parameter was used to eliminate those signals which represented pixels containing insignificant coverage by a combination of water and vegetation (using the initially developed proportion estimation algorithm proportions, may be estimated for only two classes when using a single channel). Because the water signal level in ERTS Band 7 was lower than all others in the scene, a value of zero could be used for the parameter ρ without causing false alarms. Therefore, the results given in Figure 24 are for $\rho = 0$ and varying values for the parameter τ. We see that as τ decreases the detection rate increases, with a penalty of increased false alarm rate. A false alarm rate of zero is achieved for τ values of 0.6 or greater.

For conventional recognition the parameter τ does not enter into the calculation, since each pixel is classified as either containing water (100%) or not (0%). The value of ρ, however, does need to be determined. It was found that the occurrence of false alarms was independent of ρ therefore, the value of ρ which maximized the detection rate was selected.

Before describing the test results, we present here a brief discussion of the areas which were assigned to each pixel. The instantaneous field of view of the ERTS MSS is 79 × 79 m but, since the data are oversampled along the scan direction, there is overlap in the ground patch covered by successive samples. Therefore, in order that calculations of the total area of an ERTS frame do not exceed the actual area viewed in that frame, a smaller effective size has been used in the scan direction. However, for the problem being addressed here, where the area for only one class in the scene is being estimated, one needs to consider the actual ground area viewed by each pixel. In other words, if a pond smaller than 79 × 79 m is contained within one pixel and that pixel is estimated to contain 50% water, the estimated area of the pond is 50% of 79 × 79 m and not 50% of some smaller effective area. If this same pond was seen in the overlap area of two successive pixels it would be inaccurate to use the 79 × 79 m area for each pixel since some portion of the pond would be counted twice.

In order to account for problems of this sort, three separate pixel sizes were used in computing estimated area. If the pixel containing some portion of water in excess of the threshold value fell between two pixels on the same scan line which were also identified as containing water, the pixel size for area estimates were assumed to be 79 × 57 m (the size was computed based on the 100-nautical-mile frame size and number of samples per scan line). "Water"

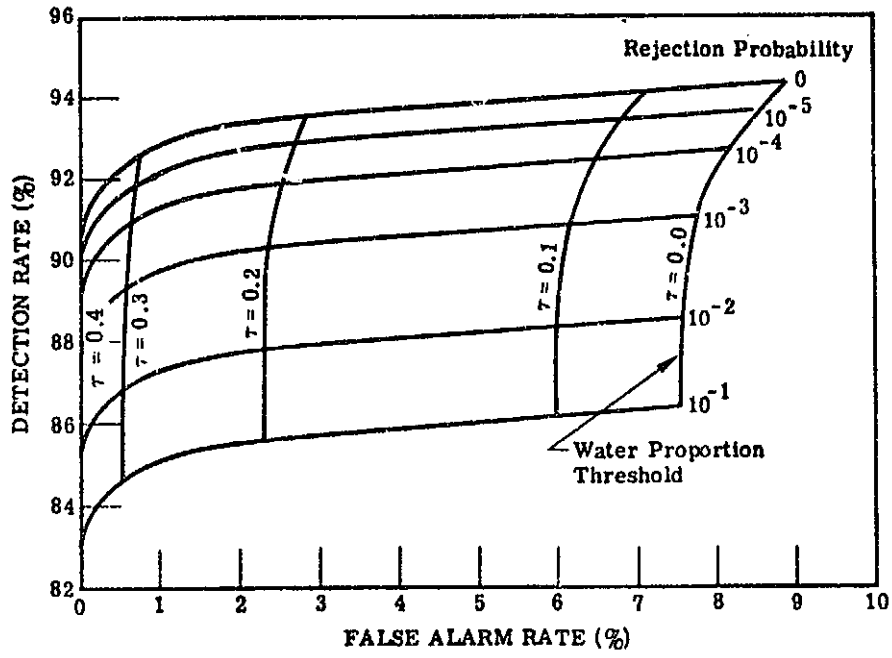

FIGURE 23. OPERATING CHARACTERISTICS OF PROPORTION ESTIMATION (3-CHANNEL)

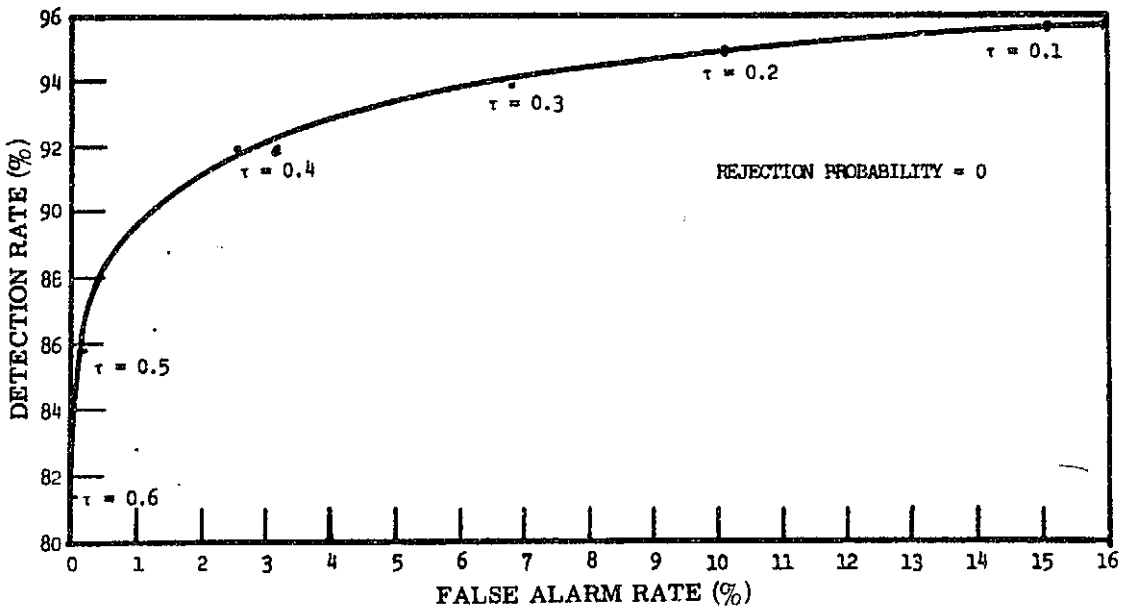

FIGURE 24. OPERATING CHARACTERISTICS OF PROPORTION ESTIMATION (1 CHANNEL: ERTS BAND 7)

pixels with one "water" neighbor along the scan line were assumed to be 79 × 68 m and "water" pixels with no "water" neighbors were assumed to be 79 × 79 m.

Water Test Results: Using the three processing algorithms described earlier, three water classification maps were generated. These are shown in Figures 25, 26, and 27 for the multi-channel proportion estimation, single-channel proportion estimation, and conventional recognition algorithms, respectively. The first two maps are printed with symbols whose density is related to the proportion of water estimated in each pixel while the conventional recognition map includes only a single symbol where water was detected implying that the entire ground area viewed in those pixels is covered with water.

Upon comparing Figures 25 through 27 with the aerial photograph in Figure 22, it is clear that the shape of the water bodies was more accurately reproduced on the multi-channel proportion estimation map and that more of the small bodies of water are detected on this map. In fact only one of the bodies of water was totally undetected.

In order to compare the area estimation results achieved on individual water bodies using the three algorithms, we present Figure 28. Here we plot on the vertical axis the ratio of area as measured from the photograph to the area determined by automatic processing. On the horizontal axis we plot the shape factor which we define as a constant times the area divided by the perimeter of the water body. Shape factor is used rather than area since water bodies with small shape factors (because of large perimeters or small size) can be expected to be less accurately estimated than those with large shape factors. This expectation is borne out on examining Figure 28, which shows that the spread in accuracy for the three methods is small for water bodies having large shape factors (relatively fewer boundary pixels) and generally increases for smaller shape factors.

The area-estimate accuracies are better using the multi-channel proportion estimate algorithm in almost every case. There are a small number of cases in which the area is slightly overestimated; however, it is possible that the areas measured from the aerial photograph were somewhat low. In general, the results using the conventional recognition algorithm were much inferior, especially for water bodies with smaller shape factors.

A summary of the results for the entire test site is shown in Table 20. Here we see that 97% of water measured from the photograph was detected using the multi-channel proportion estimation algorithm while only about 85% was detected using the other two algorithms. This difference would have been greater if fewer large lakes existed in the scene.

We have shown that, for this example, more accurate water surface area estimates are achieved by using multi-channel proportion estimation.

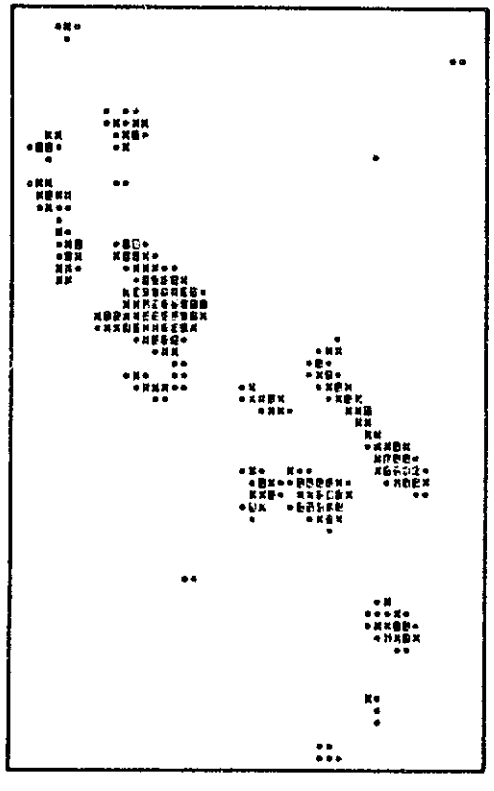

FIGURE 25. PROPORTION ESTIMATE WATER RECOGNITION MAP WITH ERTS BANDS 4, 5 AND 7

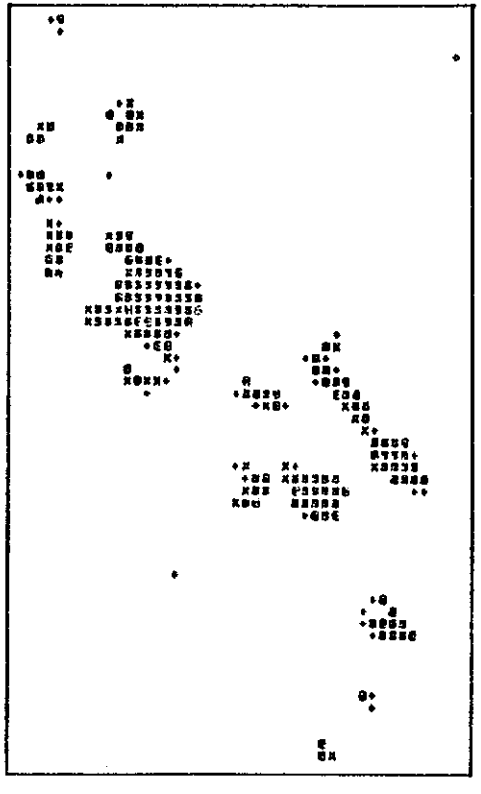

FIGURE 26. PROPORTION ESTIMATE WATER RECOGNITION MAP WITH ERTS BAND 7 ONLY

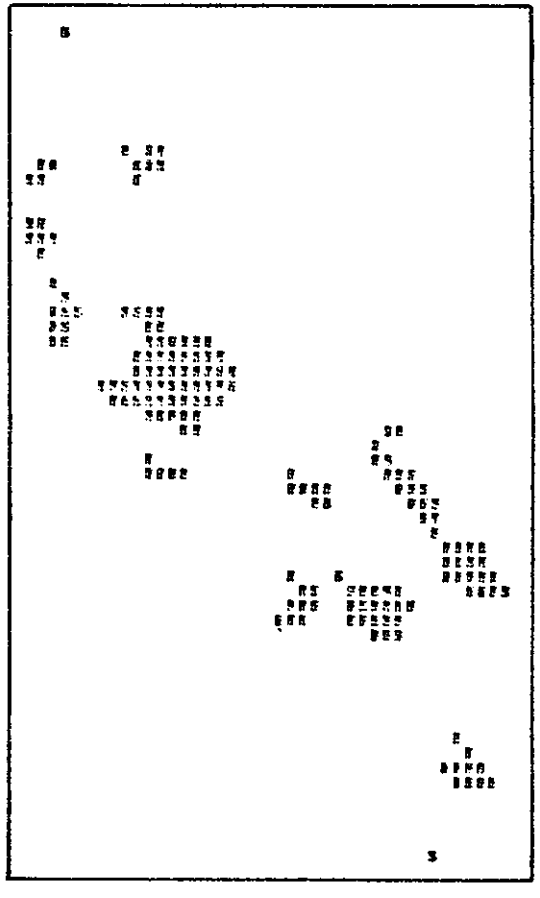

FIGURE 27. CONVENTIONAL WATER RECOGNITION MAP WITH ERTS BANDS 4, 5 AND 7

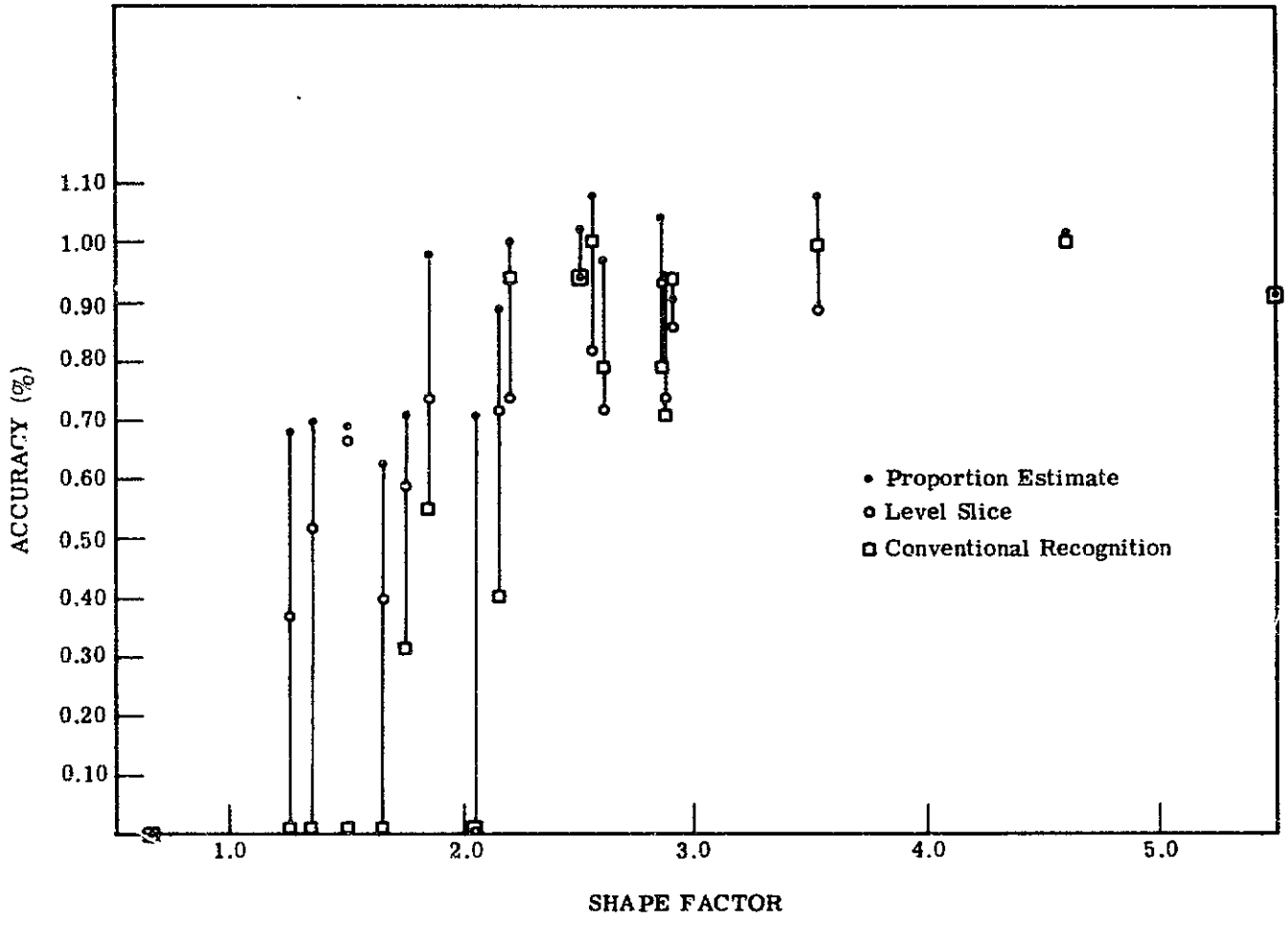

FIGURE 28. INDIVIDUAL WATER BODY AREA: ESTIMATE ACCURACY VS SHAPE FACTOR

TABLE 20. SUMMARY OF WATER AREA ESTIMATION RESULTS

	Photointerpretation	Fractional Pixel Procedures		Whole Pixel Procedure
		3-Channel Proportion Estimation	1-Channel Proportion Estimation	Conventional Recognition
Number of Water Bodies Detected	19	18	17	13
Total Water Area (Meters^2)	1,041,958	1,006,739	892,118	879,120
Percentage of Photointerpreted Area	100%	97%	86%	84%

The multi-channel proportion algorithm described above was found to be useful by Mr. Edgar A. Work Jr. of ERIM as a part of another ERTS investigation (USDI 14-16-0008-715) where water acreage determination was involved. The purpose of this investigation was to assist the U.S. Fish and Wildlife Service of the Department of the Interior in demonstrating the utility of remote sensor data for monitoring the breeding habitat of migratory waterfowl in the glaciated prairies. The results of Mr. Work's efforts are described in References [33-39].

5.3.2 PROPORTION ESTIMATION FOR AGRICULTURE

Having demonstrated that the multi-channel proportion estimation algorithm generated accurate water area estimates, attempts were undertaken to establish the utility of the algorithm for the agricultural discipline. With the limited resources available, only one agricultural data set could be examined under this contract. The ERTS data set examined was the one gathered in late August 1972 over Eaton, Ionia, and Clinton Counties in Michigan which was described in Section 4.3.

Because of the aforementioned difficulty with Band 6 of the ERTS MSS only three spectral bands were available, thereby limiting the number of signatures that could be used to four with the then available proportion estimation algorithm. Based on the importance of each ground cover, the acreage of each, and their spectral separation, four signatures (one each for corn, field beans, soybeans, and bare soil) were generated by combining signatures from among the original twelve generated for Eaton County.

The spectral separability of the resulting signatures is shown below in Table 21.

TABLE 21. SIGNATURE SPECTRAL SEPARABILITY

Signature	Separability 6 units of Standard Deviation
Corn	0.59
Field Beans	0.26
Soybeans	0.75
Soil	1.06

The separability shown represents the distance in units of standard deviation from each crop signature mean to the hyperplane formed by the remaining three crop means. These values then are a measure of the degeneracy of the signature configuration as previously illustrated in Figure 21. In this case the values, especially for field beans, were quite low indicating even before any actual proportion estimation that the results were likely to be less accurate than desired. As a contributing factor to the lack of signature spectral separability, not only was one of the four spectral bands not useful due to noise, but two of the remaining three bands (4 and 5) exhibited a high degree of correlation. As a result, very little additional information

for discriminating between the ground covers would have been lost had either of these bands not been available. (We believe that the broad spectral coverage of the ERTS-MSS bands contributes to these discrimination difficulties.)

Agriculture Test Results: Using ERTS Bands 4, 5 and 7, and the signatures for corn, field beans, soybeans and bare soil, the proportion estimation algorithm was applied to data from each of fourteen sections (1 × 1 mile areas) and to the data from the set of all fourteen sections. Two approaches were used in the application of the proportion estimation algorithm. In the first approach the proportions of the above ground covers were calculated for each non-alien pixel in the area being studied (each individual section and the collection of all sections). These proportions were then aggregated to determine the proportions of the ground covers for each area. In the second approach only one calculation of proportions was carried out for each area since the non-alien pixels forming each area were combined by averaging to effectively form a single pixel for each area. This second approach was less time consuming and it was believed that the results might be more accurate since the effect of some of the variations were being reduced by averaging.

The results of the tests are shown in Figure 29. In this figure we plot Δ which is defined as the absolute value of the difference between the true and estimated proportion. The maximum, mean, median and minimum section Δ and the combined area Δ are plotted for each ground cover and for both the pixel-by-pixel (P) and average pixel (A) approach.

The minimum section Δ's for both approaches were very small with only the minimum section Δ for soybeans and the averaging approach exceeding 0.01. The maximum section Δ's, however, ranged from 0.099 to 0.189 with the range for pixel-by-pixel being 0.099 to 0.165 and the range for averaging being 0.144 to 0.189. The mean and median Δ's for each crop were quite similar, the difference being somewhat larger for the averaging approach. The values from crop to crop were also similar, ranging from 0.035 to 0.083. Overall, for the individual sections, the results for the pixel-by-pixel approach were more accurate than those generated by the averaging approach.

The combined section results are similar in nature, with the range of Δ's for the pixel-by-pixel approach being 0.00 to 0.05 and for the averaging approach ranging from 0.041 to 0.08. In every case the combined section Δ's were (sometimes significantly) less than or equal to the mean Δ of the individual sections.

It appears that the proportion estimation algorithm produced relatively accurate results even for the situation tested here where the signatures were not ideally separated. These results, however, are not very different and in some cases are inferior to those generated using more conventional recognition algorithms. It is clear that the accuracy of the result improves

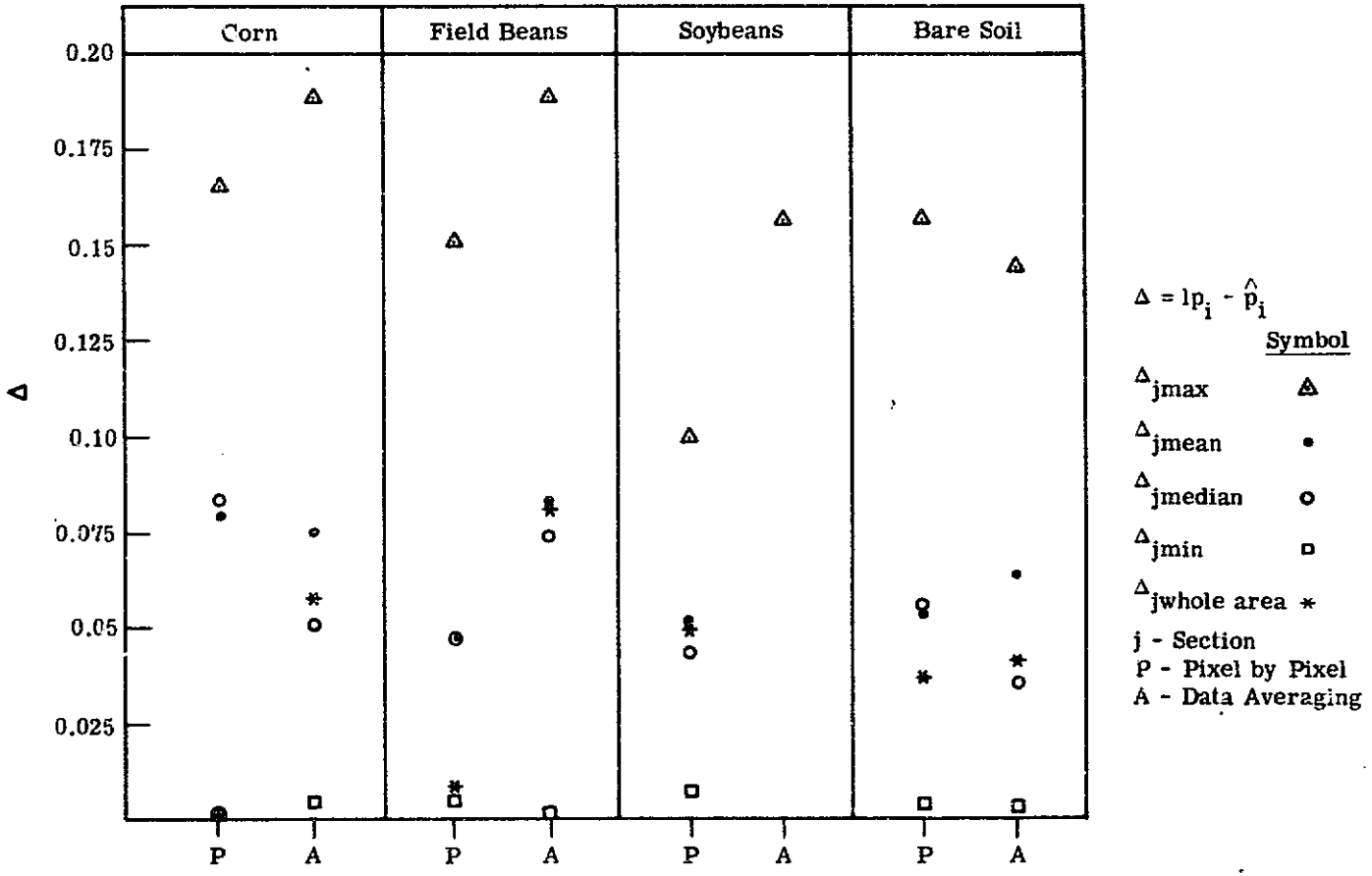

FIGURE 29. PROPORTION ESTIMATION PERFORMANCE OF AGRICULTURE

with an increase in the size of the area (i.e., number of pixels) considered. The fact that the averaging technique generated somewhat inferior results was disappointing and may be related to this particular data set. Should this be true the averaging approach, because of its economy of computation, would certainly be the most practical approach for large area inventories where it was only necessary to know the proportions of crops in a large area and not their location.

Results achieved in applying the proportion estimation algorithm to an agricultural application by another ERIM ERTS investigator were significantly more accurate [40]. In this case the problem was to accurately estimate the acreage of rice in a region where large rice fields were separated by irrigation ditches. Boundary pixels containing portions of rice and ditch were being misclassified by conventional recognition techniques with a resulting loss of acreage estimation accuracy. When the ERIM proportion estimation algorithm was applied to the boundary pixels much improved results were achieved. The acreage accuracy increased from 84.4% to 99.8%.

5.4 CONCLUSIONS AND RECOMMENDATIONS

In the beginning of this section we described the problem of proportion estimation associated with data gathered by coarse spatial resolution sensors such as the MSS of ERTS-1. We then described an approach to the solution of this problem which was developed at ERIM. The test and evaluation of this approach was described for two problems; the estimation of the proportion of water in a scene and the estimation of the proportion of agricultural crops in a scene.

For the estimation of the proportion of water in an ERTS scene we showed that the ERIM algorithm did a more accurate job of both detecting water bodies and identifying their acreage than other available techniques. As might be expected, the largest improvement was achieved on the smaller lakes and ponds which in most cases were totally undetected by more conventional techniques. Improvements were also achieved for the larger bodies of water, especially with regard to the accurate duplication of their shape on a digital map printout.

The accuracy in estimating proportions of various ground covers in an agricultural scene using the ERIM proportion estimation algorithm exhibited little or no improvement over that achievable using more conventional recognition algorithms. While this result was disappointing it was not totally surprising since only three of the four bands of ERTS data available for this test were of sufficient quality to be used, thereby reducing the overall spectral differences between the ground covers in a situation where the spectra were already similar. Nevertheless, the effect of some of the restrictions imposed by this original ERIM proportion estimation algorithm were more clearly identified.

In recent months, as a result of the information made available through this and other investigations carried out at ERIM, the proportion estimation algorithm has been modified. The modifications have eliminated some of the restrictions and limitations formerly imposed and it is our expectation that improved proportion estimation accuracies should be possible. We recommend that the modified ERIM proportion estimation algorithms be fully tested and evaluated to adequately establish their performance characteristics.

APPENDIX A
CONTAMINATED ATMOSPHERES AND REMOTE SENSING

by
Robert E. Turner
(Reprint)

Originally presented at

Third Remote Sensing of Earth Resources Conference
March 25-27, 1974

The University of Tennessee Space Institute
Tullahoma, Tennessee

and Published in Vol. III of Conference Proceedings

CONTAMINATED ATMOSPHERES AND REMOTE SENSING

Robert E. Turner*

Environmental Research Institute of Michigan
P. O. Box 618, Ann Arbor, Michigan

Abstract

The effects of absorption and multiple scattering of radiation by Earth's atmosphere, especially under hazy conditions, significantly diminish one's ability to recognize terrain features in the processing of multispectral remote sensing data. As a result, it is desirable that an atmospheric-radiative-transfer model be used to account for these systematic atmospheric variations. The radiative-transfer model presented here is used to describe the radiation field in a realistic atmosphere composed of aerosol particles which can scatter and absorb radiation by varying amounts. Using Mie scattering theory in conjunction with empirical results on basic atmospheric constituents, a detailed analysis was made to determine the single-scattering albedo vertical profile for various atmospheric states. The results of this study clearly show that the refractive index of aerosol particles is an important factor which should be taken into consideration in the processing of multispectral data.

Introduction

One of the most important aspects of the remote sensing of Earth's surface is the discrimination between specific targets and backgrounds. The multispectral method is one way of performing the discrimination, that is, one analyzes the radiation received in several wavelength intervals and assumes that surface features possess sufficiently different reflectance properties in those intervals such that a unique

* Research Physicist, Infrared and Optics Division

C-2

spectral signature exists for a class of objects. This multispectral method has been applied successfully to a number of applications[1,2] in the fields of agriculture, geology, forestry, hydrology, atmospheric science, and oceanography to name just a few.

Besides the natural or intrinsic variability in the surface features of interest, there is a variation due to the atmosphere. As the sensor passes over different regions of the atmosphere the aerosol component may change or the sun angle may change depending upon the orientation of the aircraft or spacecraft. These and other systematic variations can bias the intrinsic data which are truly representative of the objects on the surface. For this reason it is necessary to have a model which can account for these systematic variations and to generate algorithms which can be used to correct the data.

Previous studies[3,4,5] have resulted in an atmospheric-radiative-transfer model which has been used to calculate the natural radiation field in a plane-parallel, homogeneous, atmosphere bounded by a uniform Lambertian surface. The model, however, excluded absorption by gases and aerosols whereas the improved version presented here includes the effects of aerosol absorption and absorption by the gas ozone in the visible part of the spectrum.

The Radiative Transfer Model

The spectral radiance received by a downward directed sensor at some point either within or outside of the atmosphere is given by the simple equation

$$L_T = L_0 T + L_p \qquad (1)$$

in which L_T is the total spectral radiance at the sensor, L_0 is the spectral radiance at the surface, T is the spectral transmittance from the surface (target) to the sensor, and L_p is the spectral path radiance, i.e., the radiance along the path connecting the target to the sensor as a result of radiation scattered and emitted by the atmosphere. Assuming some knowledge of the atmospheric state and the surface conditions one should be able to calculate all of the quantities in Eq. (1).

The general equation which is used to describe the transfer of radiation in a horizontally homogeneous, plane-parallel, scattering, absorbing, and emitting atmosphere is given by

$$\mu \frac{dL}{d\tau} = L(\tau,\mu,\phi) - \frac{\omega_o(\tau)}{4\pi}\int_0^{2\pi}\int_{-1}^{1} p(\tau,\mu,\phi,\mu',\phi')L(\tau,\mu',\phi')d\mu'd\phi'$$

$$- \frac{\omega_o(\tau)}{4\pi} E_o e^{-\tau/\mu_o} p(\tau,\mu,\phi,-\mu_o,\phi_o) = [1-\omega_o(\tau)]B(\tau) \qquad (2)$$

where the first term on the right hand side of the equation is the diffuse radiance at optical depth τ in a direction specified by the nadir view angle $\theta(= \cos^{-1}\mu)$ and azimuth angle ϕ. The second term represents the radiation scattered from a direction (μ',ϕ') into the direction (μ,ϕ) with an angular distribution determined by the single-scattering phase function $p(\tau,\mu,\phi,\mu',\phi')$. The third term is the source term for singly-scattered solar radiation, i.e., radiation which is scattered once from the solar direction (μ_o,ϕ_o) into the direction (μ,ϕ) with an extraterrestrial solar irradiance E_o. The last term is the contribution due to thermal emission by the atmosphere with a Planck radiation function $B(\tau)$. A very important quantity in the above equation is the single-scattering albedo $\omega_o(\tau)$, a dimensionless number which indicates the amount of scattering. If $\omega_o(\tau) = 0$, there is no scattering and all of the diffuse radiance is due to thermal emission. On the other hand, if $\omega_o(\tau) = 1$, there is no absorption and all of the diffuse radiation arises from multiple scattering. For values of $\omega_o(\tau)$ between zero and one there is a combination of scattering and absorption. If we confine our attention to the visible and near infrared part of the spectrum, then the contribution from thermal emission is negligible and we can drop the last term in Eq. (2). Using a modified two-stream approximation[3,5] an approximate solution was found for the integro-differential equation of transfer for the case of homogeneous atmospheres, i.e., those in which $\omega_o(\tau)$ and $p(\tau,\mu,\phi,\mu',\phi')$ are independent of optical depth τ. The results of the analysis of this equation will be presented in the last section of this paper, but it is first necessary that we calculate the pertinent atmospheric optical parameters.

The Atmospheric State

Gases

The major permanent gas components of our atmosphere are molecular nitrogen, oxygen, and argon, none of which absorb much radiation in the visible and near infrared portion of the electromagnetic spectrum. The most important absorbers of radiation in the near infrared are ozone, water vapor, and

carbon dioxide, whereas in the visible it is the ozone Chappuis band in the range 0.440 μm to 0.74 μm which is of importance. The maximum concentration usually occurs at an altitude of 23 km.

Aerosols

Embedded in the gaseous atmosphere is a semi-permanent suspension of liquid and solid particles called an aerosol. The particles arise from a variety of natural and anthropogenic sources such as, volcanoes, forest fires, dust storms, sea spray, industrial smokestacks, and automobile exhaust. From such varied sources the particles coalesce, evaporate, and condense to produce a distribution of shapes, sizes, and compositions. The shape of liquid particles is probably that of a sphere whereas solid particles may have any shape whatever. However, for a collection of particles in random orientations we can probably assume that the scattering effect is approximately the same as that for a collection of spheres. The sizes of particles range from 10^{-7} cm to 10^{-4} cm with an approximate Gaussian type distribution. Several hazes have been suggested by Deirmendjian[6] and Junge[7], each characterized by a specific particle size distribution function. The composition of aerosols can vary from pure water to highly absorbing soot-like particles. We shall denote the composition by the complex refractive index $m(\lambda)$, i.e.,

$$m(\lambda) = m_1(\lambda) - im_2(\lambda) \qquad (3)$$

If the imaginary part, $m_2(\lambda)$ is zero the particles do not absorb any radiation, but for values of $m_2 > 0.1$ the absorption can be quite important.

Single-Scattering Albedo

Knowing the complex refractive index, the scattering, absorption, and total (extinction) cross sections can be calculated by using the standard Mie formulas, and, by selecting a particular size distribution one can calculate the absorption, scattering, and extinction coefficients as a function of wavelength λ, refractive index $m(\lambda)$, size distribution s, and altitude z. Thus, we have

$$\alpha(\lambda,m,s,z) = \alpha_R(\lambda,z) + \alpha_A(\lambda,m,s,z) \qquad (4)$$

$$\beta(\lambda,m,s,z) = \beta_R(\lambda,z) + \beta_A(\lambda,m,s,z) \qquad (5)$$

$$\kappa(\lambda,m,s,z) = \kappa_R(\lambda,z) + \kappa_A(\lambda,m,s,z) \qquad (6)$$

for the volume absorption, scattering, and extinction coefficients respectively. The first term on the right hand side of Eqs. (4), (5), and (6) represents the coefficient for the Rayleigh (pure gas) situation and the second term represents the corresponding aerosol coefficient. Now, defining an absorptivity parameter[9] f as

$$f = 1 - \frac{\beta_A(\lambda,m,s,z)}{\kappa_A(\lambda,m,s,z)} \tag{7}$$

and the single-scattering albedo ω_o as

$$\omega_o(\lambda,m,s,z) = \frac{\beta_R(\lambda,z) + \beta_A(\lambda,m,s,z)}{\kappa(\lambda,m,s,z)} \tag{8}$$

we get the following expression for ω_o:

$$\omega_o(\lambda,m,s,z) = \frac{f\beta_R(\lambda,z)-(1-f)\alpha_R(\lambda,z)}{\kappa(\lambda,m,s,z)} + 1 - f \tag{9}$$

It should be noted that if there is no aerosol absorption then $f = 0$ and if there is complete aerosol absorption, $f = 1$. These extreme conditions are illustrated in Fig. 1 for a wavelength of 0.60 μm. The values of the total extinction coefficients, $\kappa(\lambda,m,s,z)$ were taken from tables by Elterman[10] in which $\kappa(\lambda,m,s,z)$ is given in terms of wavelength, altitude, and visual range. With no aerosol absorption the albedo decreases with altitude due to ozone absorption but only by a significant amount above an altitude of 10 km. With complete aerosol absorption, the albedo increases rapidly as we go up through the lower troposphere but it decreases as we reach the ozone layer.

By varying the complex refractive index we can see the effect of ever increasing aerosol absorption. This is illustrated in Fig. 2 for a very hazy atmosphere. The $m_2 = 0.01$ case corresponds to a small amount of aerosol absorption and one can see that the albedo is rather large, especially near the surface. For the $m_2 = 1.0$, i.e., strong aerosol absorption, the albedo is much less. It should also be noted that there is a strong wavelength dependence particularly for the upper part of the atmosphere where ozone absorption is significant.

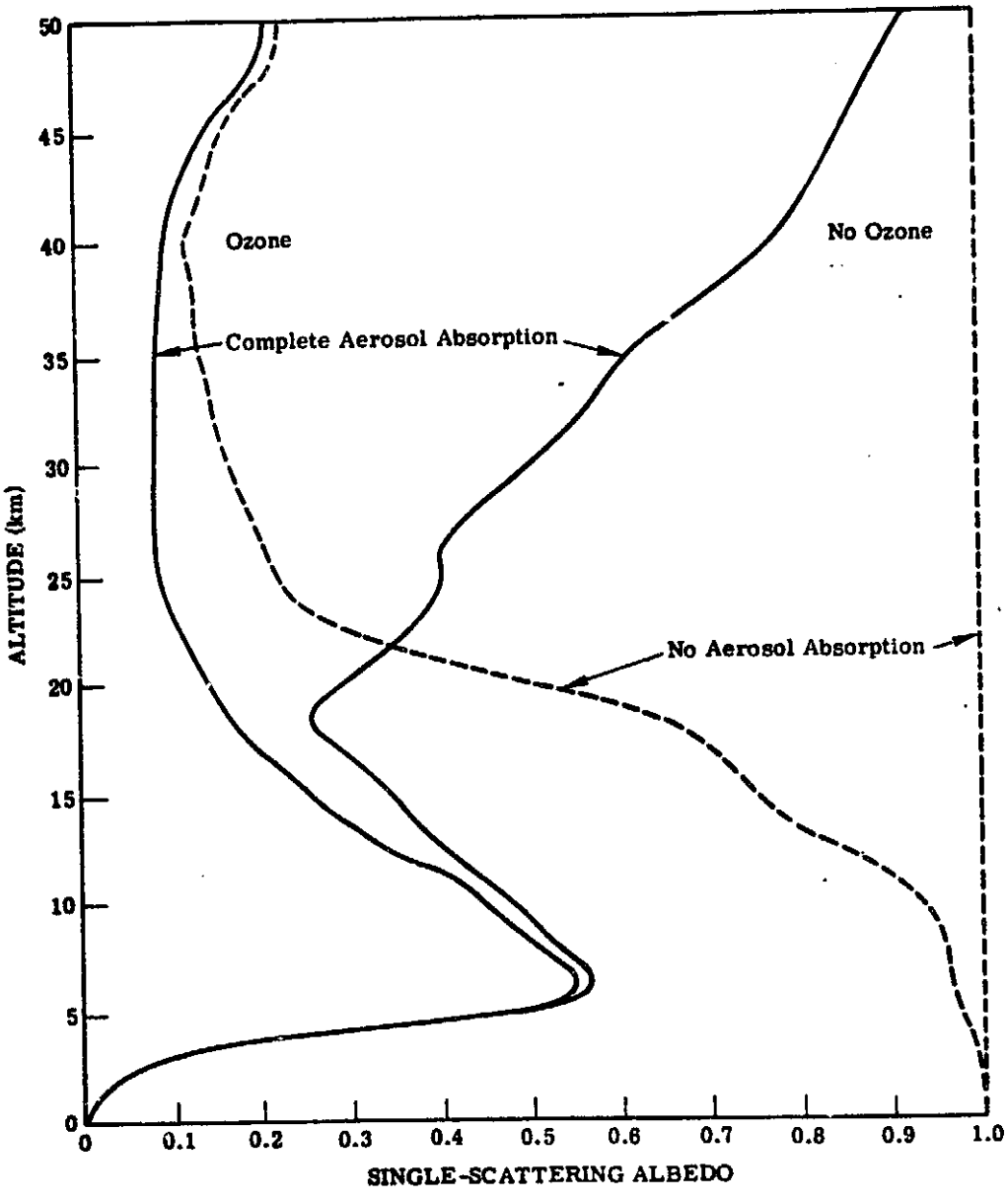

FIGURE 1. ALTITUDE PROFILE OF THE SINGLE-SCATTERING ALBEDO WITH AND WITHOUT OZONE.
Wavelength = 0.6 μm

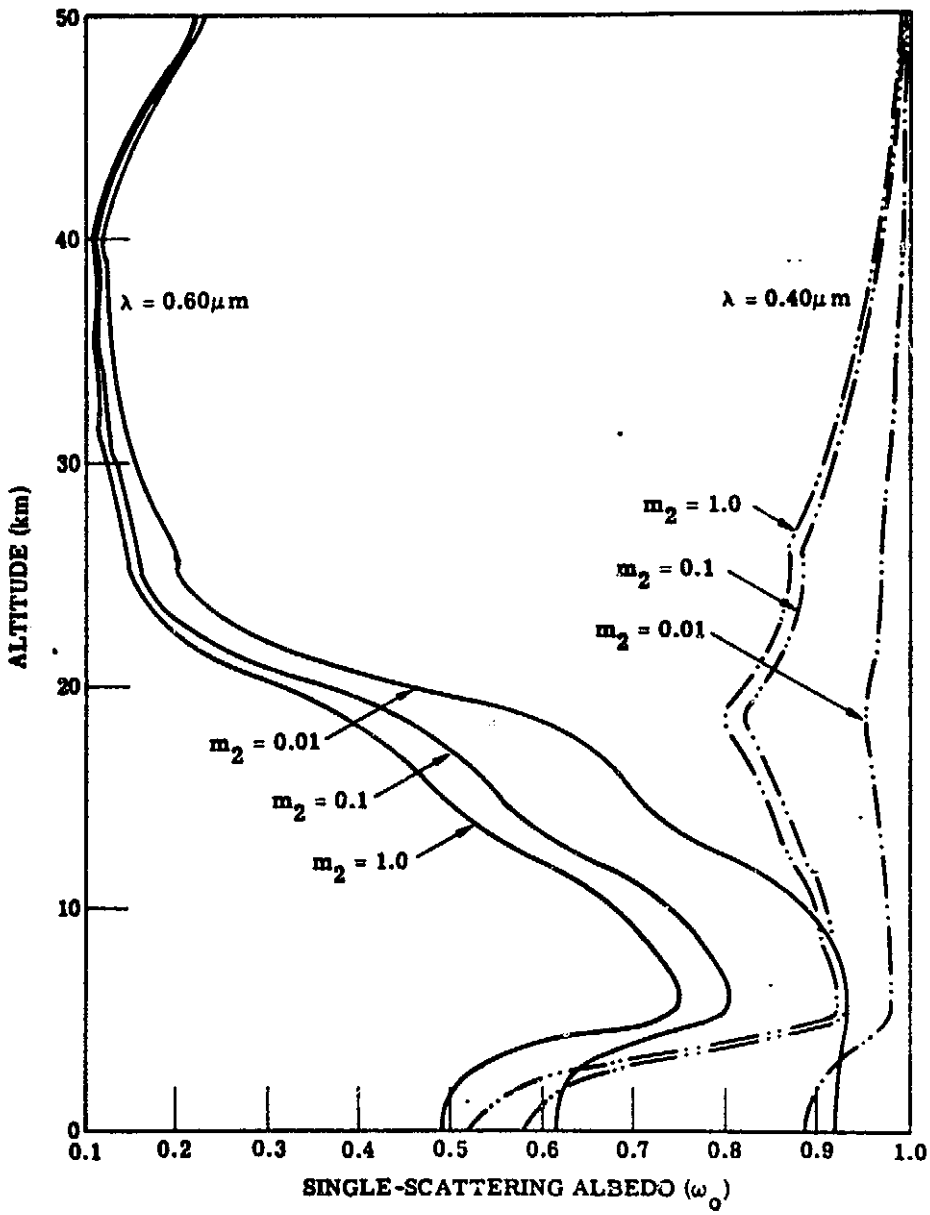

FIGURE 2. ALTITUDE PROFILE OF THE SINGLE-SCATTERING ALBEDO FOR HAZE L. Visual Range = 2 km, complex refractive index $m = 1.5 - im_2$.

Phase Functions

Tables of the single-scattering phase function have been calculated for different refractive indices. The effect of varying the amount of aerosol absorption is easily seen in Fig. 3. For the strong absorption case, the phase function is more anisotropic than in the other cases and the back-scattering ($\chi = 180$) is much less.

Atmospheric Radiation

Using an average single-scattering albedo and the single-scattering phase functions in the atmospheric radiative-transfer model we calculated the spectral radiance for various combinations of refractive indices, wavelengths, altitudes, sun angles, surface reflectances, and view angles.

Figure 4 depicts the path radiance and the total (path plus attenuated surface) radiance for a moderately hazy atmosphere. It should be noted that the non-absorption case gives a radiance almost twice that of the strong absorption case. In Fig. 5 we see the same situation for a very hazy atmosphere and in this case the ratio of the radiances is about eight. In both cases the size distribution of the aerosol particles was that corresponding to a general continental haze, called haze L.

The altitude dependence of radiance for no aerosol absorption and strong aerosol absorption is illustrated in Fig. 6 for a moderate haze. The radiance increases uniformly and approaches an asymptotic value at an altitude of about 30 km. Figure 7 depicts the same situation except that the atmosphere has more haze. In the latter case it is interesting to note that in the strong absorbing aerosol the total radiance first decreases with altitude and then gradually increases. This is due to the fact that the transmission loss is greater than the increase as a result of multiple scattering. However, as we go to greater altitudes the path radiance dominates and always causes an increase with altitude. The change in path radiance as a function of altitude for various refractive indices is illustrated in Fig. 8 for a very hazy atmosphere. As the amount of absorption increases the path radiance decreases, especially for the case of $m_2 > 0.01$, i.e., for moderate absorption. Beyond $m_2 \simeq 0.10$, the effect of an increase in the refractive index has is less noticeable.

The total spectral radiance at an altitude h is given by

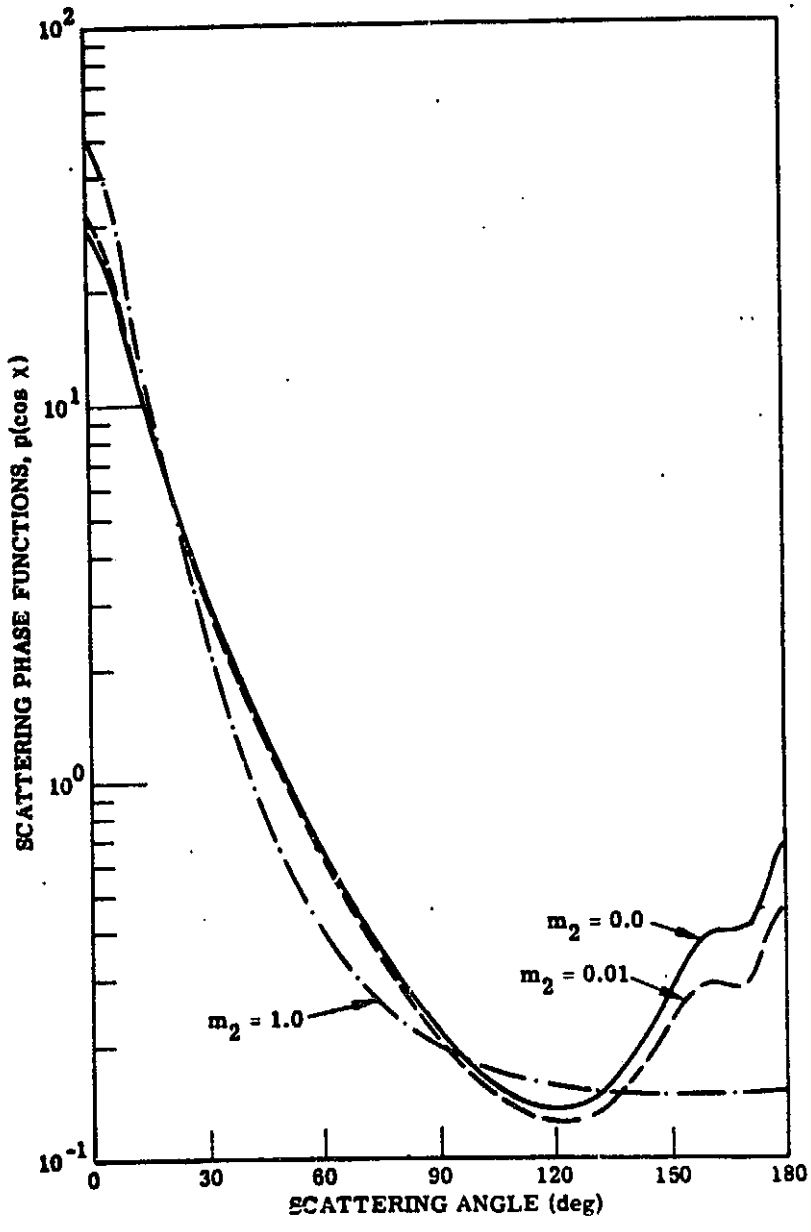

FIGURE 3. SCATTERING PHASE FUNCTIONS AS CALCULATED FROM MIE THEORY FOR HAZE L - COMPLEX REFRACTIVE INDEX $m = 1.5 - im_2$. Wavelength = 0.55 μm

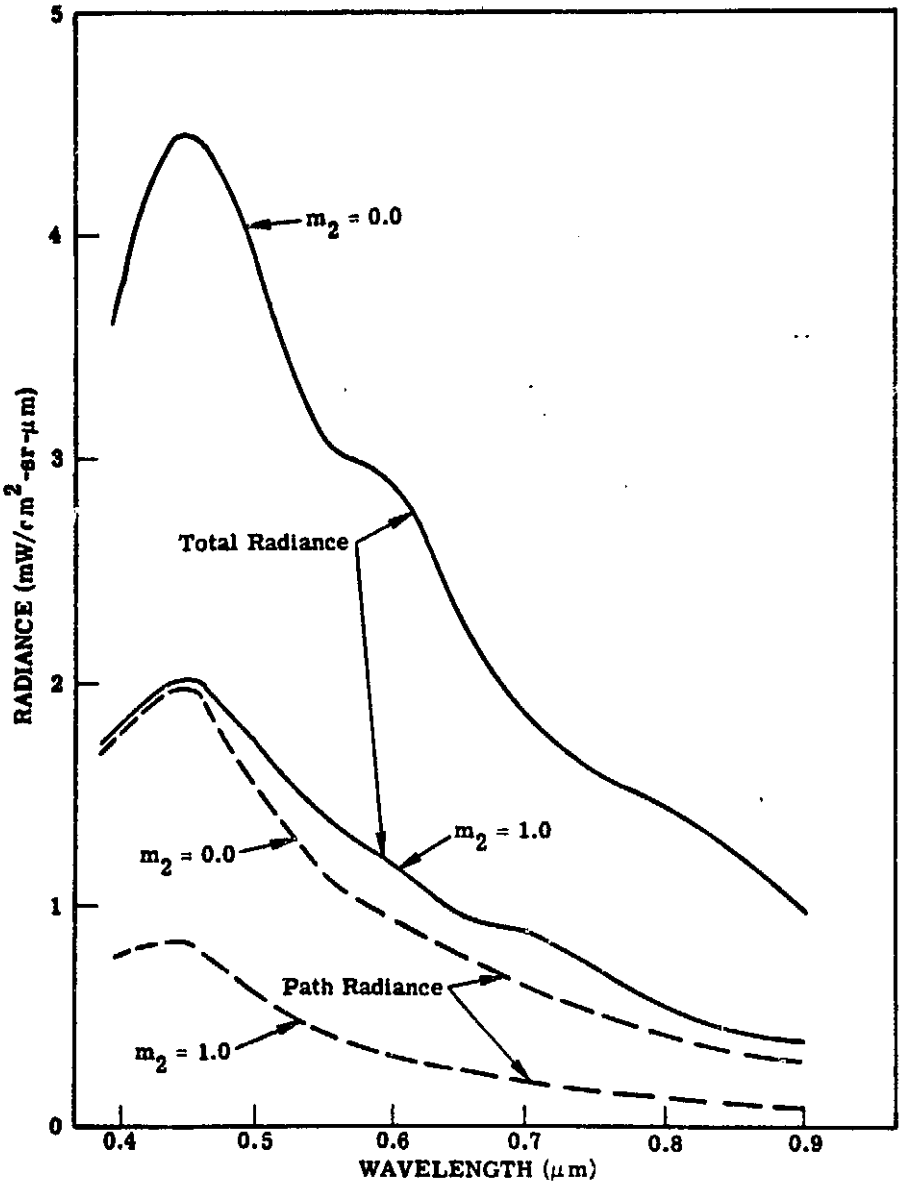

FIGURE 4. Dependence of Path Radiance and Total Radiance on Wavelength for Haze L. Altitude=1 km, Solar Zenith Angle = 30°, Nadir Angle=0°, Visual Range=23km, Target Reflectance=0.10, Background Albedo=0.10, Refractive Index $m=1.5-im_2$

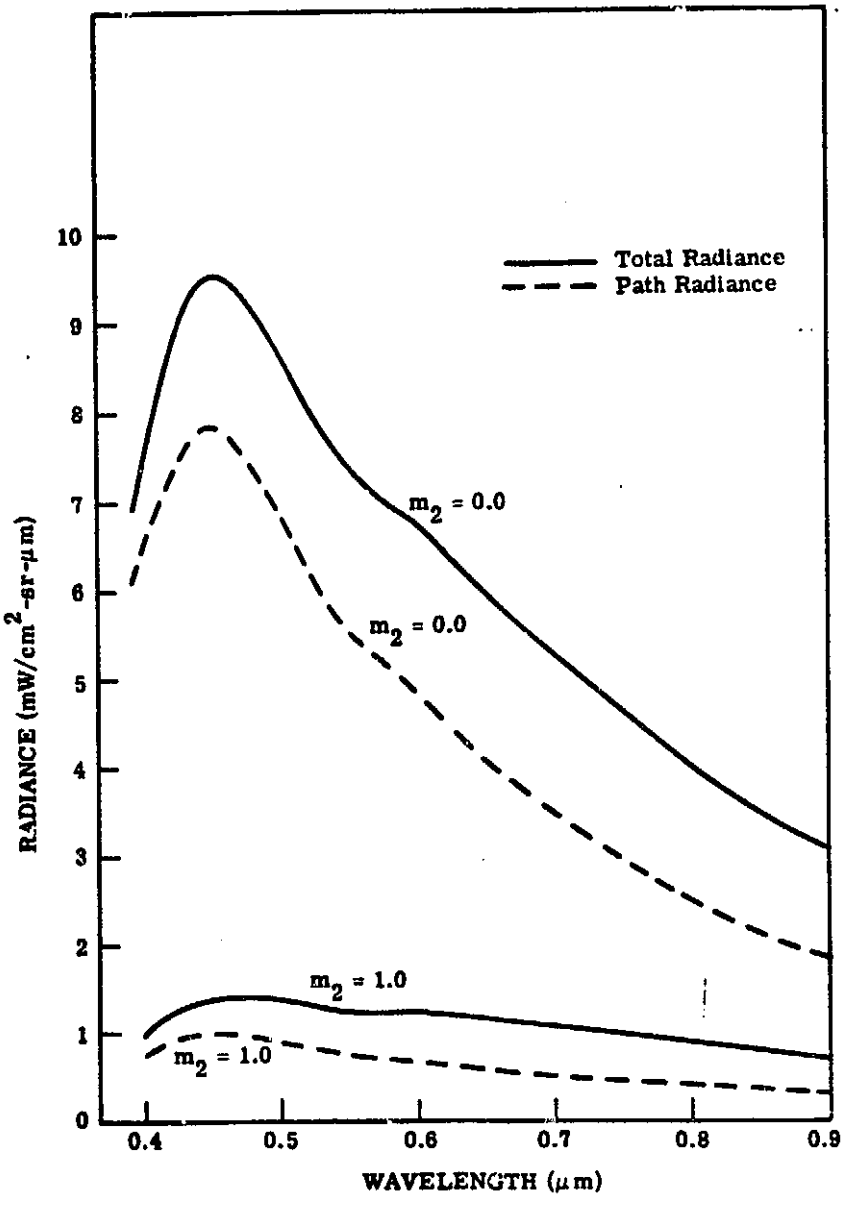

FIGURE 5. DEPENDENCE OF PATH RADIANCE AND TOTAL RADIANCE ON WAVELENGTH FOR HAZE L - VISUAL RANGE = 2 km. Altitude = 1 km, solar zenith angle = 30°, nadir angle = 0°, target reflectance = 0.1, background albedo = 0.1, complex refractive index m = 1.5 - im_2.

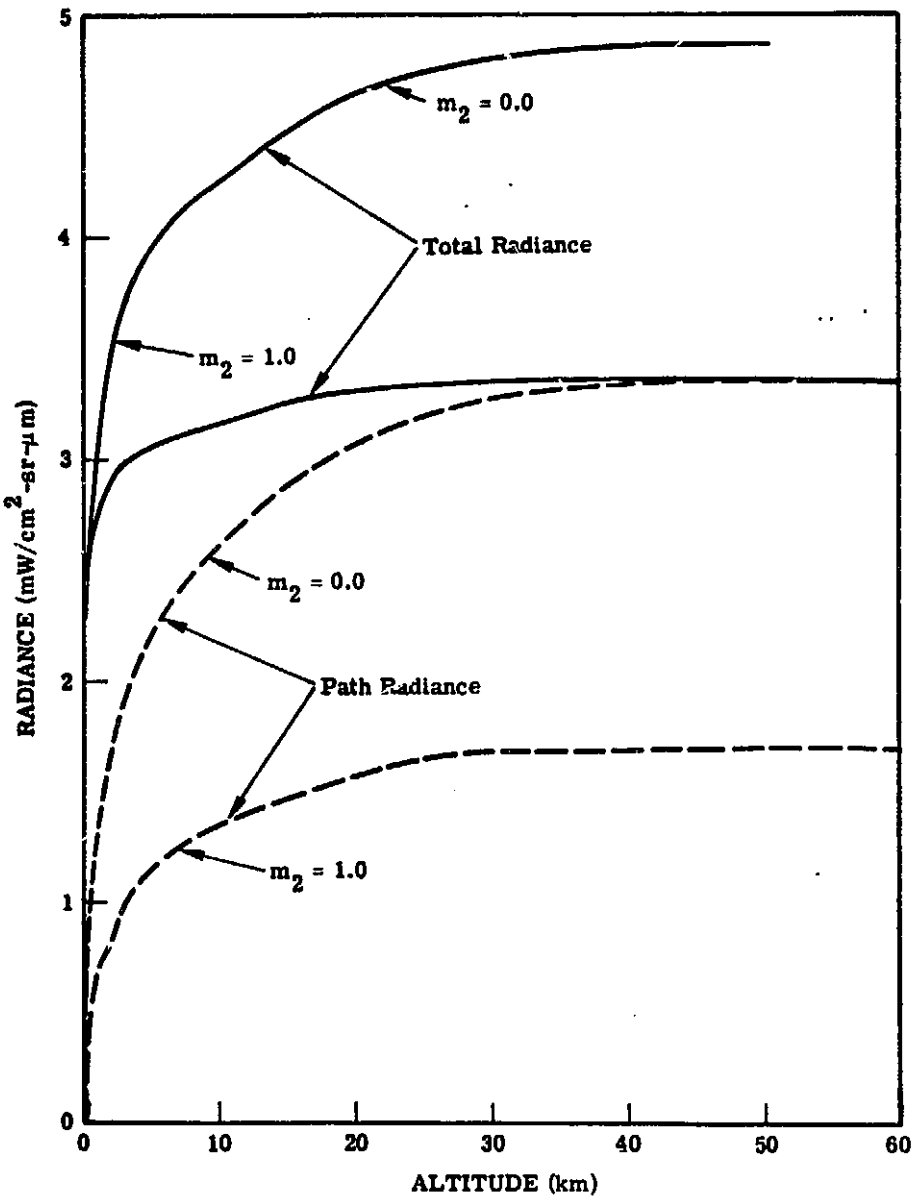

FIGURE 6. DEPENDENCE OF PATH RADIANCE AND TOTAL RADIANCE ON ALTITUDE FOR HAZE L - VISUAL RANGE = 23 km. Wavelength = 0.55 μm, solar zenith angle = 30°, nadir angle = 0°, target reflectance = 0.1, background albedo = 0.1, complex refractive index $m = 1.5 - im_2$.

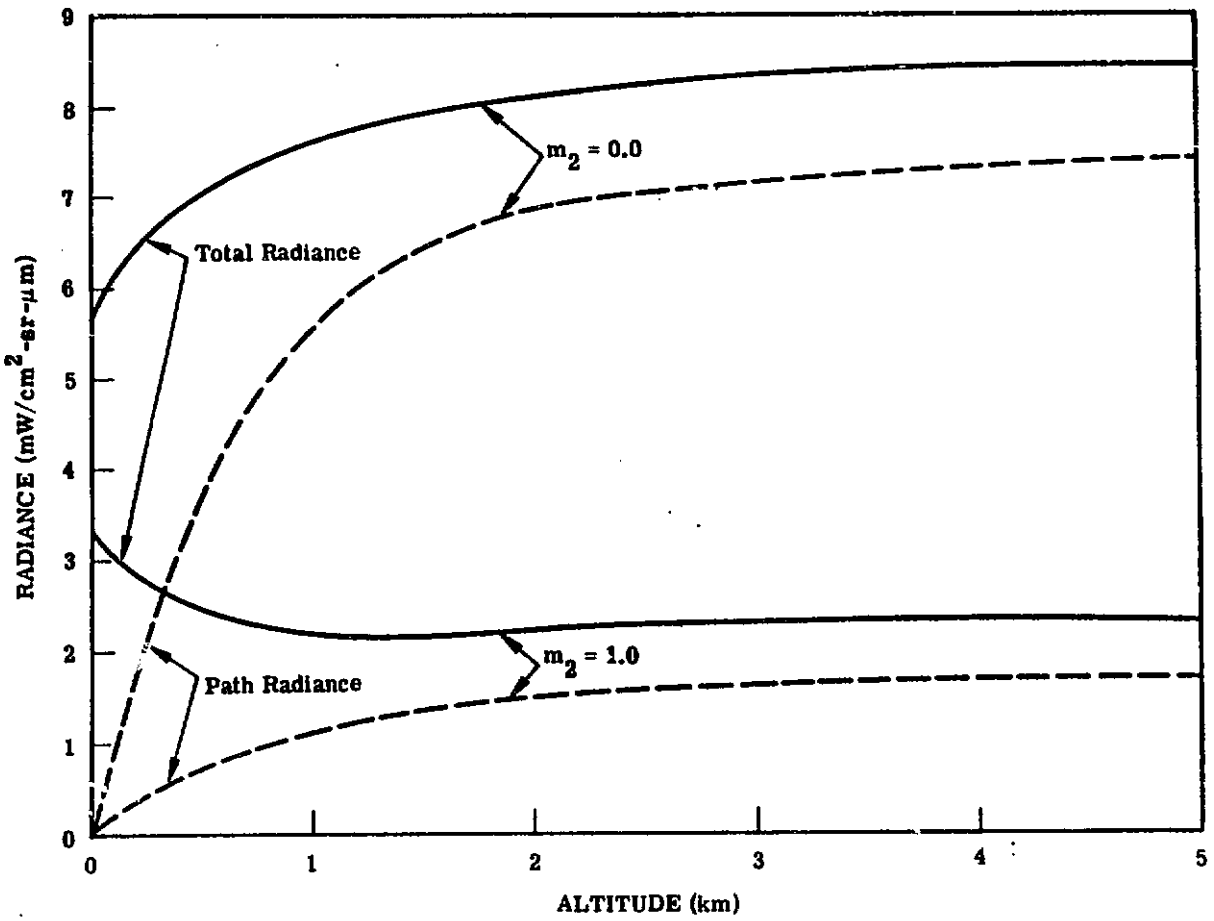

FIGURE 7. DEPENDENCE OF PATH RADIANCE AND TOTAL RADIANCE ON ALTITUDE IN THE LOWER TROPOSPHERE FOR HAZE L. Wavelength = 0.55 μm, solar zenith angle = 30°, nadir angle = 0°, visual range = 2km, target reflectance = 0.1, background albedo=0.1, complex refractive index $m=1.5-im_2$.

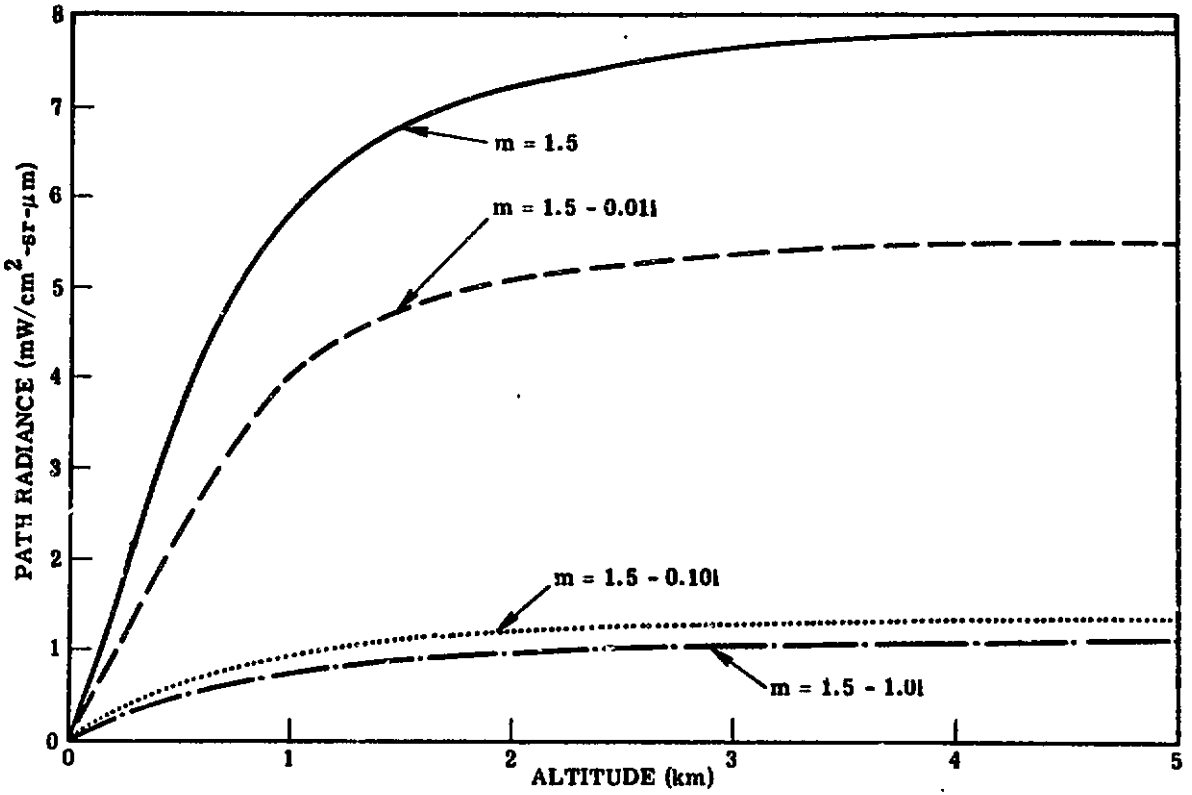

FIGURE 8. DEPENDENCE OF PATH RADIANCE ON ALTITUDE IN THE LOWER TROPOSPHERE FOR SEVERAL REFRACTIVE INDICES. Wavelength = 0.55 μm, solar zenith angle = 30°, nadir view angle = 0°, target reflectance = 0.1, background reflectance = 0.1, visual range = 2 km.

$$L_T(\lambda,h,m,s,V,\theta_o,\theta,\phi,\rho,\bar{\rho}) = L_A(\lambda,h,m,s,V,\theta_o,\theta,\rho,\bar{\rho}) + L_p(\lambda,h,m,s,V,\theta_o,\theta,\phi,\bar{\rho})$$

where L_A and L_p are the attenuated and path radiances respectively. L_A is the radiance at the surface attenuated up to the altitude h of the sensor. The quantity m is refractive index, s is the atmospheric state parameter which describes a particulate size distribution, V is the horizontal visual range at the surface, θ_o is the solar zenith angle, θ is the nadir view angle, ϕ is the azimuthal angle, and ρ and $\bar{\rho}$ are the target and background reflectances respectively. In Fig. 9 is illustrated the three radiances for a "clean", i.e., non-absorbing aerosol atmosphere and for a "contaminated" or strongly absorbing aerosol atmosphere. Here we see clearly the effect discussed earlier. The transmission loss causes a large decrease in the attenuated radiance with increasing altitude whereas just the opposite effect occurs for path radiance. In a "clean" atmosphere the path radiance does not increase fast enough to overcome the loss due to transmission, especially at low altitudes, but for contaminated atmospheres the path radiance increase is more rapid.

Finally, the effect of varying the view angle is illustrated in Fig. 10. A sensor is imagined to be located at an altitude of 2 km scanning the surface in the plane of the sun. As expected, the increasing amount of absorption causes a decrease in the path radiance and in approximately the same relative way regardless of the amount of absorption.

Conclusions

In this study of the natural radiation field in Earth's atmosphere, the atmospheric optical parameters, single-scattering albedo, and the single-scattering phase function were modeled in order to simulate the conditions for contaminated atmospheres. This was done by varying the imaginary part of the particulate refractive index which is indicative of the aerosol absorption. All degrees of atmospheric haze were studied, from a very heavy haze, characterized by a visual range of 2 km, to the clearest conditions possible, i.e., a pure Rayleigh atmosphere.

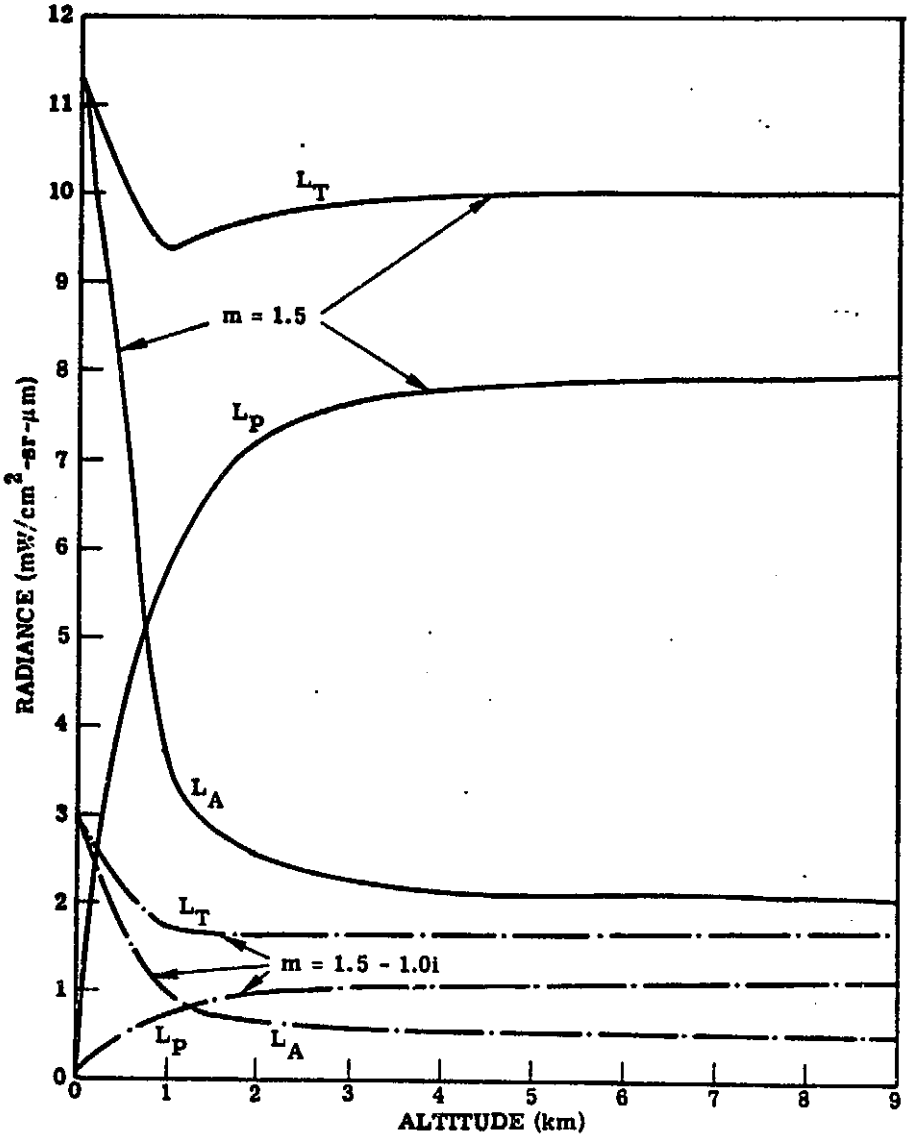

FIGURE 9. DEPENDENCE OF PATH RADIANCE, ATTENUATED RADIANCE AND TOTAL RADIANCE ON ALTITUDE FOR NO ABSORPTION AND HEAVY ABSORPTION. Wavelength = 0.55 μm, solar zenith angle = 30°, nadir view angle = 0°, target reflectance = 0.1, background reflectance = 0.1, visual range = 2 km.

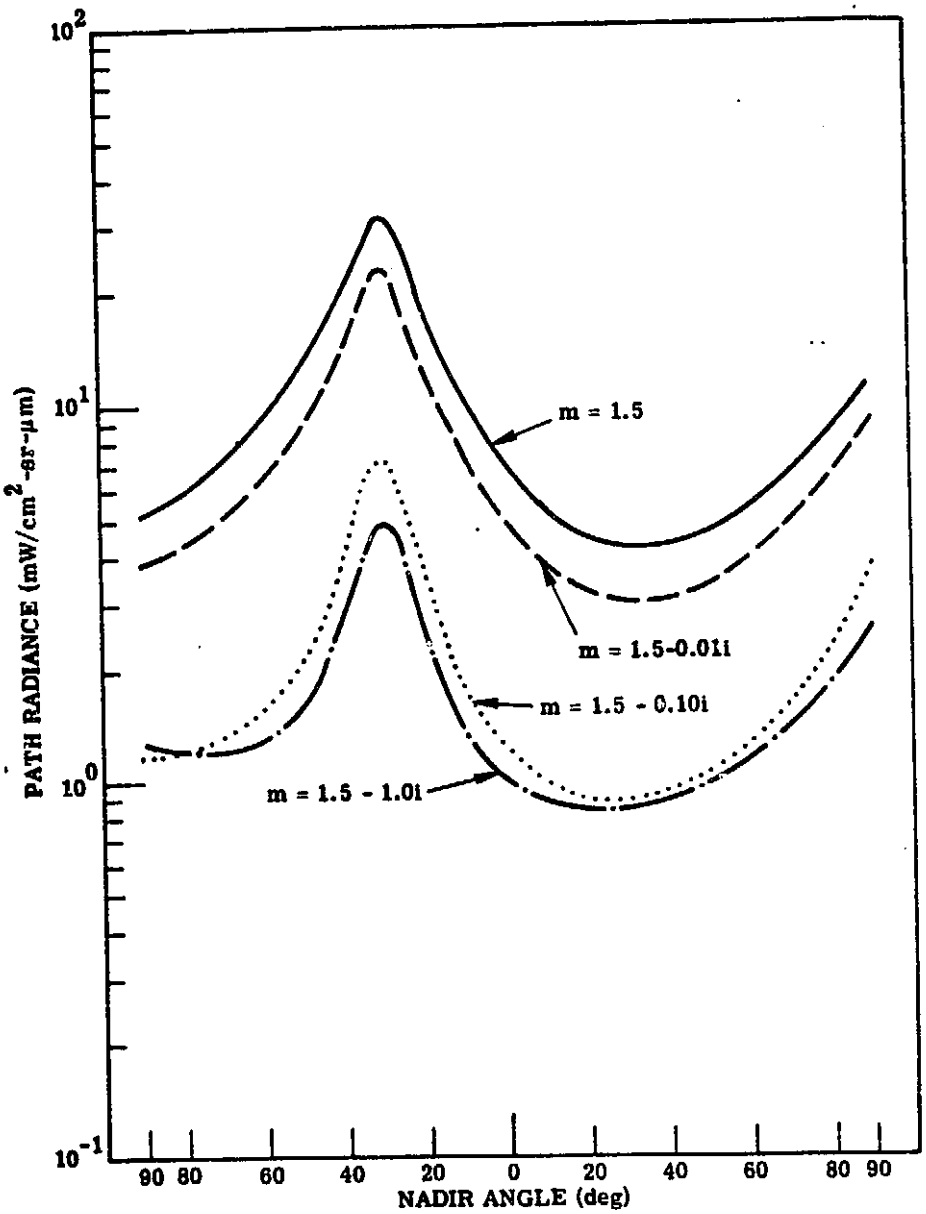

FIGURE 10. Dependence of Path Radiance on Nadir View Angle in the Solar Plane for Several Refractive Indices. Wavelength = 0.55 μm, Altitude = 2 km, Solar zenith Angle = 30°, Target Reflectance = 0.10, Background Reflectance = 0.10, Visual Range = 2 km.

The results show that by increasing the amount of absorption the radiance decreases, although in a non-linear way, i.e., eventually complete absorption is reached. Furthermore, the variation of radiance with altitude and view angle is essentially the same as for the non-absorption case.

The question naturally arises as to what value of complex refractive index does one choose in the analysis of multispectral data. For "clean" water type aerosols, the refractive index in the visible and near infrared region is real and equal to $\sim$ 1.34. On the other hand, for contaminated air filled with various amounts of silicate and soot-like particles the refractive index may be 1.55 - 0.1 i, with considerable variation in the imaginary part. In actual practice, therefore, one should conduct in situ sampling of the atmosphere, i.e., perform measurements of particulate composition and size distribution using radiometric techniques or collect air samples and perform laboratory measurements to determine refractive index. If the complex refractive index is known, along with the approximation size distribution, and the horizontal visual range, then one can relate measured radiances to the calculated ones and thereby develop techniques for the removal of atmospheric variations from multispectral data.

References

[1]Remote Sensing, With Special Reference to Agriculture and Forestry, National Academy of Sciences, Washington, D.C., 1970.

[2]Nalepka, R.F., Investigation of Multispectral Discrimination Techniques, Infrared and Optics Laboratory, Willow Run Laboratories, Institute of Science and Technology, The University of Michigan, 2264-12-F, Jan., 1970.

[3]Malila, W.A., Crane, R.B., Omarzu, C.A., and Turner, R.E., Studies of Spectral Discrimination, Infrared and Optics Laboratory, Willow Run Laboratories, Institute of Science and Technology, The University of Michigan, WRL 31650-22-T, May, 1971.

[4]Malila, W.A., Crane, R.B., and Turner, R.E., Information Extraction Techniques for Multispectral Scanner Data, Infrared and Optics Laboratory, Willow Run Laboratories, Institute of Science and Technology, The University of Michigan, WRL 31650-74-T, June, 1972.

[5]Turner, R.E., Atmospheric Effects in Remote Sensing, Remote Sensing of Earth Resources, Vol. II, Ed., F. Shahrokhi, The University of Tennessee, Tullahoma, Tennessee.

[6]Deirmendjian, D., Electromagnetic Scattering on Spherical Polydispersions, American Elsevier Publishing Company, Inc., New York, 1969.

[7]Junge, C.E., Journal Meteorol., 12, 1955.

[8]van de Hulst, H.C., Light Scattering by Small Particles, John Wiley & Sons, Inc., New York, 1957.

[9]Turner, R.E., Radiative Transfer in Real Atmospheres, Infrared and Optics Division, Environmental Research Institute of Michigan, 190100-24-T, 1974.

[10]Eltermann, L., U.V., Visible and IR Attenuation for Altitudes to 50 km., 1968, Report No. AFCRL-68-0153, Air Force Cambridge Research Laboratories, Office of Aerospace Research, Bedford, Massachusetts, 1968.

Appendix B

DETAILED RECOGNITION PERFORMANCE MATRICES

TABLE B-1. ERTS SIGNATURE EXTENSION, UNADJUSTED EATON SIGNATURES APPLIED TO IONIA AND CLINTON COUNTY DATA.(12 SIGNATURES, 7 CLASSES, 0.001 THRESHOLD.)

PERCENTS OF TOTAL NUMBER OF POINTS IN EACH CLASS

BY CLASSES OF PLOTS AND CLASSES OF SIGNATURES

CLASS	NR. PLOTS	NR. POINT	SIGNATURES.. CORN	SENESC. VEG.	SOY BEANS	ALFA	TREES	GRASS	SOIL	POINTS IN CLASS: NOT CLASD	RIGHT (OF ALL)	WRONG (OF ALL)	RIGHT (OF CLASD)	WRONG (OF CLASD)	ASS'D FROM OTHER CLASS
CORN	37	295	57.3	40.7		.3	.3	1.4		.0	57.3	42.7	57.3	42.7	5.2
SENESC. VEG.	49	258	.8	49.6	21.3	12.8		1.6	14.0	.0	64.0	36.0	64.0	36.0	30.6
SOYBEANS	6	27	3.7	3.7	92.6					.0	92.6	7.4	92.6	7.4	8.6
DECID.TREES	7	47	36.2	4.3	2.1	2.1	55.3			.0	55.3	44.7	55.3	44.7	.2
BARE SOIL	11	53							100.0	.0	100.0	.0	100.0	.0	5.7
	110	680								.0	64.4	35.6	64.4	35.6	
AVG. OVER PCINTS											64.1	35.9	64.1	35.9	
AVG. OVER PLOTS											73.8	26.2	73.8	26.2	10.0
OVER CLAS BY PCINT											69.2	30.8	69.2	30.8	
OVER CLASS BY PLOT															

TABLE B-2. ERTS SIGNATURE EXTENSION, MLA-I EATON SIGNATURES APPLIED TO IONIA AND CLINTON COUNTY DATA. (12 SIGNATURES, 7 CLASSES, 0.001 THRESHOLD.)

PERCENTS OF TOTAL NUMBER OF POINTS IN EACH CLASS

BY CLASSES OF PLOTS AND CLASSES OF SIGNATURES

			SIGNATURES..					POINTS IN CLASS					ASS'D FROM
CLASS	NR. PLOTS	NR. POINT	CORN	SOY BEANS	TREES	BARE SOIL	SENESC VEG.	NOT CLASD	RIGHT (OF ALL)	WRONG (OF ALL)	RIGHT (OF CLASD)	WRONG (OF CLASD)	OTHER CLASS
CORN	37	297	61.3	.3	26.6		11.8	.0	61.3	38.7	61.3	38.7	7.8
SOYBEANS	6	27		88.9	7.4		3.7	.0	88.9	11.1	88.9	11.1	9.0
TREES	6	47	4.3		91.5		4.2	.0	91.5	8.5	91.5	8.5	12.7
BARE SOIL	10	53				86.8	13.2	.0	86.8	13.2	86.8	13.2	4.1
SENESC. VEG.	48	260	10.8	22.3		10.0	55.0	1.9	55.0	43.1	56.1	43.9	10.6
	107	684						.7	64.0	35.2	64.5	35.5	
AVG. OVER POINTS									80.1	38.9	80.5	39.5	
AVG. OVER PLOTS									76.7	22.9	76.9	23.1	8.8
OVER CLAS BY POINT									71.5	27.7	72.0	28.0	
OVER CLASS BY PLOT													

TABLE B-3. ERTS SIGNATURE EXTENSION, MLA-II EATON SIGNATURES APPLIED TO IONIA AND CLINTON COUNTY DATA. (12 SIGNATURES, 7 CLASSES, 0.001 THRESHOLD.)

PERCENTS OF TOTAL NUMBER OF POINTS IN EACH CLASS

BY CLASSES OF PLOTS AND CLASSES OF SIGNATURES

CLASS	NR. PLOTS	NR. POINT	SIGNATURES.. CORN	SOY BEANS	TREES	BARE SOIL	SENESC VEG.	NOT CLASD	POINTS IN CLASS RIGHT (OF ALL)	WRONG	RIGHT (OF CLASD)	WRONG	ASS'D FROM OTHER CLASS
CORN	37	297	67.0	.3	19.9		12.1	.7	67.0	32.3	67.5	32.5	5.9
SOYBEANS	6	27		88.9	7.4		3.7	.0	88.9	11.1	88.9	11.1	7.3
TREES	6	47	6.4		89.4		4.3	.0	89.4	10.6	89.4	10.6	5.6
BARE SOIL	10	53				88.7	11.3	.0	88.7	11.3	88.7	11.3	4.1
SENESC. VEG.	48	260	7.7	18.1		10.0	59.2	5.0	59.2	35.8	62.3	37.7	10.6
	107	684						2.2	68.1	29.7	69.7	30.3	
AVG. OVER POINTS									63.9	34.0	64.6	35.4	
AVG. OVER PLOTS									78.6	20.2	79.3	20.7	7.5
OVER CLAS BY POINT									74.1	25.0	74.4	25.6	
OVER CLASS BY PLOT													

TABLE B-4. ERTS LOCAL RECOGNITION, UNADJUSTED IONIA-CLINTON SIGNATURES APPLIED TO IONIA AND CLINTON COUNTY DATA. (7 SIGNATURES, 5 CLASSES, 0.001 THRESHOLD.)

PERCENTS OF TOTAL NUMBER OF POINTS IN EACH CLASS

BY CLASSES OF PLOTS AND CLASSES OF SIGNATURES

CLASS	NR. PLOTS	NR. POINT	SIGNATURES.. CORN	SOY BEANS	TREES	BARE SOIL	SENESC VEG.	NOT CLASS	POINTS IN CLASS RIGHT (OF ALL)	WRONG (OF ALL)	RIGHT (OF CLASS)	WRONG (OF CLASS)	ASS'D FROM OTHER CLASS
CORN	37	297	77.4		7.7		14.8	.0	77.4	22.6	77.4	22.6	4.1
SOYBEANS	6	27		85.2	7.4		7.4	.0	85.2	14.8	85.2	14.8	4.6
TREES	6	47	8.5		87.2		4.3	.0	87.2	12.8	87.2	12.8	3.9
BARE SOIL	10	53				94.3	5.7	.0	94.3	5.7	94.3	5.7	1.4
SENESC. VEG.	48	260	4.6	11.5		3.5	76.5	3.8	76.5	15.6	79.6	20.4	12.0
	107	684											
AVG. OVER POINTS								1.5	79.4	19.2	80.6	19.4	
AVG. OVER PLOTS									75.6	20.6	75.8	21.4	
OVER CLAS BY POINT									84.1	15.1	84.8	15.2	5.2
OVER CLASS BY PLOT									78.8	19.5	78.5	19.5	

TABLE B-5. ERTS SIGNATURE EXTENSION, UNADJUSTED IONIA-CLINTON SIGNATURES APPLIED TO EATON COUNTY DATA. (7 SIGNATURES, 5 CLASSES, 0.001 THRESHOLD.)

PERCENTS OF TOTAL NUMBER OF POINTS IN EACH CLASS

BY CLASSES OF PLOTS AND CLASSES OF SIGNATURES

CLASS	NR. PLOTS	NR. POINT	SIGNATURES.. CORN	SOY BEANS	TREES	BARE SOIL	SENESC VEG.	POINTS IN CLASS NOT CLASD	RIGHT (OF ALL)	WRONG (OF ALL)	RIGHT (OF CLASD)	WRONG (OF CLASD)	ASS'D FROM OTHER CLASS
CORN	32	444	57.0		37.8		2.5	2.7	57.0	40.3	58.6	41.4	15.2
SOYBEANS	7	51		66.7	2.0		27.5	3.9	66.7	29.4	69.4	30.6	.9
TREES	5	75	4.0		93.3			2.7	93.3	4.0	95.9	4.1	22.3
BARE SOIL	5	36				80.6	16.7	2.8	80.6	16.7	82.9	17.1	1.0
SENESC. VEG.	47	258	23.6	2.7	2.7	3.1	61.6	6.2	61.6	32.2	65.7	34.3	5.1
	96	864											
AVG. OVER POINTS								3.8	63.1	33.1	65.6	34.4	
AVG. OVER PLOTS									63.3	33.8	64.7	35.3	
OVER CLAS BY POINT									71.8	24.5	74.5	25.5	6.9
OVER CLASS BY PLOT									73.2	24.5	74.5	25.5	

TABLE B-6. EELS SIGNATURE EXTENSION, MLA-I IONIA-CLINTON
SIGNATURES APPLIED TO EATON COUNTY DATA.
(7 SIGNATURES, 5 CLASSES, 0.001 THRESHOLD.)

PERCENTS OF TOTAL NUMBER OF POINTS IN EACH CLASS

BY CLASSES OF PLOTS AND CLASSES OF SIGNATURES

			SIGNATURES..					POINTS IN CLASS				ASS'D
CLASS	NR. PLOTS	NR. POINT	CORN	SOY BEANS	TREES	BARE SOIL	SENESC VEG.	NOT CLASD	RIGHT (OF ALL)	WRONG	RIGHT (OF CLASD)	WRONG	FROM OTHER CLASS
CORN	32	444	64.2		3.2		32.7	.9	64.2	35.8	64.2	35.8	4.0
SOYBEANS	7	51		74.5			25.5	.0	74.5	25.5	74.5	25.5	1.0
TREES	5	75	13.3	1.3	73.3		6.7	5.3	73.3	21.3	77.5	22.5	1.8
BARE SOIL	5	36				77.8	16.7	5.6	77.8	16.7	82.4	17.6	1.6
SENESC. VEG.	47	258	2.7	2.7		9.7	86.8	2.7	86.8	10.5	89.2	10.8	27.9
	96	864											
AVG. OVER POINTS								1.5	72.9	25.6	74.0	26.0	
AVG. OVER PLOTS									78.1	20.4	79.0	21.0	
OVER CLAS BY POINT									75.3	22.0	77.6	22.4	7.3
OVER CLASS BY PLOT									77.0	21.1	78.4	21.6	

TABLE B-7. ERTS SIGNATURE EXTENSION, MLA-II IONIA-CLINTON
SIGNATURES APPLIED TO EATON COUNTY DATA.
(7 SIGNATURES, 5 CLASSES, 0.001 THRESHOLD.)

PERCENTS OF TOTAL NUMBER OF POINTS IN EACH CLASS

BY CLASSES OF PLOTS AND CLASSES OF SIGNATURES

CLASS	NR. PLOTS	NR. POINT	SIGNATURES.. CORN	SOY BEANS	TREES	BARE SOIL	SENESC VEG.	POINTS IN CLASS NOT CLASD	RIGHT (OF ALL)	WRONG (OF ALL)	RIGHT (OF CLASD)	WRONG (OF CLASD)	ASS'D FROM OTHER CLASS
CORN	32	444	64.9		5.6		29.3	.2	64.9	34.9	65.0	35.0	4.3
SOYBEANS	7	51		74.5			25.5	.0	74.5	25.5	74.5	25.5	1.0
TREES	5	75	12.0	1.3	76.0		5.3	5.3	76.0	18.7	80.3	19.7	3.2
BARE SOIL	5	36				75.0	19.4	5.6	75.0	19.4	79.4	20.6	1.6
SENESC. VEG.	47	258	3.5	2.7		5.0	86.0	2.7	86.0	11.2	88.4	11.6	25.4
	96	864						1.6	73.1	25.2	74.4	25.6	
AVG. OVER POINTS									78.4	20.0	79.3	20.7	
AVG. OVER PLOTS									75.3	22.0	77.5	22.5	7.1
OVER CLAS BY POINT									76.6	21.5	78.0	22.0	
OVER CLASS BY PLOT													

TABLE B-8. ERTS LOCAL RECOGNITION, UNADJUSTED EATON SIGNATURES APPLIED TO EATON COUNTY DATA. (12 SIGNATURES, 7 CLASSES, 0.001 THRESHOLD.)

PERCENTS OF TOTAL NUMBER OF POINTS IN EACH CLASS

BY CLASSES OF PLOTS AND CLASSES OF SIGNATURES

			SIGNATURES..						POINTS IN CLASS				ASS'D FROM
CLASS	NR. PLOTS	NR. POINT	CORN	SOY BEANS	TREES	BARE SOIL	SENESC VEG.	NOT CLASS	RIGHT (OF ALL)	WRONG (OF ALL)	RIGHT (OF CLASS)	WRONG (OF CLASS)	OTHER CLASS
CORN	32	444	77.0	.2	10.6		11.7	.5	77.0	22.5	77.4	22.6	7.4
SOYBEANS	7	51		88.2			7.8	3.9	88.2	7.8	91.8	8.2	1.5
TREES	5	75	12.0		88.0			.0	88.0	12.0	88.0	12.0	6.1
BARE SOIL	5	36				97.2	2.8	.0	97.2	2.8	97.2	2.8	2.2
SENESC. VEG.	47	258	8.5	4.3	.4	7.0	78.3	1.6	78.3	20.2	79.5	20.5	9.4
	96	864											
AVG. OVER POINTS								.9	79.9	19.2	80.6	19.4	
AVG. OVER PLOTS									78.5	20.2	79.5	20.5	
OVER CLAS BY POINT									85.8	13.1	86.8	13.2	5.3
OVER CLASS BY PLOT									84.1	13.9	85.9	14.1	

TABLE B-9. ERTS SIGNATURE EXTENSION, ADAPTATION OF IONIA-CLINTON SIGNATURES WITHIN IONIA AND CLINTON COUNTY DATA.
(7 SIGNATURES, 5 CLASSES, ADAPTATION INTERVAL ~190 LINES.)

PERCENTS OF TOTAL NUMBER OF POINTS IN EACH CLASS

BY CLASSES OF PLOTS AND CLASSES OF SIGNATURES

CLASS	NR. PLOTS	NR. POINT	SIGNATURES.. CORN	SOY BEANS	TREES	BARE SOIL	SENESC VEG.	NOT CLASD	POINTS IN CLASS RIGHT (OF ALL)	WRONG (OF ALL)	RIGHT (OF CLASD)	WRONG (OF CLASD)	ASS'D FROM OTHER CLASS
CORN	37	297	78.1		7.4		14.5	.0	78.1	21.9	78.1	21.9	4.4
SOYBEANS	6	27		85.2	7.4		7.4	.0	85.2	14.8	85.2	14.8	4.6
TREES	6	47	8.5		87.2		4.3	.0	87.2	12.8	87.2	12.8	3.8
BARE SOIL	10	53				94.3	5.7	.0	94.3	5.7	94.3	5.7	2.4
SENESC. VEG.	48	260	5.0	11.5		5.8	77.7	.0	77.7	22.3	77.7	22.3	11.8
	107	684											
AVG. OVER POINTS								.0	80.1	19.9	80.1	19.9	
AVG. OVER PLOTS									77.3	22.7	77.3	22.7	
OVER CLAS BY PCINT									84.5	15.5	84.5	15.5	5.4
OVER CLASS BY PLOT									79.5	20.5	79.5	20.5	

TABLE B-10. ERTS SIGNATURE EXTENSION, ADAPTATION OF EATON COUNTY SIGNATURES WITHIN IONIA AND CLINTON COUNTY DATA. (7 SIGNATURES, 5 CLASSES, ADAPTATION INTERVAL ~190 LINES.)

PERCENTS OF TOTAL NUMBER OF POINTS IN EACH CLASS

BY CLASSES OF PLOTS AND CLASSES OF SIGNATURES

CLASS	NR. PLOTS	NR. POINT	SIGNATURES.. CORN	SOY BEANS	TREES	BARE SOIL	SENESC VEG.	POINTS IN CLASS: NOT CLASD	RIGHT (OF ALL)	WRONG (OF ALL)	RIGHT (OF CLASD)	WRONG (OF CLASD)	ASS'D FROM OTHER CLASS
CORN	37	297	64.0		.3		35.7	.0	64.0	36.0	64.0	36.0	5.2
SOYBEANS	6	27	3.7	85.2			11.1	.0	85.2	14.8	85.2	14.8	2.0
TREES	6	47	40.4	2.1	51.1		6.4	.0	51.1	48.9	51.1	48.9	.2
BARE SOIL	10	53				100.0		.0	100.0	.0	100.0	.0	5.1
SENESC. VEG.	48	260		4.6		12.3	83.1	.0	83.1	16.9	83.1	16.9	26.4
	107	684											
AVG. OVER POINTS								.0	74.0	26.0	74.0	26.0	
AVG. OVER PLOTS									71.7	28.3	71.7	28.3	
OVER CLAS BY POINT									76.7	23.3	76.7	23.3	7.8
OVER CLASS BY PLOT									71.8	28.2	71.8	28.2	

Appendix C
DESCRIPTION OF PROPORTION ESTIMATION PROCEDURE

In this appendix, which contains exerpts from Refs. 23 and 29, theoretical methods are developed for determination of the mixture of materials in the IFOV of a multispectral sensor when the radiation received by the sensor is composed of radiation from several object classes. In Section C.1, a mathematical model is formulated which relates the signature of a mixture of materials in the IFOV to the signatures of the constituent materials. The mathematical model is used in Section C.2 to determine the maximum likelihood estimate of the proportions of the various materials occurring in the IFOV, given an observed data point. The question of uniqueness of the estimate is also discussed. The detection of alien objects is dealt with in Section C.3. Finally, in Section C.4, the problem of estimating mixtures of materials is related to the more usual problem of identifying the material when it is assumed that the IFOV contains a single object class.

C.1 MODEL FOR SIGNATURES OF MIXTURES

When the IFOV of a multispectral scanner is large in contrast to the structure being scanned, a single resolution cell may contain a number of different object classes. Suppose the scanner has m spectral channels and that the signature of object class i, where $1 \le i \le n$, is represented by an m-dimensional Gaussian distribution with mean A_i and covariance matrix M_i. If the proportion of object class i in the resolution cell is p_i and $p = (p_1, \ldots, p_n)$, then let the signature of this combination of classes have mean A_p and covariance matrix M_p.

To find expressions for A_p and M_p, consider the following model. If the resolution cell contains elements only of object class i, assume that it contains N_i elements of this type. With each of these elements, associate a random variable with mean A_i^* and covariance matrix M_i^*. Thus, we have

$$A_i = N_i A_i^*$$

If we assume statistical independence of these N_i random variables, we have also

$$M_i = N_i M_i^*$$

Now, if the proportion of the resolution cell covered by elements of object class i is p_i, then the number of elements of this type in the resolution cell is $p_i N_i$. Thus,

$$A_p = \sum_i p_i N_i A_i^* = \sum_i p_i A_i$$

If we assume that the random variables associated with elements from different object classes are also statistically independent, we have

$$M_p = \sum_i p_i N_i M_i^* = \sum_i p_i M_i$$

Since the pure signatures are taken to be Gaussian, the distribution associated with proportion vector, p, is also Gaussian. As derived above, its parameters are given by

$$A_p = \sum_i p_i A_i$$

$$M_p = \sum_i p_i M_i$$

These formulas for A_p and M_p constitute our model for signatures of object-class combinations in terms of the signatures of the individual object classes. This model assigns a signature to each mixture of the n materials. The formula for the mean of a mixture may be interpreted geometrically. If A_1, A_2, and A_3 are the means of the pure materials, then the mean of each mixture lies in the triangle $A_1A_2A_3$ (convex hull of A_1, A_2, andA_3, which we often refer to as the signature simplex). In Fig. C.2, A' is the mean of the signature assigned to the proportion vector (1/3, 1/3, 1/3). It is the centroid of the triangle. A'' is the mean of the signature assigned to the proportion vector (0, 1/2, 1/2). It is the midpoint of line segment A_2A_3.

C.2 ESTIMATION OF PROPORTIONS

The model for the signature of a mixture is now utilized to estimate the mixture of materials in the resolution cell corresponding to the signal generated by a multispectral sensor. If the signal is represented by an m-vector y, then the maximum likelihood procedure leads to choosing a proportion vector, p, which minimizes

$$F(p) = \ell n\ |M_p| + \left\langle y - A_p,\ M_p^{-1}(y - A_p) \right\rangle$$

subject to the constraints that p be a proportion vector, i.e.;

$$\sum p_i = 1$$

and

$$p_i \geq 0 \quad 1 \leq i \leq n$$

Here $|M|$ denotes the determinant of the matrix M; M^{-1} denotes the inverse of M; $\langle u, v \rangle$ is the inner product of the vectors u and v; and y and A_p are taken as column vectors. F(p) is, except for a constant, the negative of the natural log of the Gaussian density function with mean A_p and covariance matrix M_p evaluated at the point y.

C.2.1 ESTIMATION OF PROPORTIONS IN SPECIAL CASES

Consider the special case (Case 1) where the M_i are all equal, (e.g., $M_i = M$). If M is positive definite, it can be factored into

$$M = LL^T$$

where L is a triangular matrix, and T superscript means transpose. If we define

$$z = L^{-1}y$$

$$B_i = L^{-1}A_i \quad 1 \leq i \leq n$$

$$B_p = L^{-1}A_p$$

it is easy to show (see Ref. 29) that the maximum likelihood estimate of p minimizes

$$G(p) = \left|\left|z - B_p\right|\right|^2$$

over all proportion vectors p. Here $||u||$ denotes the norm of the vector u. This minimization problem has a simple geometric interpretation. We want to find a p such that B_p is the point in the convex hull of the B_i, $1 \leq i \leq n$, which is closest to z, as illustrated in Fig. 4. Each point in the triangle $B_1B_2B_3$ (convex hull of the points B_1, B_2, and B_3) has a unique representation in the form

$$\sum_i^3 p_i B_i$$

where p is a proportion vector. B_{p^o} is the point in the triangle closest to z and p^o is the required estimate. For this example

$$p^o = 0.33, 0, 0.67$$

A more inclusive special case occurs when the M_i are all scalar multiples of some common matrix M (Case 2). If σ_i^2 is defined by

$$M_i = \sigma_i^2 M \quad 1 \leq i \leq n$$

then the maximum likelihood estimate of p minimizes

$$H(p) = m \ell n\, w_p + \frac{1}{w_p} \left|\left| z - B_p \right|\right|^2$$

over the set of proportion vectors p, where

$$w_p = \sum p_i \sigma_i^2$$

and m is the number of spectral channels.

C.2.2 UNIQUENESS OF ESTIMATES

When the covariance matrices M_i are scalar multiples of each other, the objective function H(p) is quasi-convex [41]. Then the maximum likelihood estimate of p is unique, when the (m + 1) - dimensional vectors $(1, A_i)$, $1 \leq i \leq n$, are linearly independent.

Estimates are not necessarily unique in the general case under this condition. However, if the covariance matrices are small, then estimates are almost unique. To be more precise, let r be a small, positive number, and let

$$M_{p,r} = rM_p$$

and

$$F_{p,r} = \ell n |M_{p,r}| + \left\langle y - A_p, M_{p,r}^{-1}(y - A_p) \right\rangle$$

then

$$rF_{p,r} = mr \ell n\, r + r \ell n |M_p| + \left\langle y - A_p, M_p^{-1}(y - A_p) \right\rangle$$

As r becomes smaller, $rF_{p,r}$ is approximately

$$R_p = \left\langle y - A_p, M_p^{-1}(y - A_p) \right\rangle$$

But this function is convex and is minimized by a unique p, from which we may conclude that if the covariances are small enough, R_p will approximate F_p. Thus, the unique p which minimizes R_p will be close to any p that minimizes F_p. As a result, all minimizing p's of F(p) will be close to each other and therefore will not be a source of significant error in the estimate.

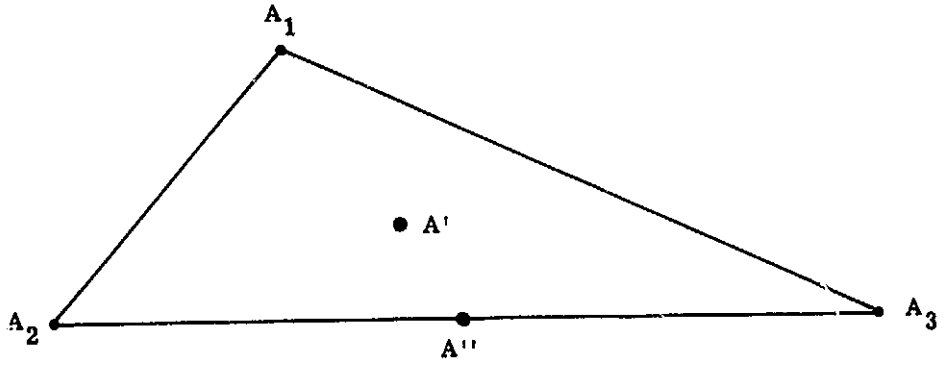

FIGURE C1. GEOMETRIC INTERPRETATION OF MEANS OF SIGNATURES OF MIXTURES

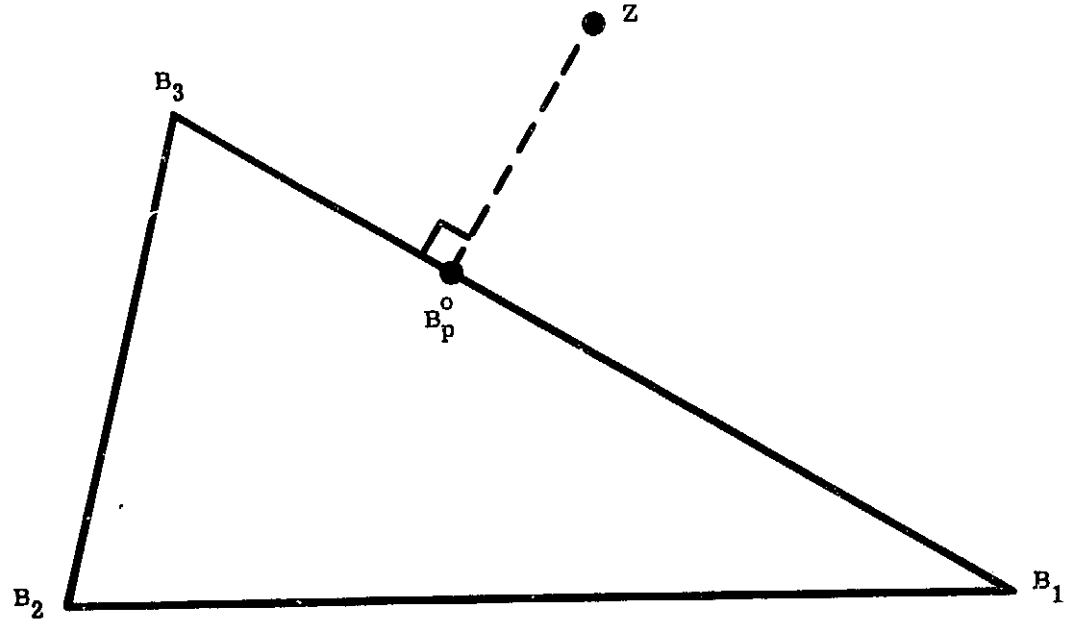

FIGURE C2. GEOMETRIC INTERPRETATION OF ESTIMATE (SPECIAL CASE)

C.3 ESTIMATION OF PROPORTIONS IN PERSPECTIVE

The solution to the problem of estimating proportions of materials in the IFOV is the logical extension of the solution of the problem of identifying the material, when it is assumed that the IFOV contains only one type of material. The procedure in the latter case is essentially to maximize the likelihood of the given data point with respect to the signatures of a finite number of possible materials. The mixture model assigns signatures to all the mixtures of a finite number of materials and maximizes the likelihood of a data point over this infinity of possibilities. Conceptually, therefore, the solutions are similar. However, the computation of the estimate of the proportion vector is more complicated than the determination of the most likely material from a limited number of alternatives.

C.4 DETECTION OF ALIEN OBJECTS

Estimating proportions of unresolved objects from a signal y is based on the assumption that the signal comes from a pixel which contains a mixture of materials. These materials are represented by known signatures that constitute the pure signature set. If the pixel should contain a material not represented in the signature set, significant additional error in the estimate of proportions may result. The amount of this error depends upon the proportion of these alien materials and the geometric relationship of their signatures to those in the pure signature set. Those materials occurring in a scene but not represented in the pure signature set are referred to as alien materials or alien objects. Procedures have been designed to reduce the error resulting from the presence of alien objects. These procedures take the form of thresholding tests—hence the designation "alien object threshold."

One might attempt to avoid the alien object problem by obtaining signatures for all materials present in the scene. This approach is usually impractical because of the large number of materials present and the impossibility of obtaining definitive signatures for many of them. An alternative is to use essentially a chi-square test as in conventional recognition processing. Some modifications are necessary when averaging procedures are also employed.

The current mixtures program contains improved procedures for dealing with alien objects. These procedures can be described most easily in terms of the pure signature set and signals after a linear transformation has been employed. After this transformation, we assume that the i-th material in the pure signature set has mean A_i, and its covariance matrix is the identity. Now given a signal (data point) y from a pixel with unknown proportions of various materials, the estimate $\hat{\lambda}$ of the proportion is obtained as follows. Let Z denote the point in the signature simplex closest to y. Then Z may be represented in the form

$$Z = A\hat{\lambda}$$

where $\hat{\lambda}$ is a proportion vector and is taken as the estimate of proportions in the pixel represented by the signal y. In order to apply an alien object test, we ask, "What is the probability that we would have observed the signal with value exceeding y if the true proportion of the pixel was $\hat{\lambda}$?" Assuming Gaussian signature distributions, this amounts to a chi-square test with n degrees of freedom, where n is the number of spectral channels used. The level of significance is determined by a value χ_o^2, which is the alien object threshold. If

$$||y - Z||^2 = ||y - A\hat{\lambda}||^2 > \chi_o^2$$

then the estimate fails the chi-square test; we then say that the pixel contains significant amounts of alien materials and make no estimate of proportions for the pixel in question. If the estimate passes the test, we accept it as the estimate of proportions of materials in the pixel in question.

REFERENCES

1. W.A. Malila, R.B. Crane, C.A. Omarzu and R.E. Turner, "Studies of Spectral Discrimination," Report No. 31650-22-T, Willow Run Laboratories of the Institute of Science and Technology, The University of Michigan, Ann Arbor, 1971.

2. R.E. Turner, W.A. Malila and R.F. Nalepka, "Importance of Atmospheric Scattering in Remote Sensing, or Everything You've Always Wanted to Know About Atmospheric Scattering But Were Afraid to Ask," Proceedings of the Seventh International Symposium on Remote Sensing of Environment, Center for Remote Sensing Information and Analysis, Willow Run Laboratories of the Institute of Science and Technology, The University of Michigan, Ann Arbor, 1971.

3. R.E. Turner, "Remote Sensing in Hazy Atmospheres," Proceedings of ACSM/ASP Meeting, Washington, D.C., March, 1972.

4. R.E. Turner, "Radiative Transfer in Model Atmospheres (Scattering)," Course Notes, Advanced Infrared Technology, The Ann Arbor Engineering Summer Conference, The University of Michigan, Ann Arbor, 1972.

5. R.E. Turner, "Radiative Transfer in Real Atmospheres," Report No. 190100-24-T, Environmental Research Institute of Michigan, Ann Arbor, 1974.

6. R.E. Turner, W.A. Malila, R.F. Nalepka and F.J. Thomson, "Influence of the Atmosphere on Remotely Sensed Data," Proceedings of SPIE Seminar on Scanners and Imagery Systems for Earth Observation, San Diego, California, 19-20 August 1974.

7. K.L. Coulson, J.V. Dave and Z. Sekera, Tables Related to Radiation Emerging from a Planetary Atmosphere with Rayleigh Scattering, University of California Press, 1960.

8. L. Elterman, "Vertical Attenuation Model with Eight Surface Meteorological Ranges 2 to 13 Kilometers," AFCRL Report No. 70-0200, Air Force Cambridge Research Laboratories, Bedford, Massachusetts, March, 1970.

9. W.A. Malila, and R.F. Nalepka, "Atmospheric Effects in ERTS-1 Data, and Advanced Information Extraction Techniques," Symposium on Significant Results Obtained from the Earth Resources Technology Satellite-1, NASA SP-327, Goddard Space Center, Greenbelt, Maryland, March 1973.

10. D.E. Pitts, W. McAllum and A.E. Dillinger, "Measurement of Atmospheric Precipitable Water Using a Solar Radiometer," NASA Technical Memorandum TMX-58129, JSC-08682, Johnson Space Center, Houston, Texas, February, 1974.

11. M.J. Duggin, "On the Natural Limitations of Target Differentiation by Means of Spectral Discrimination Techniques," Proceedings of Ninth International Symposium on Remote Sensing of Environment, the Environmental Research Institute of Michigan, Ann Arbor, 1974.

12. F.W. Kriegler, W. Malila, R. Nalepka and W. Richardson, "Preprocessing Transformations and Their Effects on Multispectral Recognition," Proceedings of Sixth International Symposium on Remote Sensing of Environment, Willow Run Laboratories of the Institute of Science and Technology, The University of Michigan, Ann Arbor, 1969.

13. R.B. Crane and W. Richardson, "Rapid Processing of Multispectral Scanner Data Using Linear Techniques," Remote Sensing of Earth Resources, Vol. 1, edited by F. Shahroklir, University of Tennessee Space Institute, Tullahoma, 1972.

14. R.B. Crane, "Adaptive Processing of Multispectral Scanner Data Using a Decision-Directed Kalman Filter," Proceedings of Ninth International Symposium on Renote Sensing of Environment, the Environmental Research Institute of Michigan, Ann Arbor, 1974.

15. F.J. Kriegler, R.E. Marshall, H. Horwitz and M. Gordon, "Adaptive Multispectral Recognition of Agricultural Crops," Proceedings of Eighth International Symposium on Remote Sensing of Environment, Environmental Research Institute of Michigan, Ann Arbor, 1972.

16. R. Henderson, "Task II, Signature Extension Techniques," Report No. 109600-6-L, NASA Contract NAS9-14123, the Environmental Research Institute of Michigan, Ann Arbor, 1974.

17. G.R. Safir, W.L. Myers, W.A. Malila and J.P. Morgenstern, "Application of ERTS-1 Data to Analysis of Agricultural Crops and Forests in Michigan," Proceedings of Symposium on Significant Results Obtained from the Earth Resources Technology Satellite-1, Vol. I, Sec. A, NASA SP-327, Goddard Space Flight Center, Greenbelt, Maryland, March 1973.

18. W.A. Malila, J.E. Sarno, T.W. Wagner, J.T. Lewis and J.D. Erickson, "The Use of ERTS Data for a Multi-Disciplinary Analysis of Michigan Resources," Report No. 197500-28-F, prepared for Michigan State University, E. Lansing, the Environmental Research Institute of Michigan, Ann Arbor, September 1974.

19. W.A. Malila, R.H. Hieber and A.P. McCleer, "Correlation of ERTS MSS Data and Earth Coordinate Systems; Proceedings of Purdue Conference on Machine Processing of Remotely Sensed Data, Lafayette, Indiana, October 1973. (NTIS No. N74-13057)

20. F.J. Thomson, et al., the Environmental Research Institute of Michigan Progress Report, 1 January-30 June 1973, Task VII, Report No. 193300-16-P, Environmental Research Institute of Michigan, Ann Arbor, 1973 (NTIS No. N73-29248)

21. W.A. Malila, and R.F. Nalepka, "Advanced Processing and Information Extraction Techniques Applied to ERTS-1 MSS Data" Proceedings of Third Earth Resources Technology Satellite-1 Symposium, NASA SP-351, Washington, D.C., December 1973.

22. H.M. Horwitz, R.F. Nalepka, P.D. Hyde and J. Morgenstern, "Estimating the Proportions of Objects within a Single Resolution Element of a Multispectral Scanner," Seventh International Symposium on Remote Sensing of Environment, Willow Run Laboratories of the Institute of Science and Technology, The University of Michigan, Ann Arbor, 1971.

23. R. Nalepka, H.M. Horwitz and P.D. Hyde, Estimating Proportions of Objects from Multispectral Data, Report No. 31650-73-T, Willow Run Laboratories of the Institute of Science and Technology, The University of Michigan, Ann Arbor, March 1972.

24. R.F. Nalepka, H.M. Horwitz, P.D. Hyde and J.P. Morgenstern, "Classification of Spatially Unresolved Objects," Proceedings of the Fourth Annual Earth Resources Program Review, NASA/MSC, Houston, Texas, January 1972.

25. R.F. Nalenka and P.D. Hyde, "Classifying Unresolved Objects from Simulated Space Data," Eighth International Symposium on Remote Sensing of Environment, the Environmental Research Institute of Michigan, Ann Arbor, 1972.

26. R.F. Nalepka and P.D. Hyde, Estimating Crop Acreage from Space-Simulated Multispectral Scanner Data, Report No. 31650-148-T, the Environmental Research Institute of Michigan, Ann Arbor, January 1973.

27. W. Richardson and H.M. Horwitz, "A Faster Algorithm for Estimating Proportions," LARS Conference on Machine Processing of Remotely Sensed Data, Purdue University, Lafayette, Indiana, October 1973.

28. H.M. Horwitz and P.O. Hyde, "Estimating Proportions of Unresolved Objects from Multispectral Data," 1973 International Symposium on Pattern Recognition, IEEE, Pattern Recognition Society, Am. Soc. of Photogrammetry, Washington, D.C., October - November 1973.

29. H.M. Horwitz, P.D. Hyde and W. Richardson, Improvements in Estimating Proportions of Objects from Multispectral Data, Report No. 190100-25-T, the Environmental Research Institute of Michigan, Ann Arbor, April 1974.

30. C.R. Hallum, "On a Model for Optimal Proportions Estimates for Category Mixtures, Eighth International Symposium on Remote Sensing of Environment, the Environmental Research Institute of Michigan, Ann Arbor, 1972.

31. D.M. Detchmendy and W.H. Pace, "A Model for Spectral Signature Variability for Mixtures," Earth Resources Observation and Information Analysis Systems Conference, University of Tennessee Space Institute, Tullahoma, 1972.

32. P. Salvato Jr., "Interactive Techniques to Estimate Signature Vectors for Mixture Processing of Multispectral Data," The Purdue Conference on Machine Processing of Remotely Sensed Data, Purdue University, Lafayette, Indiana, October 1973.

33. W.H. Pace and D.M. Detchmendy, "A Fast Algorithm for the Decomposing of Multispectral Data Into Mixtures," Second Annual Remote Sensing of Earth Resources Conference, University of Tennessee Space Institute, Tullahoma, March 1973.

34. H.M. Horwitz, J. Lewis and A. Pentland, Proportion Estimation, Task IV, Report No. 109600-3-L, NASA Contract NAS9-14123, the Environmental Research Institute of Michigan, Ann Arbor, 1974.

35. NASA, Reports on Surface Water Detection, No. JSC-08638, JSC-08639, JSC-086449 through JSC-086454, Johnson Space Center, Houston, Texas, 1973.

36. E.A. Work Jr., D.S. Gilmer and A.T. Klett, "Preliminary Evaluation of ERTS-1 for Determining Numbers and Distribution of Prairie Ponds and Lakes," Proceedings of the Symposium on Significant Results Obtained from the Earth Resources Technology Satellite-1, Vol. 1, NASA SP-327, Goddard Space Flight Center, Greenbelt, Maryland, March 1973.

37. E.A. Work Jr., D.S. Gilmer and A.T. Klett, "Utility of ERTS for Monitoring the Breeding Habitat of Migratory Waterfowl," Proceedings of the Third Earth Resources Technology Satellite-1 Symposium, pp. 1671-1685, Vol. I and pp. 102-113, Vol. II., Goddard Space Flight Center, Greenbelt, Maryland, December 1973.

38. E.A. Work Jr., and F.J. Thomson, A Study of Waterfowl Habitat in North Dakota Using Remote Sensing Techniques: Phase II," Report No. 10100-12-T, the Environmental Research Institute of Michigan, Ann Arbor, 1974.

39. E.A. Work Jr., "Application of the Earth Resources Technology Satellite for Monitoring the Breeding Habitat of Migratory Waterfowl in the Glaciated Prairies," Master's Thesis, The University of Michigan, University Microfilms, Ann Arbor, Michigan, (Thesis Abstr. M-6698), 1974.

40. F.J. Thomson, "Crop Species Recognition and Mensuration in the Sacramento Valley," Symposium on Significant Results Obtained from the Earth Resources Technology Satellite-1, Vol. 1, NASA SP-327, Goddard Space Flight Center, Greenbelt, Maryland, March 1973.

41. C. Berge and A. Ghouila-Houri, Programming Games, and Transportation Networks, John Wiley Inc., New York, 1965.